POLITECNICO DI MILANO

Facoltà di Ingegneria Industriale

Corso di Laurea in
Ingegneria Energetica

Hybrid repowering of a coal-fired power plant with an Integrated Solar Combined Cycle (ISCC) in Australia

Relatore: Prof. Giampaolo MANZOLINI

Co-relatore: Ing. Andrea GIOSTRI

Tesi di Laurea di:

Martino BONIARDI Matr. 735628

Anno Accademico 2010 - 2011

Acknowledgement

Foremost, I would like to express my sincere gratitude to my supervisor Prof. Giampaolo Manzolini for the continuous support of my thesis, for his patience, motivation and insightful comments. His guidance helped me in all the time writing this thesis. Besides my advisor, I would like to thank Andrea Giostri for all the time given to me, for his precious help in starting up and develop the work and for be always present for any clarification I needed.

My sincere thanks also go to Ing. Attilio Pigneri, a co-supervisor and a friend, for his patience, encouragement and knowledge, for offering me the opportunity of a 5-months internship in their group in Sydney, and for leading me working on my first steps. I owe my deepest gratitude to Dr. Iain McGill, a special person that made my 6-month international exchange in Sydney possible, for having made me feel at ease from the first moment I arrived at University of New South Wales and for revolutionizing the concept I had of "Professor". Also I thank my friend Manuel for his wittiness, humor and for sharing unforgettable moments inside and outside the UNSW.

A special thank goes to Mario, Guido, Marco, Eugenio, Andrea e Riccardo for all the time spent together in the last years and for being not just fellow students but Friends with a capital F. I also would like to thank all unmentioned friends and people who know to be an important part of my life.

Lastly, the biggest thank goes to my family: to my parents Vincenzo and Raffaella, for supporting me spiritually throughout my life and for giving me the concrete opportunity to write this thesis after a path of studies rich in unforgettable experiences abroad, to my brother Giacomo for the great respect I always perceive and to my grandfather Gianni, for having always made me feel his unlimited faith in me.

An enormous thank to Mattia, that has confirmed day by day to be nothing less than a stepbrother.

I really care for saying an endless thank to Clarissa, my life's companion, for being that easily by my side.

Ringraziamenti

Innanzitutto, vorrei esprimere la mia sincera gratitudine al mio relatore Prof. Giampaolo Manzolini per il continuo sostegno dato alla mia tesi, per la sua pazienza, per la motivazione e per i suoi illuminanti commenti. Inoltre, vorrei ringraziare Andrea Giostri per tutto il tempo che mi ha dedicato, per il suo prezioso aiuto per avviare e sviluppare il lavoro e per essere stato sempre presente per qualsiasi chiarimento.

Un ringraziamento sincero va anche all'Ing. Attilio Pigneri, un correlatore ed un amico, per la sua pazienza, per l'incoraggiamento, per aver messo a disposizione la sua conoscenza e per avermi offerto l'opportunità di uno stage di cinque mesi nella loro sede di Sydney. Devo la mia più profonda gratitudine al Dott. Iain McGill, una persona speciale senza la quale lo scambio internazionale in Australia non sarebbe stato possibile; lo ringrazio per avermi fatto sentire a mio agio fin dal primo momento in cui sono arrivato alla University of New South Wales e per aver rivoluzionato il concetto che avevo di "Professore". Ringrazio anche il mio amico Manuel per la sua arguzia, per il suo umorismo e per la condivisione di momenti indimenticabili dentro e fuori la UNSW.

Un ringraziamento speciale va a Mario, Guido, Marco, Eugenio, Andrea e Riccardo per tutto il tempo passato insieme negli ultimi anni e per essere non solo compagni, ma amici con la A maiuscola. Vorrei anche ringraziare tutte le persone non esplicitamente citate e gli amici che sanno di essere una parte importante della mia vita.

Il ringraziamento più grande va alla mia famiglia: ai miei genitori Vincenzo e Raffaella, per avermi supportato a occhi chiusi in ogni istante della mia vita e per avermi dato l'opportunità concreta di scrivere questa tesi, dopo un percorso di studi ricco di esperienze indimenticabili all'estero; Grazie a mio fratello Giacomo, per la grande stima che mi fa percepire continuamente e a mio nonno, Gianni, per non aver mai nascosto la sua illimitata fiducia in me.

Un enorme grazie a Mattia, che ha confermato di essere ogni giorno un fratello, anche se non di sangue.
Tengo in particolar modo a concludere con un grazie Infinito a Clarissa, compagna della mia vita, per la sua semplicità e spontaneità nello starmi così splendidamente vicino.

To Raffaella, Vincenzo e Gianni

Table of contents

Abstract

The paper has the aim of study an alternative way for using solar energy, as hybrid integration in traditional fossil fuelled systems, made with large solar thermal CSP (*Concentrating Solar Power*). Even if there are some advances in solar-alone power generation, efficiencies are still too low and costs too high to compete with conventional facilities. Hybrid systems can be very attractive for reducing this gap.
In Chapter 1 a complete and detailed analysis on concentrating solar power principle and physics is lead. In this chapter the solar resource is studied through all the conversion processes from its origin to end-use. It will be shown also the reason of solar radiation concentration and its technical limits, focusing on parabolic trough collectors.
In Chapter 2 different possibilities for hybrid integration are analysed, with a particular focus on ISCCs (*Integrated Solar Combined Cycles*) enlightening technical and energy advantages and disadvantages of numerous sub-solutions such as the DSG (*Direct Steam Generation) one*, expressly chosen for the case study in Chapter 4.
In Chapter 3 the economical and political frame of solar technologies is analysed, in order to give a wider context, able to stay more in touch with real mechanisms and issues. At first, the LCOE (*Levilized Cost Of Electricity*) index construction is explained and, for each obtained LCOE value, its cost structure is studied, with the aim of seeing the possibilities for a cost reduction. After that, both short-term and long-term decision-making strategies are analysed, ending with the Australian political and governmental actions to incentivise the development of CSP.
In Chapter 4 all abovementioned notions are put in practice creating a case study that analyse a hybrid repowering of a coal-fired power plant with an ISCC in Australia. The study is conducted in Thermoflex engineering software, by recreating the coal-based layout as first step, by simulating its substitution with NGCC (*Natural Gas Combined Cycle*) as second step, by converting it into ISCC as third step and by computing off-design conditions as fourth and last step.

Keywords:

ISCC, Integrated solar combined cycle, Hybrid repowering, CSP, solar thermal, DSG

Sommario

La trattazione si pone l'obbiettivo di studiare un'opportunità alternativa per l'utilizzo dell'energia solare, sottoforma di integrazione ibrida di sistemi CSP (*Concentrating Solar Power*) in sistemi tradizionali basati su combustibili fossili. Nonostante i progressi degli ultimi anni nella generazione di potenza da sistemi esclusivamente solari, i rendimenti risultano essere ancora troppo bassi e i costi che ne derivano non riescono a competere con i sistemi tradizionali. I sistemi ibridi rappresentano un'opportunità molto interessante e più che concreta per ridurre questo gap.
Nel Capitolo 1 è condotta un'analisi dettagliata sui principi fisici dei sistemi CSP. La risorsa solare è studiata attraverso tutti quei processi di conversione energetica che la portano dalla sua origine (il Sole) all'utilizzatore finale. Sono inoltre evidenziati i punti di forza del processo di concentrazione e i suoi limiti tecnici. Un particolare focus è riservato ai sistemi a concentrazione parabolica.
Nel Capitolo 2 sono analizzate tutte le principali possibilità di integrazione solare ibrida, con particolare attenzione rivolta ai cicli combinati solari (ISCC, *Integrated Solar Combined Cycles*). Sono quindi stati evidenziati i vantaggi e gli svantaggi, da un punto di vista tecnico ed economico, delle diverse soluzioni come quella con generazione diretta di vapore (DSG, *Direct Steam Generation*) scelta per il case study illustrato nel Capitolo 4.
Il Capitolo 3 è incentrato sul contesto economico e politico delle tecnologie CSP, con l'obbiettivo di allargare la visuale, andando a vedere come questa tecnologia si inserisce nel mondo reale e nel mercato dell'energia. Lo studio inizia con una trattazione dettagliata dell'indice LCOE (*Levilized Cost Of Electricity*) evidenziando poi, per i valori trovati, la composizione dei costi, e cercando possibili soluzioni per la loro riduzione. Sono quindi analizzate le basi delle strategie decisionali sia a breve termine, sia a lungo termine, per poi concludere con una trattazione sulle azioni politico-governative dello Stato australiano atte ad incentivare lo sviluppo delle tecnologie solari.
Nel Capitolo 4 tutte le sopracitate nozioni sono state messe in pratica creando un case study che analizza il repowering ibrido di una centrale a carbone con un ISCC in Australia. Lo studio è condotto con il software dedicato Thermoflex, ricreando il layout a carbone come primo step, simulando la sua sostituzione con un NGCC (*Natural Gas Combined Cycle*) come secondo step, convertendo quest'ultimo in un ISCC come terzo step ed effettuando i calcoli delle prestazioni off-design come quarto ed ultimo step.

Parole chiave:

ISCC, ciclo combinato solare, CSP, solare a concentrazione, DSG, repowering ibrido

Introduction

Nowadays, most of growing energy demand is satisfied by consuming increasingly limited fossil fuels. Not only fossil fuels do have a limited life but also their combustion process has serious negative impacts on our environment. Solar energy represents one of the most interesting technologies to avoid both this depletion and environmental wrecking, because it is unlimited, clean and free.
But in order to give a context to solar energy production, a critical observation must be addressed upstream, to energy demand and consumption. In engineering science, the most important index in every conversion process is its efficiency; the greater efficiency is the best the process. But the energy demand/consumption ratio has efficiency lower than 0,5, because more than 50% of generated energy in the world is thrown to waste (Prof. S. Carrà, *Adkronos*). How do we have to rate this conversion? What is the sense of exerting for designing a water pump with increased mass flow if the pipes where water flows are full of holes? I personally believe that the priority of R&D efforts must be addressed for reducing those senseless wastes, because this is the best and the most intelligent way to increase the percentage of share of renewable energy, with no need to build new facilities.
In a parallel (but secondary) path, existing fossil-fuelled installation must be gradually replaced over years by renewable systems to bring back a natural balance that has manifestly been lost, because, today, the world consumption exceed for 50% the total resources provided by our planet (*WWF Living Planet report 2010*). This means that Earth is no more renewable and, since it is a closed system, if we don't improve on our behaviour, it is doomed to scientifically finish in the next centuries. Unfortunately, this dramatic scenario has been confirmed by the recent Durban United Nations climate change conference (2011).
I am convinced that we have all the possibilities to get out of troubles, and this thesis represent one among infinite solutions for achieving this target. In particular, hybrid solar repowering can represent the first step of a gradual change that start modifying, "internally" and in the right direction, existing polluting energy generation system with a relevant CO_2 reduction, as confirmed from the case study proposed in Chapter 4.
I really hope this thesis will be interpreted this way and not as the umpteenth way to have a return on image to justify the perseverance of a behaviour that has leaded to the dramatic situation that everybody is obliged to face.

Chapter 1. Introduction to Concentrating Solar Power (CSP) principles and physics

1.1 The origin of solar fuel

The light beam emission coming from the Sun is a consequence of its continuous reactions that convert mass into energy. These are nuclear fusion reactions with hydrogen, of which the Sun is composed for more than 75%, as the main element.
The basic thermo-nuclear reaction of the sun is expressed in equation 1.1

$$4\,{}^{1}H \xrightarrow{Fusion} {}^{4}He + 2e^{+} + 2\nu + 2\gamma \qquad (1.1)$$

Where ${}^{1}H$ is a proton, He is a Helium atomic nucleus, e^{+} is a positron, ν is a neutrino and γ is energy available as gamma rays.

The four Hydrogen atoms, which melt at the status of plasma, form a Helium nucleus. Among the four present electrons, two complete the atom of Helium while the remaining two combine with the positrons (one each) releasing further energy. This reaction can stand because two protons loose their positive charge to give rise to the neutrons of the Helium nucleus.
But this reaction takes place with a mass fault: the sum of the chemical products' masses is lower than the one of reagents. In particular, for the Sun, this lack is equal to $4{,}7653\times10^{-29}$ kg that, put in the famous Einstein equation[1], gives a total amount of $4{,}28284\times10^{-12}$ J of energy.
In the overall balance, the Sun "loses" $4{,}3\times10^{9}$ kg/s and this means that the chemical reaction expressed in equation 1.1 takes place 10^{38} times every second, emitting $3{,}845\times10^{20}$ MW of total power.

Now, with the value of the Sun's surface known ($6{,}089\times10^{12}$ km^2), it is possible to calculate the irradiation (I_{sun}) [MW/m^2] at the surface level (see equation 1.2)

[1] $E = mc^2$, where E represents energy [J], m represents the mass [kg] and c represents the speed of light [m/s]. This equation sets the material equivalence between mass and energy.

$$I_{sun} = \frac{3,845 \cdot 10^{20}\ MW}{6,089 \cdot 10^{12}\ km^2} = 63,17\ \left[\frac{MW}{m^2}\right] \quad (1.2)$$

The irradiation that hits the outer layer of the atmosphere is much lower than the one leaving the Sun's surface because of the distance between them. This, of course, can be calculated (see equation 1.3) with a power balance, once known the Sun-Earth distance (variable during a year from $1,471 \times 10^8$ km to $1,521 \times 10^8$ km):

$$I_{earth} = \frac{I_{sun} 4\pi R_{sun}^2}{4\pi R_{sun-earth}^2} = 1325 \div 1417\ \left[\frac{W}{m^2}\right] \quad (1.3)$$

where R_{sun} is the Sun's radius and $R_{sun\text{-}earth}$ is the distance between Sun and Earth.

Furthermore, with the hypothesis of the Sun behaving as a black body (and so as bot a perfect emitter and absorber), is possible to calculate both its surface average temperature by using the Stefan-Boltzmann law (see equation 1.4) and its emitted energy (E_λ) as a function of the wavelength of radiation by using the Planck law (see equation 1.5)

$$I_{sun} = \sigma T_{sun}^4 \rightarrow T_{sun} = 5777\ [K] \quad (1.4)$$

$$E_\lambda = \frac{3,74 \cdot 10^8}{\lambda^5 \left[e^{\frac{1440}{\lambda T}} - 1\right]} \quad \left[\frac{W}{m^2 \cdot \mu m}\right] \quad (1.5)$$

where σ is the Stephan-Boltzmann constant (equal to $5,67 \times 10^{-8}$ W/m^{2}K), λ [μm] is solar radiation wavelength.

These last steps are the basis to obtain the black body emission spectrum, which can be compared with empirical reference measurements made both outside atmosphere and at sea level (see figure 1.1)

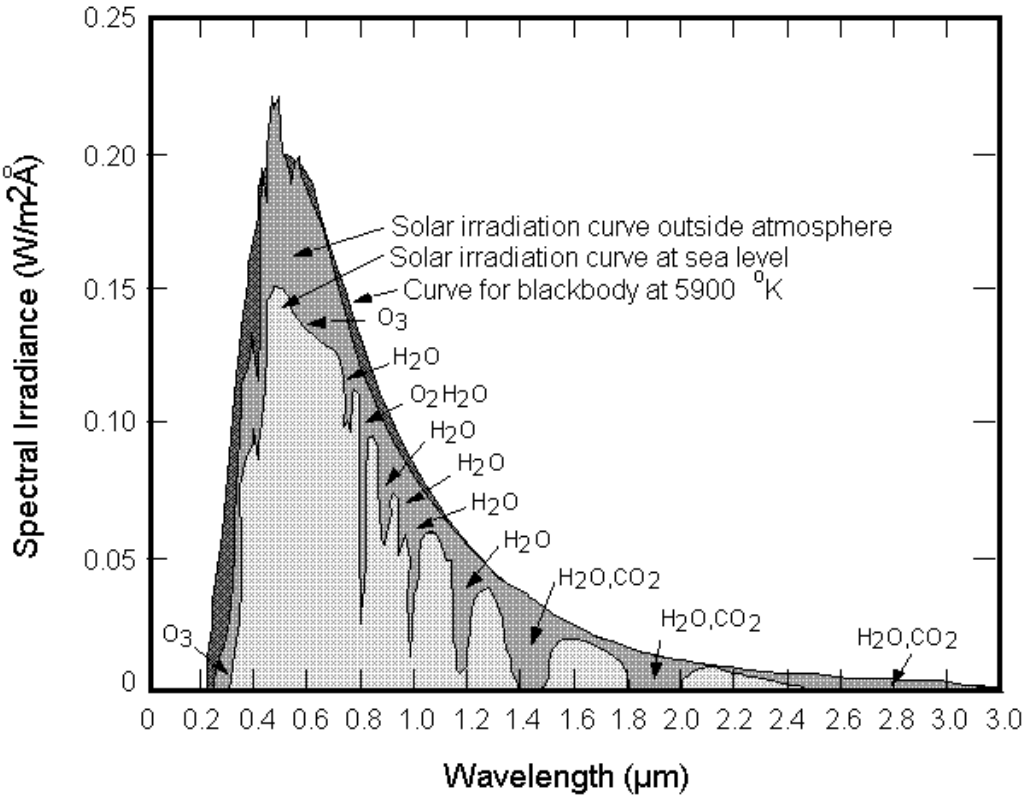

Source: Centre for Space Resource, University of Texas at Austin

Figure 1.1 – Spectral irradiance of three cases: blackbody at a temperature of 5900 K, outside atmosphere and at sea level.

It can be noticed that the spectral irradiance outside atmosphere faithfully follows the path traced by the emission spectrum of 5900 K blackbody, with a discrepancy only at its peak (better approximated by a curve referred to a 6300 K temperature blackbody).
What is significantly different is the spectral irradiance at sea level, inside atmosphere. On average it is much lower than both previous curves with low reduction peaks due to gases (such as O_3, O_2, CO_2 and H_2O) present in the

atmospheric layer. This cut is proportional to the crossed *air mass*[2], so that if the thickness grows the available energy decrease.
Three main optical processes drive this phenomenon of modification: *diffraction*, *scattering* and *reflection*. These are a function of the relative position between the terrestrial axis and Sun's orbit because

1.2 Why concentrate solar radiation?

Solar concentration increases energy quality because of higher temperatures that maximize capacity for generating mechanical work. In accord with the second law of thermodynamics, the higher the operating top temperature is, the higher the efficiency of a heat machine. The top temperature is strongly dependent on non-ideal parameters due to a real environment that interact with receivers. In particular, the machine operating temperature is directly dependent on the solar receiver outlet temperature.
With the use of solar concentration the solar receiver surface can be significantly reduced, minimizing infrared losses and reducing production costs too.

A CSP system is characterized by the use of an optical device, made by mirrors (more frequently used) or lenses, that works concentrating the incident solar radiation received on its ad-hoc shaped surface, the *collector surface* (A_c), onto the much smaller *absorber surface* A_{abs} (a pipe, often simply called *absorber*). The ratio between these two surfaces determines the value of the *concentration ratio* (*C*) (see equation 1.6). For a further analysis see paragraph 1.4.

$$\boldsymbol{C = A_{abs}/A_c} \tag{1.6}$$

In an ideal solar thermal power plant, thought with ideal concentrators, with solar receiver performing as a blackbody (therefore having only emission losses) and with a heat engine, typically a turbine, operating under Carnot ideal efficiency, the system efficiency can be written as

[2] The *air mass* expressed by $\boldsymbol{a.m.} = {}^{\mathbf{1}}/_{\boldsymbol{sin\beta}}$ where β is the *tilt angle [°],* defined as the angle between a surface perpendicular to sun's rays and ground

$$\frac{\dot{Q}}{A} = \alpha C \cdot DNI - \sigma\varepsilon(T_{abs}^4 - T_{amb}^4) \quad (1.7)$$

showing the dependence on its two kind of losses, both radiative and convective, (see equation 1.7), where α, τ and ε are respectively the hemispheric absorbance, the transmittance and the hemispherical emittance of the absorber, Q dotted is the useful power at the outlet of the solar receiver [W], A is the absorber aperture surface [m^2], σ the Stefan-Boltzmann constant [equal to $5{,}67\times10^{-8}$ W/(m^2 K^4)], DNI is the Direct Normal Irradiance [W/m^2], T_{abs} and T_{amb} respectively the absorber and ambient temperatures [K].
Concentrated solar radiation that hits the absorber increases its temperature and, consequently, its losses towards the environment. The thermal fluid flowing in the receiver pipe cools the absorber and, at equilibrium state, the gain of solar radiation equals the useful energy transferred to the cooling fluid (Q dotted) plus the infrared emission losses.

The efficiency of the solar receiver (see equation 1.8) can be obtained from the above equations and is defined as the ratio between the power gain flux and the solar energy flux incident on the absorber:

$$\eta_{rec} = \frac{\dot{Q}}{A} \cdot \frac{1}{C \cdot DNI} \quad (1.8)$$

Now, by substituting the equation 1.7 in equation 1.8 is possible to write down the thermal efficiency of the receiver (see equation 1.9) as a function of its parameters and variables;

$$\eta_{rec} = \alpha - \sigma\varepsilon \cdot \frac{T_{abs}^4 - T_{amb}^4}{C \cdot DNI} \quad (1.9)$$

In Figure 1.2 the equation 1.9 is plotted as a function of the concentrating ratio C, showing the evolution of collector global efficiency versus temperature and

concentration ratio itself, including the ideal Carnot cycle efficiency[3] too.

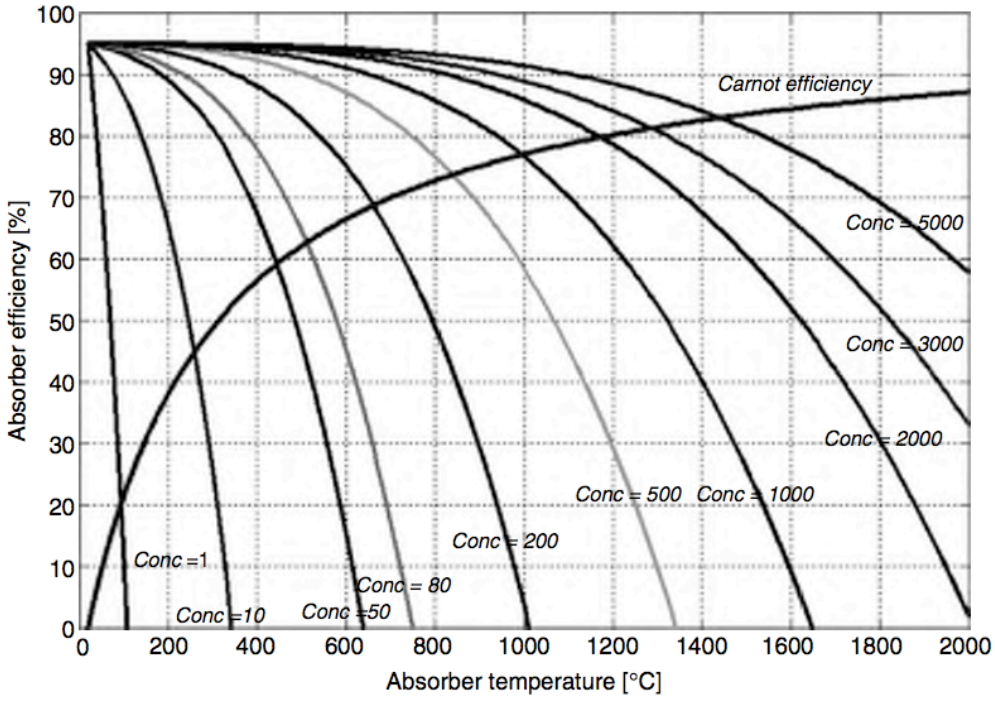

Source: F.Kreith, D. Goswami, *Handbook of energy efficiency and renewable energy, (2007)*

Figure 1.2 – efficiency of a solar receiver as a function of its absorber temperature, its concentration ratio, assuming an ambient temperature of 20 °C, a DNI of 770 W/m^2 and α = ε = 0,95.

Both equation 1.9 and its graphical representation in Figure 1.2, clearly lead to the following four conclusions:

(1) Considering an unvaried DNI, the higher the concentration ratio is, the better the collector efficiency

(2) Collector efficiency decreases with absorber temperature rise because of higher radiative losses

[3] The Carnot cycle efficiency is the ideal efficiency for reversible processes that increases with temperature and set the thermodynamic limit of the conversion efficiency (Kreith, Goswami, 2007). It is defined as $\eta_{Carnot} = \frac{T_{abs} - T_{amb}}{T_{abs}}$.

(3) The maximum theoretical collector efficiency is when $T_{abs} = T_{amb}$ and is equal to the hemispherical absorptivity (α)

(4) The higher the effective hemispherical emissivity (ε) is, the lower the collector efficiency

If we consider equation 1.7 in an unvaried system (and so with fixed technical and physic parameters A, C, DNI, σ, T_{amb}), there is a value of the temperature of the absorber that equals gains and losses, with the result of having no useful heat (Q dotted). This is the exact definition of the *stagnation temperature*, outlined in Figure 1.3 with different lines describing a variation in the hemispherical emissivity (ε).

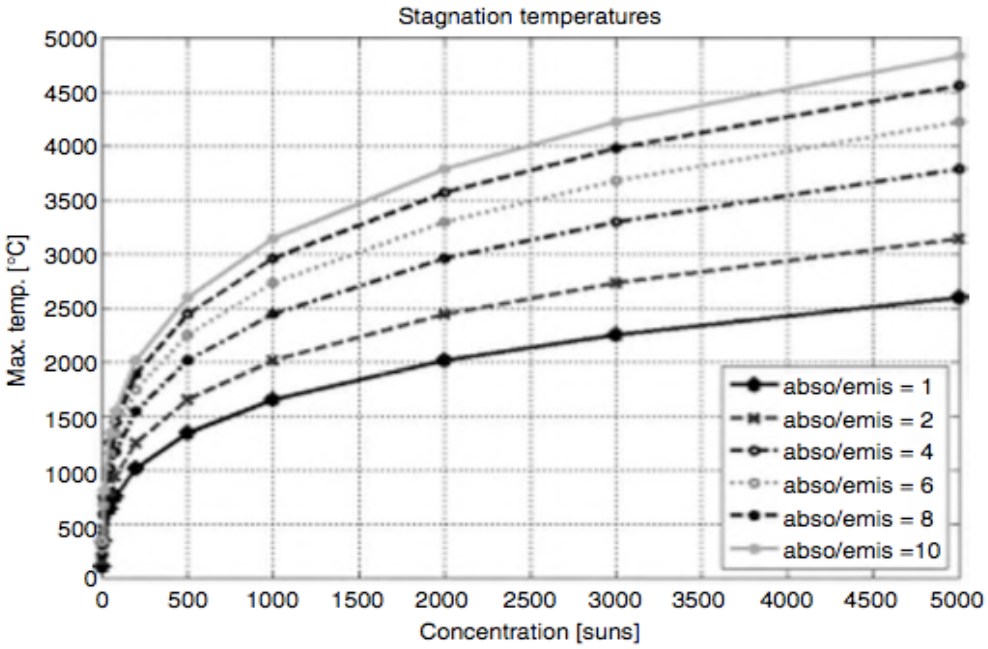

Source: F.Kreith, D. Goswami, *Handbook of energy efficiency and renewable energy, (2007)*

Figure 1.3 – Stagnation temperatures for a general solar absorber, as a function of the concentration ratio, with a DNI of 770W/m^2, an ambient temperature of 20°C, α=1 and varying ε

The stagnation limit temperature, and thus the maximum temperature of the absorber, is calculated in equation 1.10, in its turn obtained from equation 1.9:

$$T_{abs,max} = \left(\frac{\alpha \cdot C \cdot DNI}{\varepsilon \cdot \sigma} + T_{amb}^4\right) \quad (1.10)$$

To increase the maximum achievable temperature of the absorber, its external surface is made with a selective material able to change its behavior according to the wavelength of incident concentrated solar radiation. Looking at Figure 1.4, the material has an operational range, usually up to 2 μm wavelengths, where intense radiation (green curve peak) overlaps low emissivity behaviour of the material; beyond this interval, the emissivity behaviour turns high for the considered wavelengths (red curve after the 2) but is cut by the treated surface (blue line).

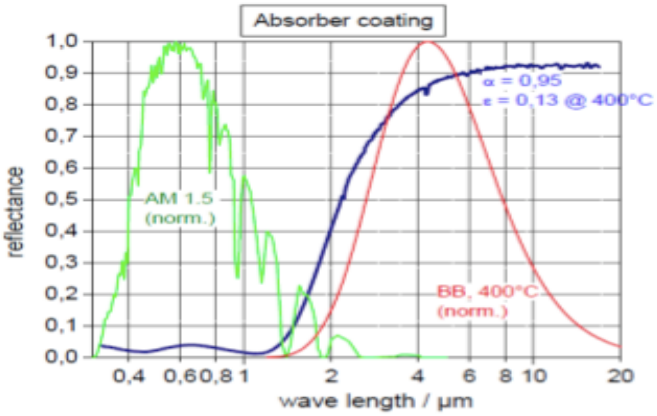

Source: L.Pistocchini, *Concentrating solar power*

Fig. 1.4 – Selective behaviour of a treated surface

The positive contribution of emissivity reduction is much higher than the negative one caused by reflection and this strongly minimizes thermal losses.
A non-selective absorber (so with $\alpha = \varepsilon = 1$) reaches approximately 95 °C in stagnation condition, with no concentration and for given solar irradiance, while a selective coating enables much higher temperatures to be reached, and that is mandatory for concentrating solar systems. For instance, for a CSP

installation with C=1000, the maximum temperature (for α/ε = 1) is higher than 1600 °C and rises to approximately 3200 °C for α/ε = 10.
So, in terms of receiver efficiency, high solar concentration and low temperatures are the best compromise, mostly because, for a given concentration ratio, there is a threshold temperature at which radiation losses increase dramatically.
When analysing a theoretical CSP system, however, we should take into consideration the whole conversion system and so the union of the solar receiver with the thermal engine. The combined efficiency (expressed in the simple equation 1.11) of both systems represents the ideal efficiency of the conversion of solar radiation into mechanical work.

$$\eta_{tot} = \eta_{rec} \cdot \eta_{Carnot} \tag{1.11}$$

This combined efficiency of both the solar receiver and heat engine has been plotted in Figure 1.5, as a function of concentration ratio and temperature:

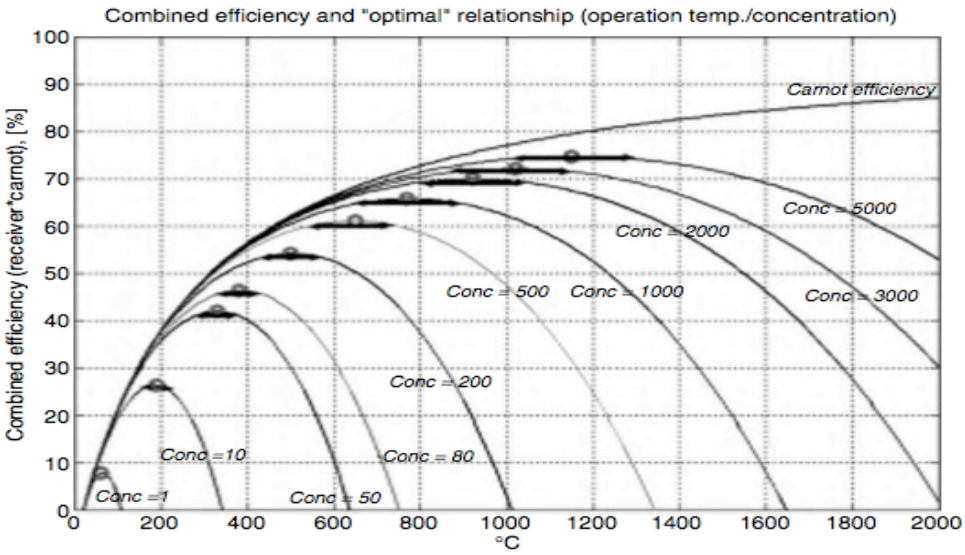

Source: F.Kreith, D. Goswami, *Handbook of energy efficiency and renewable energy, (2007)*

Figure 1.5 – Combined efficiency of both the solar receiver and the heat engine, varying as a function of different concentration ratios and temperatures of the absorber, with fixed DNI (770 W/m^2), ambient temperature (20 °C) and α = ε = 1.

In Figure 1.5 is observed that for each particular concentration ratio the efficiency has a bell-shaped trend, increasing with temperature up to an upper limit, since the Carnot term prevails. Once the peak is achieved infrared losses negative contribution overcomes Carnot term positive one causing a decrement in efficiency up to 0%.
So, as a result, it may be concluded that for any ideal receiver, with its intrinsic concentration factor, there is an optimum temperature (the ones correspondent to the each peak of the chart in Figure 1.5) that, thus, can be obtained imposing derivative of efficiency as a function of temperature equal to zero;
The optimum temperature is calculated from the resolution of a particular polynomial expression (see equation 1.12), obtained by substituting equation 1.7, equation 1.8 and equation 1.10 into equation the mathematical formulation of Carnot efficiency (see note number three of this chapter):

$$\boldsymbol{4\sigma T_{abs}^5 - 3\sigma\varepsilon T_{amb} T_{abs}^4 - \left(\sigma T_{amb}^5 + \alpha C\phi T_{amb}\right) = 0} \qquad (1.12)$$

In conclusion, to answer the main question presented as title of this paragraph, solar concentration is mandatory to both convert solar energy into mechanical work of heat engine and increase operating temperatures (up to a limit obtained in equation 1.12) for maximizing the efficiency of the system.

1.3 CSP systems technical limits

The main weaknesses of a concentrating solar power system derive from optical losses phenomena during the concentration process, due to intrinsic characteristics of the radiation source.
At first, especially in cloudy days, there is a part of solar radiation, called *diffuse radiation*, which cannot be concentred by optical systems; therefore only *direct* (or *beam*) *radiation* can be used.
Secondly, because of the issue explained above, CSP systems need to follow the suns' path during the whole day to exploit as much direct radiation as possible; this means costly and quite sophisticated mechanical devices able to track the sun, to optimize the incidence angle of solar radiation.
Thirdly, the modifications in the route from Sun's surface to Earth's one must. In fact, dispersion and absorption effects on the solar photosphere modify the ideal blackbody distribution of the expected irradiance. Furthermore, the extra-

terrestrial irradiance is modified as it enters the atmosphere because of absorption and multiple dispersions (such as reflection and scattering).
That is why radiance distribution is usually considered as split into two main regions, the central solar disc and the circumsolar region. The ratio between the circumsolar irradiance and beam radiation depends on the atmospheric conditions, but its monthly average is usually lower than 5% for well sunny sites.
Fourthly, when sun's rays come on earth surface, it must be taken into consideration that they are not completely collimated, but have a 32° subtended solid angle, equivalent to an angle of 0,2664°. Therefore, even an ideal parabolic concentrator would reflect the image of the sun on a point having the same point-to-mirror solid angle. So, when designing a real solar concentrator and the aperture of a solar receiver, it is necessary to take into account the minimum size of the spot at a given distance.
There are also some optical deviations due for example to waviness errors in the curvature of mirrors (see Figure 1.6) or to temporary deformations caused by wind or, more, to possible tracking errors in the drive mechanism.

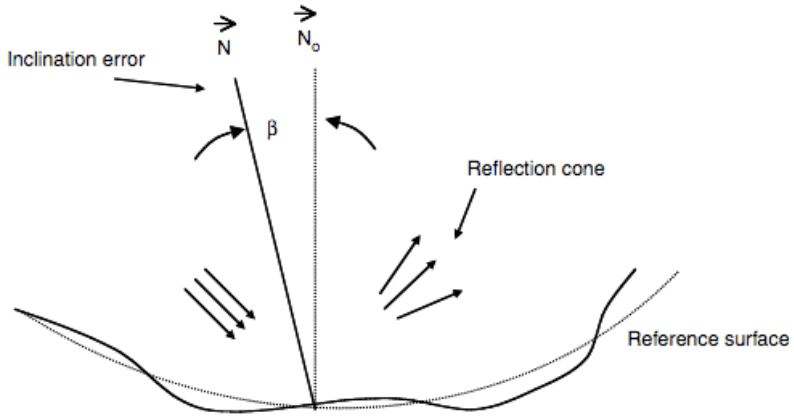

Source: F.Kreith, D. Goswami, *Handbook of energy efficiency and renewable energy, (2007)*

Figure 1.6 – Representation of the typical optical error produced by a deficient curvature of the concentrator mirror

There are thus practical physical issues decreasing the *beam quality* of a real concentrator in comparison to the unit, ideal one. The beam quality of a

concentrator can be expressed (see equation 1.13) as the total standard deviation (σ_{bq}) by means of three parameters related to each particular optical error.

$$\boldsymbol{\sigma_{bq} = \sqrt{\sigma_{sp+wav}^2 + \sigma_{curv}^2 + \sigma_{track}^2}} \quad (1.13)$$

where σ_{sp+wav} is the beam standard deviation due to radiation specularity and wavinesses, σ_{curv} is the beam standard deviation caused by imperfect curving, σ_{track} is the beam standard deviation deriving from tracking system errors.

Furthermore, a consequence of the union of all the abovementioned errors, instead of an ideal point focus parabolic concentrator (see Figure 1.7, right side) the energy profile can be approximated to a Gaussian shape on a flat-surface absorber (See Figure 1.7, left side).

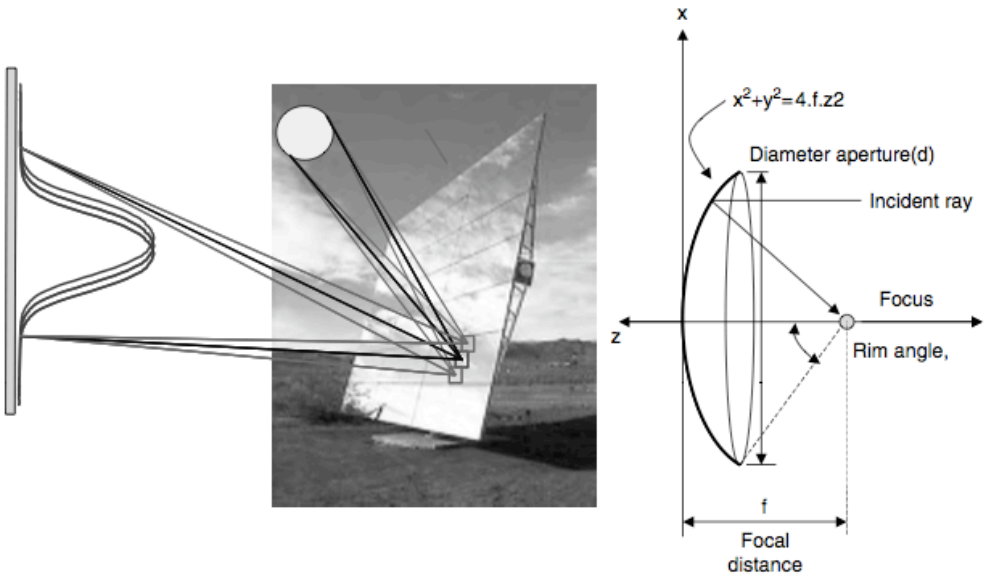

Source: F.Kreith, D. Goswami, *Handbook of energy efficiency and renewable energy, (2007)*

Figure 1.7 – Configuration of an ideal parabolic concentrator (right side) and effect of the size of the sun on the reflected image with a real heliostat (left side)

The total error of the image, also known as "degraded sun" is the convolution of all error phenomena; this is mathematically summarized in equation 1.14:

$$\boldsymbol{\sigma_{tot} = \sqrt{\sigma^2_{sunshape} + \sigma^2_{bq}}} \tag{1.14}$$

where $\sigma_{sunshape}$ is the standard deviation due to the abovementioned sunshape that causes imperfect parallelism of sun's rays.
However, the main interest of solar concentrator designers is maximizing the energy flux and not the quality of the image. An angle of 0,2664° is a good value for comparing the range of optical imperfections; in fact, those errors deflecting the reflection rays much less than 0,2664° (4,65 mrad) are of a minor importance, while higher deviations (mainly the ones that exceed 0,3438°, the equivalent of 6 mrad) drastically contribute to the reduction of concentration of solar radiation at the receiver aperture and, thus, to energy flux losses.

1.4 The solar concentration ratio

The simplest and most promising geometrical concentrator, which has become undoubtedly the most widely used in CSP systems, is the parabola. Parabolas are imaging concentrators that focus all incident rays onto a focal point located on the optical axis (see again the left part of Figure 1.7). The following correlation is valid for most solar concentrators [4]:

$$\boldsymbol{\frac{f}{d} = \frac{1}{4tan(\theta/2)}} \tag{1.15}$$

where *f* is the focal distance, *d* is the aperture diameter of the concentrator and θ is the rim angle.
An f/d ratio of 0,6, for example, is referred to a paraboloid with a rim angle of 45° and it increases as the rim angle decreases (see Figure 1.8).

[4] Equation 1.15 is deducted from the equation describing the geometry of a *parabolic dish*: $x^2+y^2 = 4fz$, where *x* and *y* are the coordinates on the aperture plane and *z* is the distance prom the plane to the vertex. A parabolic dish is a portion of a paraboloid that, in its turn, comes from a parabola axis spin.

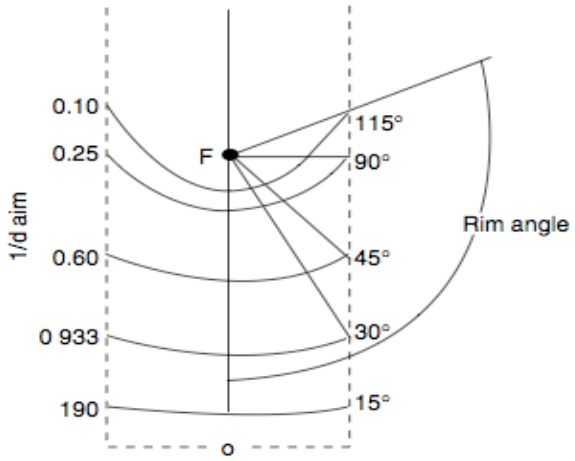

Source: F.Kreith, D. Goswami, *Handbook of energy efficiency and renewable energy, (2007)*

Figure 1.8 – Illustration of the dependance between f/d ratio vs. rim angle for a parabolic concentrator

That is why the focal point of parabolic concentrators with very small rim angles and very little curvature is far from the reflecting surface. Because of this relation CSP systems using external tubular receivers use large rim angles and short focal lengths, while the ones that use cavity receivers with smaller apertures need to use small rim angles.

Going on, there is an equation (number 1.16) that describes the minimum concentration ratio as a function of the rim angle of the parabola, for a given beam quality (σ_{bq}):

$$C_{min} = \frac{sin^2\theta \, cos^2(\theta + \sigma_{bq})}{sin^2\sigma_{bq}} \tag{1.16}$$

In terms of solar concentration, taking equation 1.16 as reference, it can be obtained that a 45° rim angle is the optimum value for any beam quality (see

Figure 1.9). Therefore an *f/d* ratio of 0,6 represents the optimal focal length-to-diameter parameter in a parabolic concentrator.

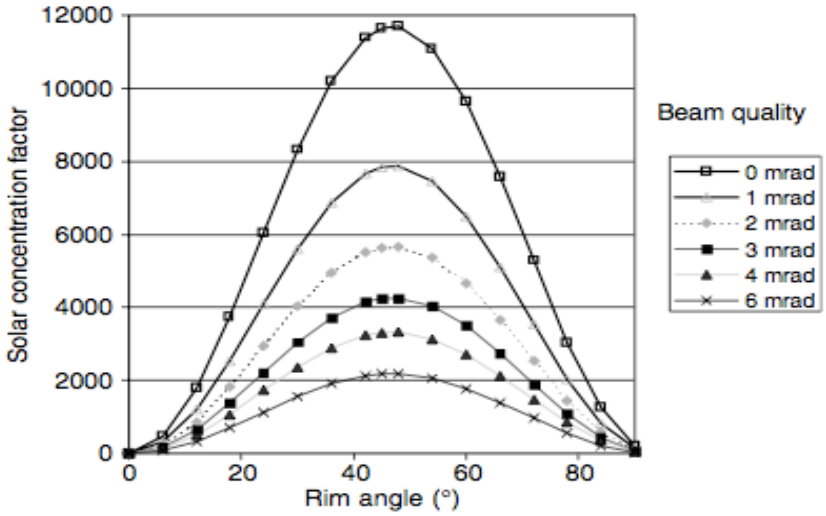

Source: F.Kreith, D. Goswami, *Handbook of energy efficiency and renewable energy, (2007)*

Figure 1.9 – Variation of minimum concentration ratio for a parabola, as a function of rim angle and beam quality

In terms of thermodynamics, the upper limit for the concentration ratio is ideally set by the size of the sun and not by the beam quality. The maximum theoretical concentration ratio for both 2D (linear concentrators) and 3D (circular concentrators) system, with refraction index n =1, has been calculated respectively in equations 1.17 and 1.18:

$$C_{MAX,2D} = \frac{1}{sin\theta_s} \leq 215 \tag{1.17}$$

$$C_{MAX,3D} = \frac{1}{sin^2\theta_s} \leq 46200 \tag{1.18}$$

where θ_s is the semi-angle subtended by the sun and equals $4{,}653\times10^{-3}$ rad.

For real concentrators, however, the maximum C is much lower than $C_{MAX,3D}$ because of the abovementioned microscopic and macroscopic physical, optical and mechanical errors.

1.5 PTCs (Parabolic Trough Collectors) performances and losses

Summarizing what said since now, the three main parameters required for designing a PTC are the concentration ratio, the acceptance angle and the rim angle. Concentration ratio, in addition to equation 1.6, can be expressed with another equation (number 1.19) basing on the geometry drawn in Figure 1.10:

$$\boldsymbol{C = \frac{l_A}{\pi \cdot d_0}} \tag{1.19}$$

where d_0 is the outer diameter of the absorber (receiver pipe) and l_A the parabola width.

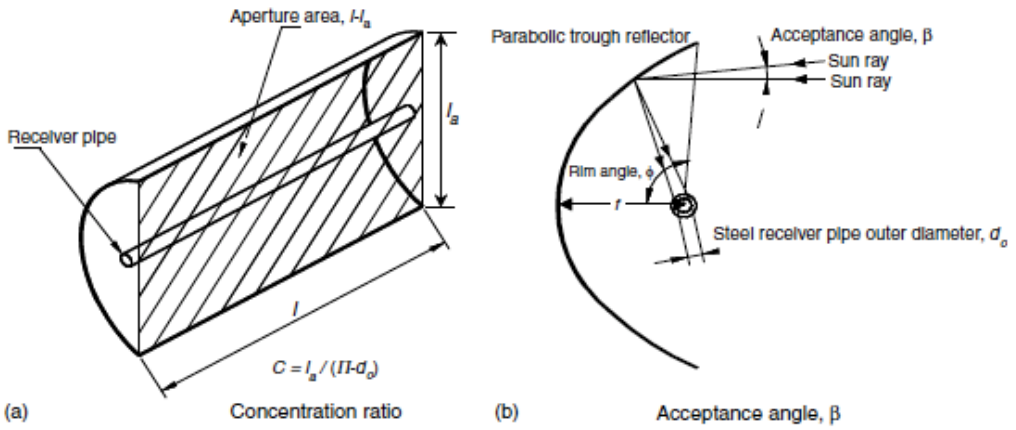

Source: F.Kreith, D. Goswami, *Handbook of energy efficiency and renewable energy, (2007)*

Figure 1.10 – Concentration ratio, acceptance and rim angles of a PTC

The wider the acceptance angle, the less accurate the tracking system has to be, because the position of the mirrors doesn't need to be updated that frequently. On the contrary, if the acceptance angle is small, the minimum variation of the relative position of the parabola in respect of the sun changes the reflection physics, increasing optical losses if the system lacks in accuracy. The most cost-effective acceptance solid angles[5] for tracking systems are the one between 1° and 2° because smaller ones would require too accurate, and thus costly, tracking systems.
Rim angles, mentioned in paragraph 1.4, have a higher value of their width, set in a 70-to-100 degrees range. Too small rim angles would reduce the aperture surface too much, while above 110° they costly but ineffective, because they increase the total reflecting surface without increasing the aperture width.

When solar radiation hits the mirrored surface of a parabolic trough collector, a significant amount of it is lost. Losses can be categorised into three main types, *optical* losses, *thermal* losses and *geometrical* losses, more accurately analysed in the next three sub-paragraphs.

1.5.1 Optical losses

This kind of losses is associated to the four main parameters ruling the physical phenomena of optics and, thus, the optical concentration process (see Figure 1.11).

[5] The solid angle is the two-dimensional angle in three-dimensional space that an object subtends at a point. It is a measure of how large that object appears to an observer looking from that point. An object's solid angle is equal to the area of the segment of unit sphere (centered at the vertex of the angle) restricted by the object.

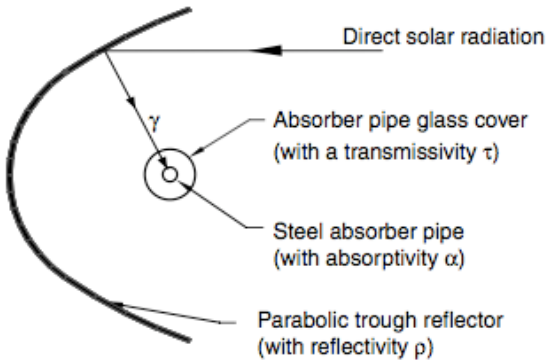

Source: F.Kreith, D. Goswami, *Handbook of energy efficiency and renewable energy, (2007)*

Figure 1.11 – Key parameters for optical losses in parabolic trough collectors

These four parameters can be resumed as:

(1) *Reflectivity* (ρ) of the collector mirrored reflecting surface. This index is expressed as the ratio between the portion of the reflected radiation and the unitary incident radiation. The typical value for this parameter in PTCs is set to 0,9. Being lower than 1, it means that there is no way to have the whole incident radiation to be reflected, as a small portion is always lost.

(2) *Intercept factor* (γ). It quantises the optical errors already represented in Figure 1.6 that deviate reflected radiation from its ideal path, so that part of the radiation doesn't hit the glass cover of the absorber or the inner receiver pipe. This parameter is thus expressed as the ratio between the radiation hitting the absorber and the total radiation reflected by the collectors and has a typical value of 0,95.

(3) *Transmissivity* (τ) of the glass tube. Part of the reflected radiation hitting the receiver is not able to pass through the glass cover that surrounds the receiver pipe. This index is calculated with the ratio between the portion of radiation that passes through the glassy cover of the receiver and the total amount of radiation that hits its outer surface. Its value is usually set aroun 0,93.

(4) *Absorptivity* (α) of the absorber selective coating. This index indicates how much the material is able to absorb radiation that hits its surface. It expression is thus the ratio between absorbed radiation and total radiation hitting its outer surface. It is usually set to 0,95

By multiplying those parameters and considering a 0° radiation incidence angle on the aperture, the *peak optical efficiency* ($\eta_{OPT,0°}$) is obtained (see equation 1.20). Its value ranges from 0,70 to 0,76 for clean and well-manufactured concentrators

$$\eta_{OPT,0°} = \rho \cdot \gamma \cdot \tau \cdot \alpha \tag{1.20}$$

1.5.2 Thermal losses

Thermal losses are due to a heat exchange from the collector towards the environment. These losses can be resumed in the radiative heat loss from the absorber pipe to the ambient and the convective and conductive heat losses from the absorber pipe to its outer glass cover (see the detailed scheme in Figure 1.12).

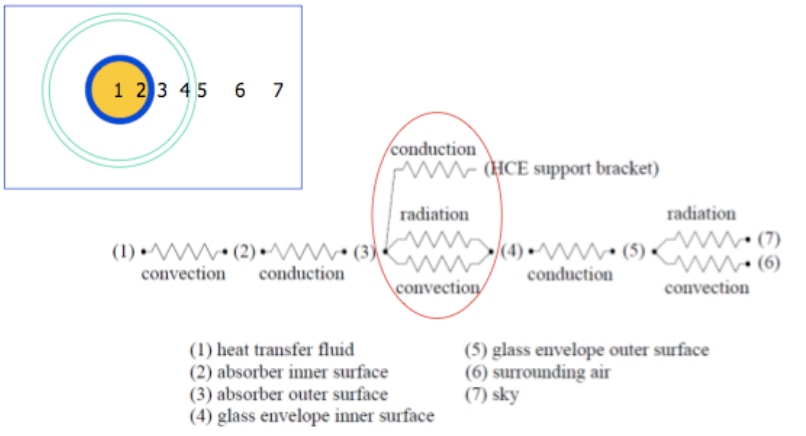

Source: L. Pistocchini, Concentrating solar power

Fig. 1.12 – heat transfer scheme for the absorbing pipeline of a CSP solar trough system

In order to have a value including all these heat transfer mechanisms, it is a good practice to include them in a thermal loss global coefficient (U_L), given in W/m^{2}K units per square meter of the steel absorber pipe surface. The thermal loss coefficient can be expressed with a second-order polynomial equation (number 1.21) with *a*, *b* and *c* coefficients experimentally calculated:

$$\boldsymbol{U_L = a + b(T_{ABS} - T_{AMB}) + c(T_{ABS} - T_{AMB})^2} \qquad (1.21)$$

Typical values of U_L are lower than 5 W/m^{2}K for absorber tubes with vacuum in the space between the inner pipe and the outer glass tube. To ensure good coating durability, high-vacuum conditions are required because of the low thermal stability in hot air of the cement coatings.

1.5.3 Geometrical losses

This third group of losses is due to a single parameter: the *incidence angle* (ϕ) of direct solar radiation on the aperture plane of the collector. The incidence angle is the one between the normal to the aperture plane of the collector and the suns' vectors (see figure 1.13), both referred to a plane perpendicular to the collector axis. The incidence angle thus depends on the day of the year and on the considered hour of the day.

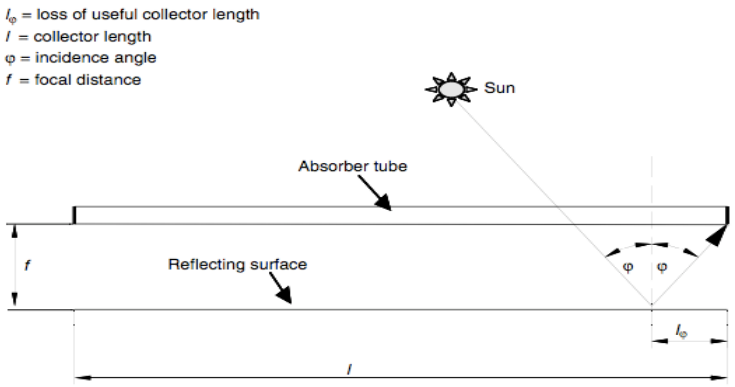

Source: F.Kreith, D. Goswami, *Handbook of energy efficiency and renewable energy, (2007)*

Figure 1.13 – Geometry of physic process due to the incidence angle

This is a very important factor because the useful portion of the direct solar radiation for a PTC is directly proportional to the cosine of ϕ angle. Furthermore, the incidence angle of direct solar radiation reduces the aperture area of a parabolic trough collector in an amount A_E, called the geometrical "end losses" of the considered collector and calculated in equations 1.22 and 1.23.

$$\boldsymbol{A_E = l_a l_f = l_a f_m tan\varphi} \tag{1.22}$$

$$\boldsymbol{f_m = f + (l_a^2/48f)} \tag{1.23}$$

where l_a is the parabola width, l is the collector length, f is the focal distance of the parabolic trough concentrator, f_m is the mean focal distance in a cross section of the parabolic trough concentrator and f is the incidence angle of the direct solar radiation.
Because of this angle, the solar radiation doesn't hit the mirrored surface perpendicularly (see figure 1.14) affecting, among others, mirror reflectivity, selective coating absorptivity, intercept factor and absorber outer glass transmissivity, because these parameters are not isotropic.

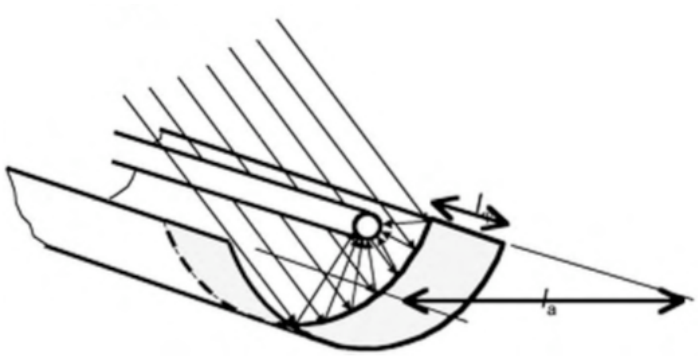

Source: F.Kreith, D. Goswami, *Handbook of energy efficiency and renewable energy, (2007)*

Figure 1.14 - 3D representation of the incidence angle effect on a PTC

For a parabolic trough concentrator, all the consequences of the incidence angle on the optical efficiency and useful aperture area is quantified with a

resuming parameter called *incidence angle modifier* (K_φ) that includes both optical and geometrical losses due to an incidence angle greater than 0°.[6]

1.6 PTC efficiencies and energy balance

The analysis done in the previous paragraph is the basis for understanding the overall performance and behaviour of a PTC, represented by its *global efficiency* (η_{global}) (see equation 1.24), thought as the ratio between the portion of energy that is effectively transferred to the fluid and the total energy that hits the collector after leaving the sun

$$\boldsymbol{\eta_{global} = \frac{\dot{Q}_{cf}}{\dot{Q}_{sc}}} \qquad (1.24)^7$$

The global efficiency of the collector is graphically represented in figure 1.15, as a function of its three main loss parameters (and thus efficiencies) analysed in sub-paragraphs 1.5.1, 1.5.2 and 1.5.3.

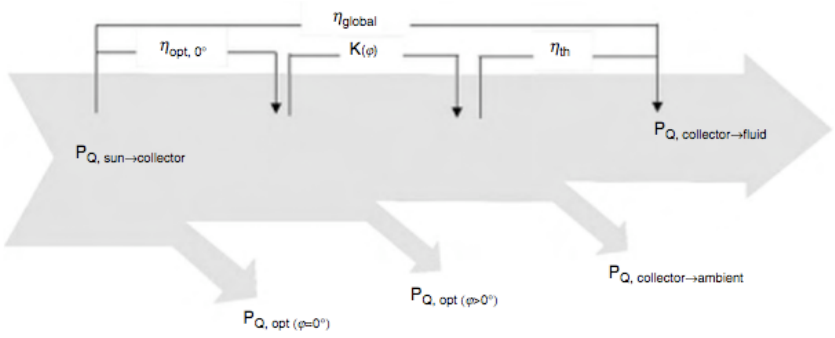

Source: F.Kreith, D. Goswami, *Handbook of energy efficiency and renewable energy, (2007)*

Figure 1.15 – Efficiencies and losses diagram in a parabolic trough collector

[6] The incidence angle modifier directly depends on the incidence angle, and is given by a polynomial equation so that it is equal to 0 for φ = 90° and to 1 for φ = 0°

[7] pedix "*c*" stand for *collector*, pedix "*f*" stand for *fluid* and pedix "*s*" stand for *sun*.

The global efficiency, in fact, is composed by the optical efficiency (calculated basing on an incidence angle of 0°), the geometrical efficiency (calculated according to an incidence angle wider than 0°), and the thermal efficiency.

The net output thermal power transferred to the fluid by a PTC could be easily calculated if the fluid mass flow and its inlet and outlet temperatures are known. However, these data are not known during the solar field design phase and thus the expected net thermal output has to be theoretically calculated starting from the environmental measures of the DNI, ambient air temperature, incidence angle and also PTC geometrical, optical and thermal parameters (see equation 1.25).

$$\dot{Q}_{cf} = \dot{Q}_{sc} \cdot \eta_{global} = A_C \cdot DNI \cdot cos(\varphi) \eta_{opt,0^\circ} K_\varphi \eta_{th} F_e \qquad (1.25)$$

where A_C is again the collector aperture surface, $\eta_{opt,0^\circ}$ is the optical efficiency, η_{th} is the thermal efficiency, while F_e ($0 < F_e < 1$) is the *soiling factor* and takes into account the progressive reduction of the nominal optical efficiency due to soiling of mirrors and glass tubes after every periodic wash. F_e is usually set to approximately 0,97.
However, from a practical point of view, it is easier to calculate thermal losses from the collector to the ambient instead of the thermal efficiency. In this case equation 1.25 turns into equation 1.26.

$$\dot{Q}_{cf} = A_C \cdot DNI \cdot cos(\varphi) \eta_{opt,0^\circ} K_\varphi F_e - U_L \pi d_0 l (T_{abs} - T_{amb}) \qquad (1.26)$$

where all the parameters have been already explained.

Keeping in mind the last expression of Q_{cf} (dotted) found in equation 1.26, both equations 1.19 and 1.24, the global efficiency of the collector (η_{glob}) can be re-written as its final and most common expression (equation 1.27):

$$\eta_{glob} = \frac{A_C \cdot DNI \cdot cos(\varphi) \eta_{opt,0^\circ} K_\varphi F_e}{\dot{Q}_{sc}} - \frac{U_L (T_{abs} - T_{amb})}{\dot{Q}_{sc} \cdot C} \qquad (1.27)$$

In conclusion, we could ideally divide equation 1.27 into two sides, the one on the left of the minus represents the positive thermal contribution for warming up the working fluid while the one on the right side of the minus is the expression of the negative thermal contribution due to the thermal losses from the collector to the environment.

Chapter 2. Matching fossil fuels with the sun: solar thermal aided power generation

Nowadays, most power is generated by consumption of fossil fuels that have serious and universally recognized negative impacts on our environment. To start inverting the course, clean and non-depleting sources must be taken into account to aid existing polluting power plants to decrease their harmful emissions. But this is just the first step to do in the target of a complete conversion.
Solar energy represents undoubtedly one of the most attractive resources in this context, even if a lot of criticisms have been addressed to it. If we consider an entirely sun-based facility the main problem is the reliability of the main power source (solar radiation) that makes it still very costly and not satisfactory in terms of productivity. Keeping in mind the definition of the ACF (*Annual Capacity Factor*), described as the ratio of the total annual hours in which a power plant generates energy with the 8760 hours in a year, solar facilities swing around 20-25% and this is a very low value if compared to the 90-92% of both coal-fired power plants and CCGTs (*Combined Cycle Gas Turbines*).
This is mostly due to the fact that at night there is no sun and thus the facility is not able to produce energy; during the day production proceeds but is strongly dependant on weather conditions. A not bright-sky day or even only the transit of a long cloud would slump the energy output on a level that is much lower than the one of the nominal design.

But what if we try to use both systems together?

Coal power plants, IGCCs and solar thermal energy systems are all mature technologies, each with their strengths and weaknesses, that can be integrated each other, coal-solar and IGCC-solar, for a *solar aided power generation* (SAPG). Most people see this opportunity as a way to pull down emissions to stay below legal limits having, as cascade effect, a big return on image. I personally hope and believe this is something more, the very first step of a growing consciousness that indicates a whole new and alternative greener course.

2.1 Solar aided power generation

The basis of SAPG technology substantially consist in using solar thermal energy to warm-up the fuel, saving part of the usual fuel consumption in the HRSG (for IGCCs) or bled-off steam in regenerative Rankine power cycles. Therefore SAPG contribution can be seen as capability of assisting fossil-fuelled power stations to increase generating capacity during the peak hours or, more intelligently, as possibility to reduce its greenhouse gas emissions. The SAPG technology is thought to be the most efficient, economic and low risk solar system to generate power as it possesses a lot of advantages:

(1) The SAPG technology has higher thermodynamic first and second law exergy efficiency over both traditional coal-fired and solar alone power stations. (See paragraph 3.1.1 for further details).
(2) Utilizing the existing infrastructure and grid of conventional power stations SAPG has low implementation costs but high social, technical, environmental and economic benefits.
(3) The SAPG technology can be applied to both new build power stations and to modify existing ones, with no risks.
(4) The thermal storage is not necessary as for the solar alone systems. The SAPG is not expected to work clock round but this is not a problem for the energy output because in low radiation periods fuel provides the thermal work for the temporarily unproductive solar system
(5) The SAPG is modular and flexible in its implementation. It can be installed in different steps according to the capital expenditure of the investors
(6) The SAPG involves traditional power industries and operators into the renewable technology with the effects of beginning its spread in conventional markets, assist them to generate greener electricity and fulfilling targets set by governments
(7) With a large adoption of SAPG technology the whole weaving factory of CSP benefits by increasing more and more its competitiveness in the energy market panorama.

We can make a first division of the SAPG technologies for existing carbon power plants repowering as well as for conventional IGCCs, with a final hybrid system dependant on the main sources considered. We can find *coal-solar thermal* plants and *ISCCs*. We will see in detail both of these solutions in paragraph 3.2.

At first, we will take as reference the result of a case study[8] on the third power unit of Loy Yang power station in Victoria State (Australia), to demonstrate both the energetic and the exergetic advantages of the SAPG systems.

2.1.1 Energetic advantages of SAPG

The considered system is shown in Figure 3.1 and is a 500MW brown-coal power generation unit with one RH (*re-heater*) and a group of six sub-units composed by five feedwater heaters plus one deareator.

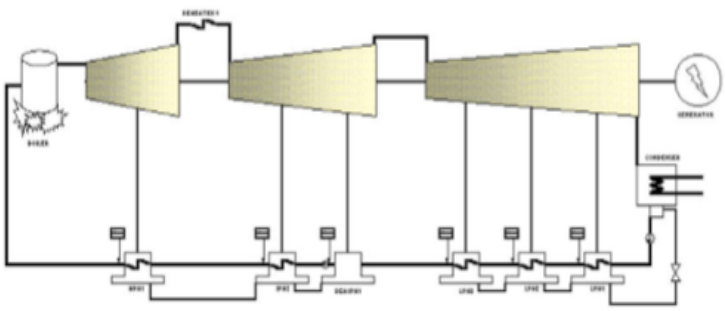

Figure 3.1 – Steam cycle structure diagram for unit 3, Loy Yang power station

For the chosen installation, the basic simulation of the unaltered unit has given a global cycle efficiency of 46,13%. At this point three possible scenarios have been examined:

(1) 100% replacement of the five closed feedwater heaters
(2) 10% replacement of the five closed feedwater heaters
(3) 100% replacement of the IPH2 (*intermediate pressure heater*), the first heater after the re-heating process

The results of the simulations are shown in Table 3.1. Before focusing on values one clarification must be made; the return on saved fuel time is different from the PBT (*Pay-back Time*) because thi last index must be built

[8] Source: E. Hu, Y. Yang, A. Nishimura, F. Yilmaz, A. Kouzani, *Solar thermal aided power generation*

taking into account feed-in tariffs and States incentives, lower O&M costs and also the imminent arrival of the "carbon tax" that should highly penalize polluting facilities. Thus, in terms of years the PBT should be significantly lower. Considering all this parameters I think that a halving on the return on saved fuel parameter can be considered as an appropriate approximation to build an estimation of the PBT index.

Table 3.1 – Results of the Loy Yang power ststion study

Type of replacement	*Case 1*	*Case 2*	*Case 3*
Cycle efficiency increase	*6,65%*	*0,64%*	*2,03%*
Additional income	*0,61 M$*	*0,61 M$*	*0,5 M$*
CO2 reduction	*3,15%*	*0,31%*	*1,02%*
Fuel saving	*2,76 M$*	*268 k$*	*0,9 M$*
Collector area	*854613 sqm*	*92640 sqm*	*219010 sqm*
Collector investment	*101,7 M$*	*11,1 M$*	*24 M$*
Return on fuel saved	*36,8 years*	*12,7 years*	*17,25 years*

Considering the same power output of the unaltered unit (500MW) to keep the same production target even for the three repowering cases, the benefit in terms of performances of this hybridization is particularly clear in Case 1, where an increase of 6,65% on the cycle overall efficiency is noted. On the other hand a very large land occupation must be noticed.

2.1.2 Exergetic advantages of SAPG

We are going to take as reference the same cycle scheme of the previous sub-paragraph (Figure 3.1).

In the conventional regenerative Rankine cycles, the feedwater is at a relatively low temperature and is heated by the steam extracted from the turbine. This nevertheless causes a big exergy loss because of a difference in in the temperature profiles of feed water and extracted steam. This exergy loss could be reduced increasing the number of extraction stages and/or feedwater heaters but it is not practical because of a higher complexity in the installation design.

This is exactly the place where the solar thermal system can aid the power generation because the solar thermal energy is hot enough to replace the extracted steam to heat the feedwater in low temperature, but also in all, regenerative stages in the Rankine cycle, according to the potentialities of the solar field. In the considered study, to enlighten the exergetic advantages a first approach theoretical analysis is conducted on a single-stage regenerative Rankine cycle (Figure 3.2) with the aim of extracting equations regulating the process.

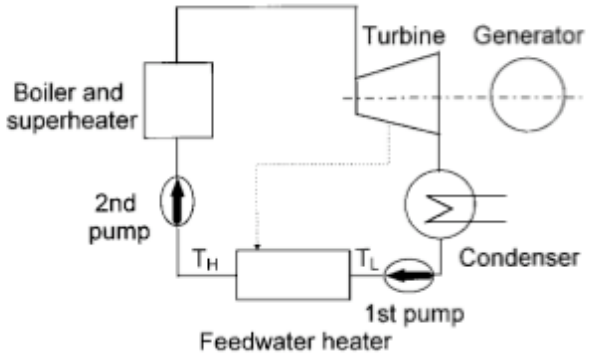

Figure 3.2 – Scheme of a generic single-stage regenerative Rankine cycle

The role of a study on exergy is to take into account not only the quantity of energy in a system but also its quality. The quality of an energy stream depends on the work potential available from the stream itself, where the capacity for the stream to do work depends on the differences with the outer environment. If a unit of heat flows from a source at a constant temperature T_H to the surrounding ambient at a temperature T_A, with a reversible heat engine, the maximum work the heat can do is called exergy of the heat at a temperature T_H. In the solar energy (or, better, solar heat) case, the exergy of the solar irradiation (EX_S) is

$$\boldsymbol{EX_S = [1 - \frac{4T_A}{3T_S}(1 - 0,28\ln f)] \cdot Q_S} \qquad (3.1)$$

where T_S is the temperature of the sun, f equals $1,3 \times 10^{-5}$ and is called "dilution factor" and Q_S is the solar heat, that in a SAPG system is the heat

used to replace the steam stream extracted from the turbine and heat feedwater. So, its value is

$$\boldsymbol{Q_s = \dot{m} \cdot \Delta h = \dot{m} \cdot C_P \cdot (T_H - T_L)} \qquad (3.2)$$

with $\dot{m}$ representing the mass flow rate of the feedwater in the feedwater heater, C_P the mean specific heat capacity of the feedwater and Δh the specific enthalpy difference of the feedwater at the extremes of the feedwater heaters.
Is now possible to obtain the net solar exergy efficiency ($\eta_{EX,S}$) of the SAPG system

$$\boldsymbol{\eta_{EX,S} = \Delta W / EX_S} \qquad (3.3)$$

where ΔW represents the extra work generated by the turbine due to the saved bled-off steam.

Whit these parameters defined, is now possible refer the results of the study done to a multi-stage regenerative system of reference (Figure 3.3) with three regenerations. The state of the working fluid at every point of the cycle have been assumed unchanged with or without solar aided feedwater heating while only the flow rate will increase in the turbine with the SAPG system. All the thermodynamic points are summarized in Table 3.2.

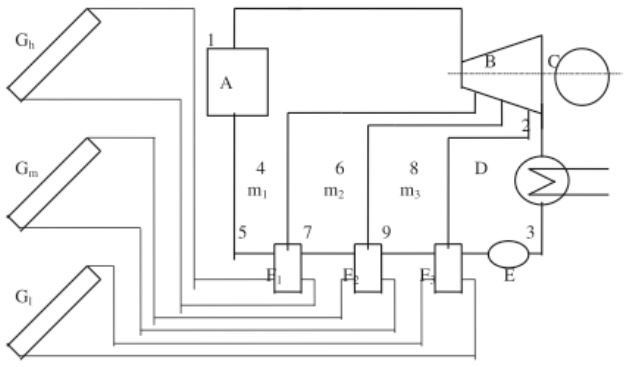

Figure 3.3 - Scheme of a generic three-stage regenerative Rankine cycle

Table 3.2 – Key thermodynamic points of the three-stage regenerative cycle

Point in Fig. 3	P (kPa, absolute)	t (°C)	h (kJ/kg)
1. Turbine inlet	16500	538	3404.78
2. Turbine exhaust	7	38.83	1993.92
3. Condensed water	7	38.83	162.7
4. High pressure extracted steam	6000	369.82	3097.15
5. High-stage heater outlet	6000	275.6	1213.4
6. Medium pressure extracted steam	1000	179.9	2701.53
7. Medium-stage heater outlet	1000	179.9	762.81
8. Low pressure extracted steam	101.3	100	2326.44
9. Low-stage heater outlet	101.3	100	419.04

Note: the weight fraction of the extracted steam $m_1 = 0.193$ $m_2 = 0.1215$, $m_3 = 0.0812$.

For this particular study the ambient temperature is set to 298 K (25 °C) and the temperature difference for heat transfer in the condenser to 10 °C.
Two main cases have been considered; the first, Case 1, is just for reference because made basing on flat plate collectors able to reach 110 °C highest temperature while the second, Case 2, is based on evacuated tube collectors able to reach a maximum temperature of 286 °C. Again, in Case 1, the extraction stage closed is just number 3 while Case 2 has all the three stages closed.
Please notice that this is just a theoretical and conceptual analysis about the exergy benefits for SAPG systems, with the aim of providing its energetic strengths; this clarification is due to the fact that the theoretical crux remains more than valid, even if the analysis conducted in the case study of this thesis (see Chapter 4) is focused on a ISCC-DSG (Integrated solar combined cycle with *Direct Steam Generation*) system with parabolic trough collectors able to reach much higher temperatures (up to about 400°C) and generate steam as working fluid.

All the results of the simulations are shown in Table 3.3.

Table 3.3 – Analysis on the two SAPG systems

	Case 1	Case 2
Phase of the heat carrier of the aided energy	Liquid	Liquid
Highest temperature of the aided energy, °C	110	286
The stage(s) closed	Stage 3 only	All stages
Extra work done by the saved steam ΔW, kJ/(kg steam generated in boiler)	27	325.9
The aided solar heat input Q_s, kJ/(kg steam generated in boiler)	175.72	1050.7
Thermal efficiency of the solar energy in the aided system η_1 ($\eta_1 = \Delta W/Q$), %	15.37	30.12
Exergy contained in the aided solar energy Ex_s, kJ/(kg steam generated in boiler), using Eq. (1):	163.1	975.4
Net solar exergy efficiency in the SAPG, %, η_{sex} in Eq. (3)	16.6	33.4
Work increased (comparing with the conventional regenerative Rankine cycle) ($\Delta W/W_0$), %	2.5	30.04

With these values, the advantages of solar aided power generation are clear, especially in terms of net solar exergy efficiency of the whole SAPG system (from 16,6 % of Case 1 to 33,4 % of Case 2) and work increase (+30,04% in Case 2). In both cases, by using solar energy to replace the extracted steam in order to heat feedwater in a regenerative Rankine cycle of a power plant, have significant improvements on both energy and exergy efficiencies. The higher the temperature of the aiding heat source is, the more performances of the system grow.

In conclusion, with the big advantages of a global efficiency growth and lower polluting greenhouse emissions and without the problem of variability in power output of traditional solar-alone facilities, the concept of the solar aided power systems can be a really significant solution.

2.2 Classification of systems for solar thermal repowering

A solar electric generating system power plant is mainly composed of two main parts, the solar field and the power block. According to the power block characteristics, its fuel used and the type of working fluid heated by the solar field, there are some possible configurations for repowering. I have summarized those configurations in three main systems: *Hybrid coal-solar thermal* systems and two different *ISCC* systems.

2.2.1 Hybrid coal-solar thermal repowering

Heat absorption process of water, which is the working fluid in coal-fired units, can be divided into three stages: preheating, evaporating and superheating processes. Those processes are made through heaters, economizers, water-cooled walls and superheaters. Considering the poor heat transfer impact of the superheating process, only preheating and evaporating is suitable to use solar heat for the selected purposes. Thus, we can now enlighten three main sub-layouts:

Preheating process system

The system (Figure 3.4) has a collector field connected in parallel with the powerhouse feedwater heaters and operates at their same inlet and outlet temperatures. In this case the collector field works as the feedwater heaters group, supplying the boiler with hot water. Since part of the feedwater is diverted to the solar field, the flow rate is varied and so, with a constant mainstream flow, heat absorption in the boiler is unchanged but the bleed-of steam from the turbine varies and, thus, its power output.

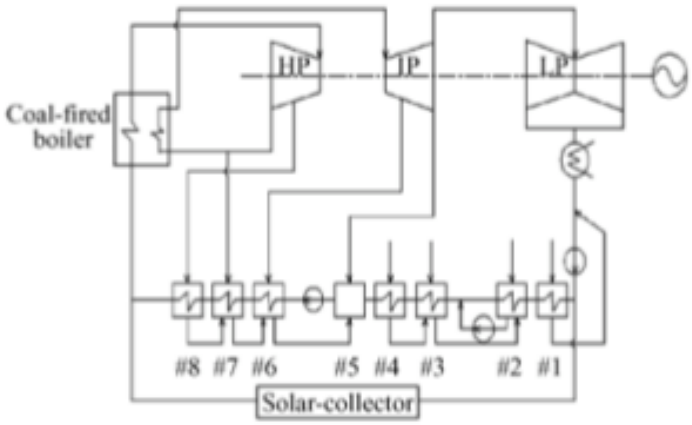

Figure 3.4 – Hybrid coal-solar thermal system with solar field working in the preheating stage

Evaporating process systems

This system (Figure 3.5) has the collector field connected in parallel with the economizer and water-water cooled wall of a conventional coal-fired boiler. The collector field receives part of the water from the discharge of feedwater heaters and generates saturated steam at the outlet. The saturated steam, mixed with the remaining part of the water that passes through economizer and water-cooled wall, flows through the boiler drum and then enters the superheater to raise the steam temperature to the steam turbine inlet temperature. The collector exit is kept at saturation temperature during variable radiation conditions by adjusting the feedwater flow rate through it. In this arrangement, steam bled from the turbine for the feedwater heaters does not vary as water flow is diverted to the collector. Thus, the steam turbine output is constant with no dependence on the flow distribution between the boiler and the collector. In this case heat absorption in the collector is affected.

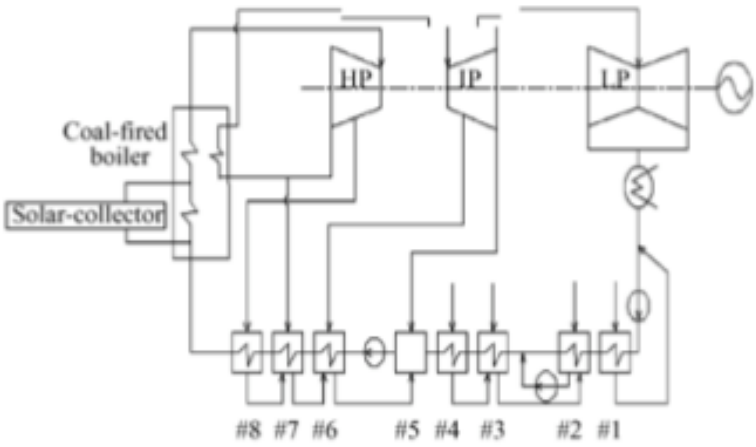

Figure 3.5 – Hybrid coal-solar thermal system with solar field working in the evaporating stage

Preheating and evaporating process systems

This system (Figure 3.6) is a combination of the two previous arrangements where the collector field is connected in parallel with every stage of heating, the economizer, the water-cooled wall and the feedwater heaters. The feedwater at the collector inlet is at the condenser temperature while the outlet one generates saturated steam that will be mixed with the steam coming from

conventional exchange surfaces then sent to the boiler drum. In this third case, both boiler heat absorption and steam turbine output varies when the feedwater is diverted to the solar field.

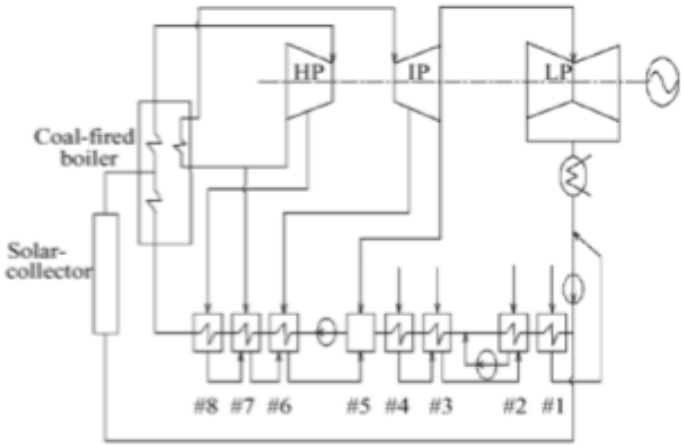

Fig 3.6 - Hybrid coal-solar thermal system with solar field working in bot preheating and evaporating stages

To see the performances and behaviour of those three configurations, the study[9] takes as reference three sizes of coal-fired power units with respectively 125MW, 200MW and 300 MW of output. The case taken as reference is the use of the SAPG system just to decrease fossil fuel consumption, keeping the electricity output of the power plant constant. Coal saved rate and solar-to-electricity efficiency are used to evaluate the thermal and economic benefits (see Figure 3.7) compared to the reference value of a conventional coal-fired installation with no solar heat input.
A clarification must be done because the results are lower than the real ones because all drawbacks of the solarisation (e.g. additional pressure drop) have been assigned to the solar system.

[9] Source: Y. Cui, Y. Yang, J. Chen, *Utilization of solar energy in a coal-fired plant*

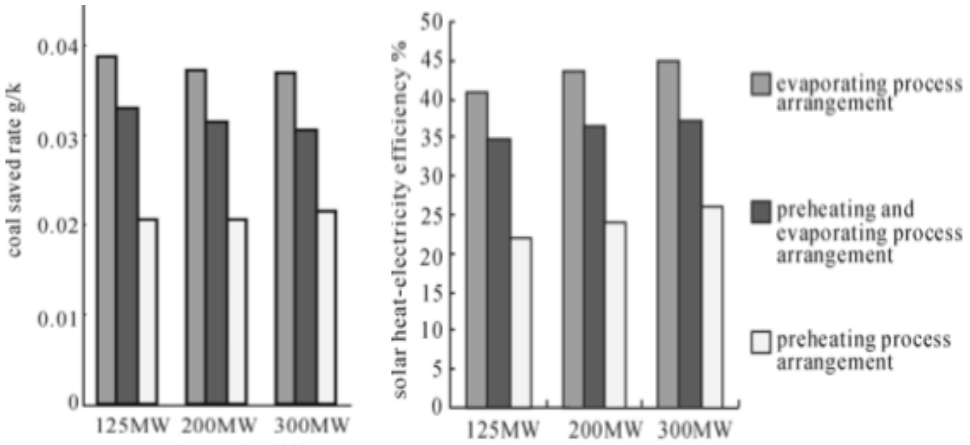

Figure 3.7 – Coal saved rate [g/kWh] and percentage solar-to-heat electricity efficiency for different integration arrangement in various capacity coal-fired units

The graphs in Figure 3.7 show that fuel saved potential is bigger in small capacity units while net incremental solar efficiency is higher in larger units, whatever coal-solar integration arrangements are used. Using the solar field to evaporate water is the best solution, while preheating water is the worst choice among the three different arrangements. But even though the preheating process has the worst efficiency, the results obtained in the study indicates that the solar heat-to-electricity efficiency is still high, at about 20% and, after considering the effect of solar field efficiency, its entire efficiency is almost equal to the yearly solar heat-to-electricity efficiency of solar-only power plants, attested approximately at 14%. Considering a 300MW coal-fired plant with parabolic trough collectors, the annual solar heat-to-electricity efficiency can attain to 27%.

2.2.2 Integrated Solar Combined Cycles (ISCCs)

This hybrid concept has a CST (*Concentrating Solar Thermal*) system employed to generate steam, than fed to the HRSG (*Heat Recovery Steam Generator*) of the power plant. Also in this case, with a required oversized steam turbine, the operation of the fossil power plant is unchanged.
The main advantages of an ISCC includes the one written in paragraph 3.1 for SAPG such as a fossil consumption decrease, low-risk and low-cost systems integration, grid connection without any new transmission infrastructure, significant CO_2 emission reduction without onerous carbon capture units.

More, one of the biggest strong points of ISCCs is the concrete possibility to avoid the installation of the energy storage system with the consequential saving for such a big voice in the capital expenditure balance.

ISCC is a relatively new concept. Recently a few parabolic trough-based ISCC installations are being developed with some installations finished and operational such as the 450MW NGCC (*Natural Gas Combined Cycle*) located in Morocco with a new 20MW trough-based CST system able to supply steam at 400 °C. A further example is a 130 MW NGCC in Algeria, again with a 20MW trough-based CST system completed in the second semester of 2010.
Currently, ISCC technology is only being applied to NGCC plants without CO_2 capture. However coal-fired power plants are also good candidates for ISCC implementation. From April 2010, there is a trough-based 4 MW demonstration plant in Colorado able to increase the power output of an existing 53-year-old coal-fired plant. However IGCCs seem to be better candidates for ISCC implementation.

As referred in a recent publication[10], ISCC are seen as a potential key benefit for green house gases emission, especially if coupled with CCS (*Carbon Capture and Storage*) systems of nowadays numerous IGCCs. In principle, a CST steam system could be incorporated to a fossil power plant with capture. The key benefit would be a greenhouse gases emissions reduction of almost 100%, with approximately 90% work made by CCS and the remaining by adding the solar field. Very high costs of this solution must be noticed.

Considering ISCC systems only, a preliminary division can be made, creating two categories related to their type of cycle and, thus, working fluid used. We can find *ISCC-HTF*, characterized by a closed solar cycle with thermal oil (such as Therminol-VP1) as working fluid or *ISCC-DSG* systems that, on the contrary, have open cycle and use almost pure water as working fluid.

ISCC-HTF

The system layout is shown in Figure 3.8. It consist in an a traditional IGCC scheme with a solar field with collectors (parabolic-shaped have been considered) that focus the sun's direct radiation on the receiver in which HTF (*Heat Transfer Fluid*) flows to be heated up to almost 400 °C. The hot

[10] Source: G. Odorica-Garcia, A. Vidal Delgado, A. Fernandez Garcia, *Novel integration options of concentrating solar thermal technology with fossil-fuelled and CO_2 capture processes*

working fluid is sent to the power block and flows trough a series of exchangers supplying the necessary heat to generate steam for the bottom Rankine cycle. By now (2011) this is the most used technology.

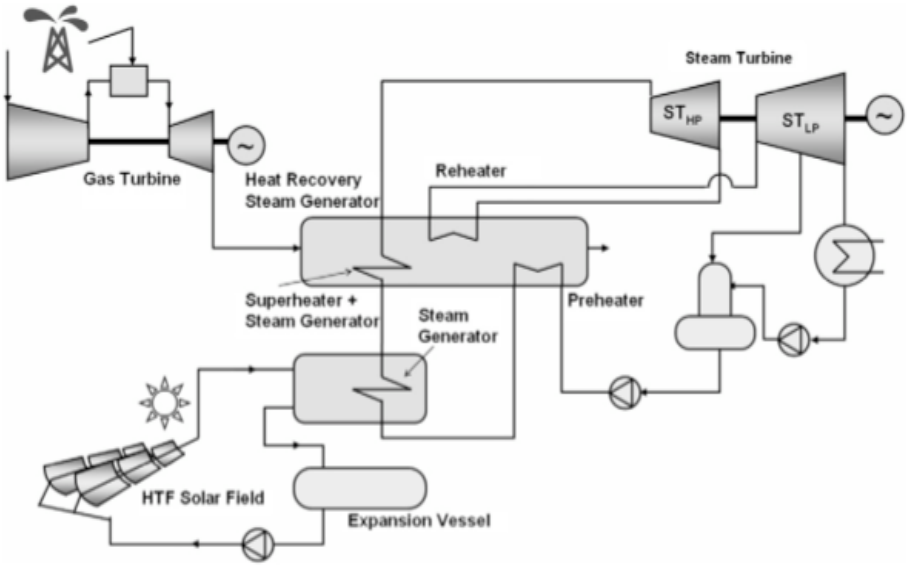

Figure 3.8 – Conventional layout of an ISCC-HTF with a parabolic trough-based solar field

ISCC-DSG

This system (figured in Figure 3.9) is similar to the one described above but uses another thermal vector as working fluid: water. DSG is the acronym of *Direct Steam Generation*; In fact, at the outlet section of the collectors flows superheated steam, generated directly in the solar field. This layout presents several advantages compared to conventional ISCC-HTF systems; for example there is no need of an intermediate heat exchanger between solar field and power cycle, resulting in a lower capital investment and in lower thermodynamic losses that increase overall efficiency. Water, even if has worse performances compared to thermal oil, is much cheaper, not toxic and not flammable, so that the risk of dangerous fire hazards, usually caused by fluid leaks, doesn't exist at all.

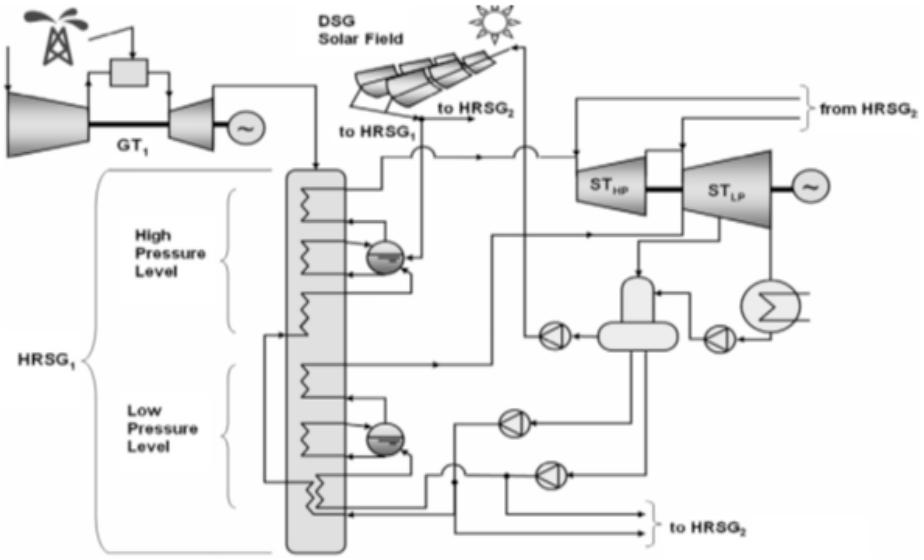

Figure 3.9 - Conventional layout of an ISCC-DSG with a parabolic trough-based solar field

This scheme refers to a 220 MW_e IGCC power plant[11]. As it can be seen there is only one bled-off steam line from the turbine and is directly linked to the deareator. Liquid water at deareator exit is pumped proportionally in the HRSG and in the solar field, according to the solar radiation real-time measurements.
The most important thing to enlighten is that the solar system is coupled to the HP (*High Pressure*) stage. In fact, high pressures are the best operational range for a DSG solar field, because pressure drop in the collector loop is reduced and overall efficiency increases. Again, in theory, if the solar thermal system operates at a high-pressure level, its energy can be used at the highest temperature level, with obvious thermodynamic benefits.
The figured facility works in the following two modes:

(1) When there is no sun, ISCC-DSG operates as a conventional IGCC power plant, avoiding problems related to start-ups and shutdowns that, on the contrary, are typical of solar-alone power plants because of a massive presence of metal in the solar field that need to be heated up.

[11] source: M.J. Montes, A. Rovira, M. Muñoz, J.M. Martìnez-Val, *Performance analysis of an Integrated Solar Combined Cycle using Direct Steam Generation in parabolic trough collectors*

(2) At solar hours the plant operates as a ISCC-DSG, fully taking advantage of its potentialities. The plant consists of two main parts, a gas turbine working for the "top" Brayton gas-fired cycle and a gas turbine for the "bottom" Rankine steam cycle, both aided by the solar field. Compared to a traditional combined cycle ISCCs have the further advantage of not experiencing production drops in hot days but, vice versa, more energy production from the solar field.

2.2.3 Performances of ISCCs compared to solar thermal-alone power plants

Considering an averagely very sunny place with its both seasonal and daily variation of radiation intensity, the energy production is attested at approximately 3000-3200 hours of energy without the thermal storage system. And that's the maximum a solar-alone system can achieve while it is not if we consider IGCCs. In the technical assessment the main parameter considered is, again, its net heat-to-electricity efficiency. This parameter (Formula 3.4) is the gross electrical energy produced by solar thermal power plants minus internal energy consumption, all divided by heat added to the cycle of the power plant:

$$\eta_{StE} = \frac{\dot{P}_{EL,Sol} - \dot{P}_{AUX}}{\dot{Q}_{TOT,Sol}} \qquad (3.4)$$

In the reference study[12] three different system layouts have been compared; one ISCC-DSG, one ISCC-HTF and a classic SEGS (*Solar-alone Electric Generating System*), all located in Isfahan, Iran.

Monthly average direct normal solar irradiation and relative sunny hours in every month of the year are shown in Table 3.4.

[12] Source: H. Nezammahalleh, F. Farhadi, M. Tanhaemami, *Conceptual design and techno-economic assessment of integrated solar combined cycle system with DSG technology*

Table 3.4 – Solar data of Isfahan (Samimi, 1994)

The months of year (in Iranian calendar)	Monthly average of direct normal irradiation (W/m^2) in sunny hours	Number of sunny hours
The first month of spring (1)	836.5	7.28
The second month of spring (2)	833.3	8.58
The third month of spring (3)	825.8	10.85
The first month of summer (4)	822.3	11.37
The second month of summer (5)	819.8	11.10
The third month of summer (6)	826.5	10.55
The first month of autumn (7)	818.0	9.34
The second month of autumn (8)	794.7	7.6
The third month of autumn (9)	767.0	6.48
The first month of winter (10)	770.2	6.18
The second month of winter (11)	798.5	6.6
The third month of winter (12)	824.9	7.14

First month of the Iranian calendar corresponds to 21 March to 21 April; the seventh month, as its name implies, corresponds to 21 September to 21 October. The same for October (8th month), November (9th month), and December (10th month).

In relation to DNI, the production of energy of the solar thermal demonstrate what said once more what said at the end of sub-paragraph 3.2.2 that is the fact that, on the contrary of traditional IGCC where warm climates cause a performance drop, solar thermal system have a significant rise of it (see Figure 3.10).

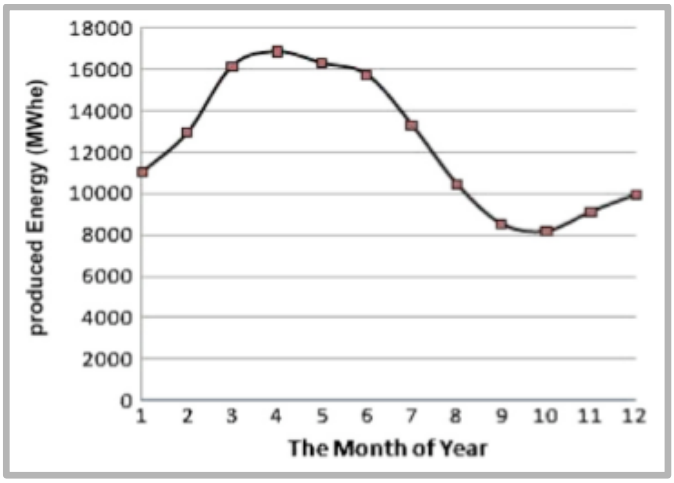

Figure 3.10 – Energy production of the sola field, based on enthalpy changes in the solar component of ISCC-DSG related to the Iranian calendar (see footnote on Table 3.4)

Finally two main evaluations are treated. The first is the one concerning η_{StE} that has been put in a graph (see Figure 3.11) basing on theoretical maximum *capacity factor*[13]

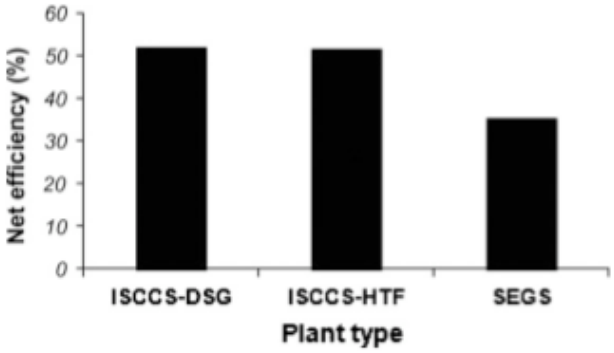

Figure 3.11 – Heat-to-electricity net efficiency of different cases at maximum capacity

While the second and last one (Figure 3.12) put in a graph a key issue of our present, the emission of CO_2. Among all greenhouse gases (CO_2, H_2O, CH_4, N_2O, O_3), in fact, CO_2 is the most harmful one with more than 30% emission originated from fossil fuels combustion. The analysis is once more done basing on theoretical maximum *capacity factor.*

[13] *Capacity factor* is the index that measures the reliability of an energy source. In fact, it takes into account only the effective period of energy production of a power plant and is described as the ratio between effective period of production and the maximum achievable in theory, the whole year with its 8760 hours.

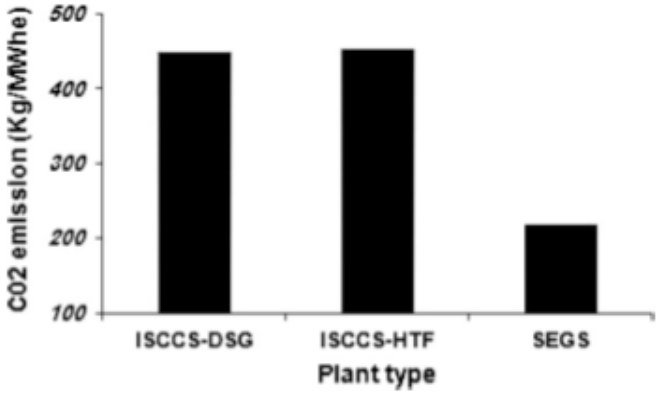

Figure 3.12 – CO_2 emissions of the three plant layouts at their maximum capacity factor

As conclusion, in both last two Figures (3.11 and 3.12) the better performances of ISCC-DSG compared to ISCC-HTF are clear. In particular the ISCC-DSG will produce 2,5% lower carbon emission than ISCC-HTF. In a 30-year period the ISCC-DSG will avoid about 365 million kilograms of CO_2 in atmosphere.
The graphical differences may seem quite meagre. That's true but a further reasoning must be done, thinking about DSG lower installation cost, lower O&M, no toxicity and no problems of flammability. Thus, ISCC-DSG systems would surely represent a very interesting alternative to ISCC-HTF and that is why in the analysis made in Chapter 4, on solar thermal repowering of Munmorah power station in New South Wales (Australia), we have taken ISCC-DSG as reference layout for the new system.

Chapter 3. Solar technologies economics and Australian policy context

In this chapter we will discuss on the economical and political frame of solar technologies, in order to give a wider context, able to stay more in touch with real mechanisms and issues. We will start from explaining the LCOE (*Levilized Cost Of Electricity*) index, one of the most important parameters for financial decision-making in the energy field. Subsequently, we will see how the LCOE is obtained and what it is used for. For each obtained LCOE global value we will work to fragment it into its main cost listings to build a cost structure, with the aim of seeing the possibilities for a cost reduction.
After that we will have a global outlook on both short-term and long-term decision-making strategies, indexes and parameters, in order to be introduced to the Australian political context. This last step has been built showing governmental actions to incentivise the development of CSP.

3.1 The LCOE index

Referring to the electricity market price, it is very useful to analyse the *Levelized Cost Of Electricity* (LCOE), a parameter able to give a very intuitive comparison between the overall costs of each technology. A particular LCOE model (the Long Running Marginal Cost, LRMC) is used in the first part of the analysis in order to give a specific value, expressed in $/MWh, for each energy source.

3.1.1 How is the LCOE calculated?

Among all the costs, the initial capital expenditure to build a new power station is always the biggest one. In this analysis it is called the *Overnight capital cost* (*I*) and comprises:

- The *main power island*: defined as the core components of a generation plant (i.e. turbine, generator, boiler)
- The *balance of plant*: comprises auxiliary equipment (i.e. fuel processing, cooling systems, etc.)

- Site acquisition, planning and permitting costs
- Pre-development and development costs
- Electricity grid connection, gas pipeline or fuel connection costs
- Aggregate commissioning costs (i.e. fuel consumption, if applicable)
- Project management and contingencies

Thus, the overnight capital cost can be written as:

$$\boldsymbol{I = gc_j \cdot 1000 \cdot icap_j} \tag{2.1}$$

where gc_j [$/kW] is the greenfield overnight capital cost for the considered energy source j and $icap_j$ [MW] is the installed capacity of the mentioned plant.

This index needs to be adapted to the presence of plant economies of scale both in terms of number of generating units and of unit sizes, because the design of a plant often involves more than just one power-generating unit, changing the associated capital cost value.
Taking this into account, the overnight capital cost (I) can be upgraded to an annual index referred to plant j and unit i, and needs to be actualized for each year with the inflation based escalation rate:

$$\boldsymbol{I_j = \frac{O_{ij}(t) \cdot I}{(1+r)^j}} \tag{2.2}$$

where $O_{ij}(t)$ [%] is the total allocation expenditure associated, yearly, to the power plant j and given to unit i, r [%] is the cost of capital, t is the variable referring to each particular year considered at the moment of the calculation. I has been explained in equation 2.1

Another crucial cost listing is fuel. According to the technology, fuel costs can be very significant in the overall economic balance, especially, for example, for both gas-powered and oil-powered plants and, in general, for conventional fossil fuelled systems. Fuel incidence is highly dependant on three main factors: the constant *heat rate* of each generator, calculated as the ratio

between the amount of heat generated for each energy unit converted, the *unity cost* of raw fuel and the *annual capacity factor*, calculated as the ratio between the yearly maximum theoretical operational time (8760 hours) and the one able to convert and produce the usable energy output.
Thus, in order to calculate fuel cost incidence, the following equation has been used:

$$\boldsymbol{FC_j} = \frac{\frac{\boldsymbol{HR_j \cdot UFC_j}}{\boldsymbol{1000}} \cdot \boldsymbol{ACF_j} \cdot \boldsymbol{icap_j} \cdot \boldsymbol{8760}}{(\boldsymbol{1+r})^{\boldsymbol{j}}} \tag{2.3}$$

where HR_j [kJ/kWh] is the heat rate of the considered power source, UFC_j [$/GJ] is the unitary cost of the fuel used in the considered power station, ACF_j [%] is the annual capacity factor of the considered system. $icap_j$, r and t have already been explained in previous equations [2.1] and [2.2].

There are two more costs that need to be faced during operation period of the built plant: the ones for fixed operation and maintenance *(FOM)* and the ones for variable operation and maintenance *(VOM)*. For almost every plant, fixed costs dominate the mix of operation and maintenance costs (i.e. about 57% for CCGT systems, about 86% for coa-fired facilities and even much more for renewable power generation systems such as wind farms or any solar power system).

Each kind of O&M cost stream can be calculated with:

$$\boldsymbol{FOM} = \frac{\boldsymbol{icap_j \cdot FOM_j}}{(\boldsymbol{1+r})^{\boldsymbol{j}}} \tag{2.4}$$

$$\boldsymbol{VOM} = \frac{\boldsymbol{icap_j \cdot ACF_j \cdot 8760 \cdot VOM_j}}{(\boldsymbol{1+r})^{\boldsymbol{j}}} \tag{2.5}$$

$$\boldsymbol{O\&M = FOM + VOM} \tag{2.6}$$

where thus FOM_j [$/year] is the annual expenditure for fixed operation and maintenance, while VOM_j [$/year] is the annual expenditure for variable O&M.

The abovementioned values are the main cost listing of the cash flow. Furthermore, before finishing the economic analysis to obtain the *Levelized Cost of Electricity* (LCOE) index, some additional financial and quantitative indexes need to be calculated; these are the *Present Worth* (PW), the *Equivalent Annual Worth* (EAW) and the total amount of energy generated in the lifetime of the considered power system, called *NES*. Respectively:

$$\boldsymbol{PW(I) = \sum_{j=0}^{n} I_j} \tag{2.7}$$

$$\boldsymbol{EAW(I) = PW(I) \cdot crf} \tag{2.8}$$

$$\boldsymbol{NES = icap_j \cdot 1000 \cdot ACF\_j \cdot 8760 \cdot lifetime_j} \tag{2.9}$$

where *crf* [%] stands for *capital recovery factor*, the percentage of the initial cost that must be paid yearly for the whole duration of the loan, and $lifetime_j$ is obviously the lifetime of the considered power source.

It is now possible, using all the formulae calculated above, obtain the final value of the LCOE [$/MWh] by using:

$$\boldsymbol{LCOE = \frac{EAW(I) + \sum_{j=o}^{n} FC_j + O\&M}{NES} \cdot 1000} \tag{2.10}$$

To build up the whole analysis with the aim of obtaining the final LCOE index, some assumptions have been taken as reference, from a partial actualization (mostly focused on CSP overnight capital costs) of a publication by P.Simshauser[14]. All hypotheses have been resumed in table 3.1:

[14] Source: P.Simshauser, *The hidden costs of wind generation in a thermal power system: what cost?* (2010). AGL applied economics and policy research.

Table 3.1 - Key assumption for producing LCOE estimates

Plant Type	*Installed Capacity [MW]*	*Greenfield overnight capital cost [$/KW]*	*N° Units [MW]*	*Unit Heat Rate [kJ/kWh]*	*Unit fuel cost [$/GJ]*	*Capacity Factor (%)*	*Fixed O&M [$/MW/a]*	*Variable O&M [$/MWh]*	*Capital Works [%]*	*Aux Load [%]*
Black Coal	*1000*	*2200*	*2*	*9000*	*1*	*92*	*48000*	*1*	*0,25*	*7*
Brown Coal	*1000*	*2600*	*2*	*11250*	*0,4*	*92*	*55000*	*1,3*	*0,25*	*8*
CCGT	*380*	*1368*	*1*	*7000*	*4*	*92*	*31000*	*3*	*0,05*	*2*
OCGT	*600*	*985*	*4*	*11500*	*4,5*	*92*	*13000*	*8*	*0,05*	*0,5*
Nuclear	*1400*	*5100*	*2*	*10500*	*0,5*	*92*	*84000*	*5*	*0,05*	*7*
Wind	*100*	*2900*	*50*	*0*	*0*	*35*	*40000*	*1*	*0,05*	*2*
Biomass	*50*	*3000*	*1*	*10500*	*1,5*	*50*	*120000*	*2*	*0,05*	*7*
CSP	*10*	*3300*	*1*	*0*	*0*	*23*	*55000*	*0*	*0,05*	*0,5*
Hybrid CSP	*10*	*1815*	*1*	*0*	*0*	*23*	*55000*	*0*	*0,05*	*0,5*

The result of the simulation gives a lot of food for thought and a quite clear reference frame. As can be seen on Figure 3.1, basing on the assumptions made above, the base load thermal technologies range from black coal 42,5 $/MWh to a peak cost of 59 $/MWh for OCGT. The LCOE of nuclear technology is set to 86,3 $/MWh. The remaining technologies in the chart are all renewables and have a cost ranging from the 119,43 of biomass to the 234,7 $/MWh for CSP technology. In the middle of this interval we can find wind technologies, with a cost of 119,4 $/MWh. What clearly emerges is the big gap between almost every technology and large solar thermal, that remain very expensive at the moment, and because of this, are not yet attractive on the NEM.

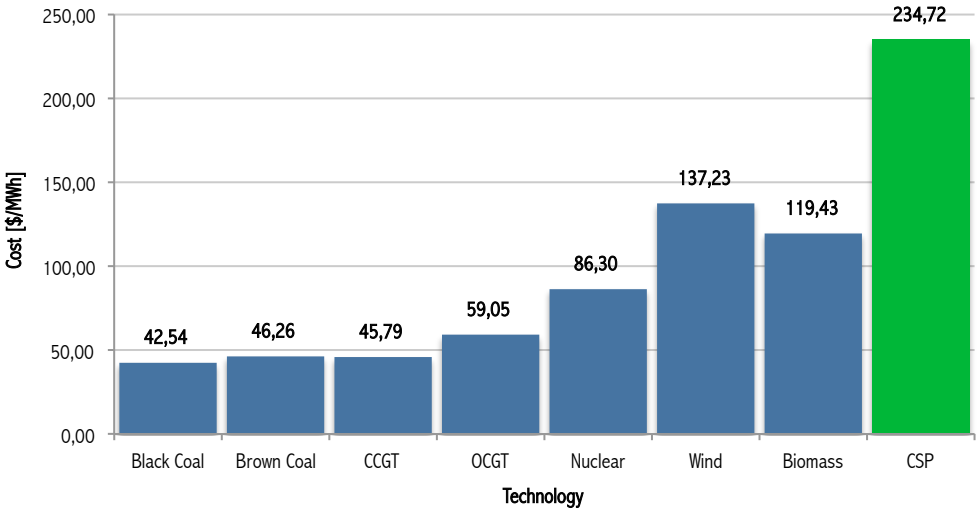

Figure 3.1 – Results of LCOE calculation

But *how could we pull down costs of solar thermal technologies to increase their competitiveness in the energy market?*

This thesis will analyse one of these opportunity for CSP systems: their integration of with traditional fossil-fuelled facilities, trying to create and exploit new synergies able to reduce capital expenditures. For example, with a hybrid-solar system there is no need to have a thermal storage because of the presence of the HRSG, able to generate power when there is no Sun. Again, hybrid-repowering options could cut land costs, could decrease expenditures for the power block. More, considering an installation with DSG (*direct steam generation*), there is no need for any thermal exchange, and thus no secondary HTF (*Heat Thermal Fluid*) system.
All these option will be further discussed and analysed in the next paragraphs and chapters, ending with the case study presented in chapter 4, where a hybrid DSG solar repowering has been deeply analysed.

3.2 Solar technologies cost structure

The LCOE index gives a first outlook on the situation of solar technologies in the NEM context and their big gap with other energy sources. The analysis needs now to be addressed on how to reduce this gap that separates solar

technologies from all other cheaper ways to produce electricity, both conventional and unconventional.
The first thing to do is to analyse the cost structure of each technology, focusing then on large solar thermal one. From the database used to construct the LCOE graph, it is possible to divide costs into four main categories (fixed O&M costs, variable O&M costs, fuel costs, EAW investment costs) and stack them to re-built a new LCOE stacked columns chart, which takes into account how costs are divided and their weight in the total balance. The result of the calculation is shown in Figure 3.2.

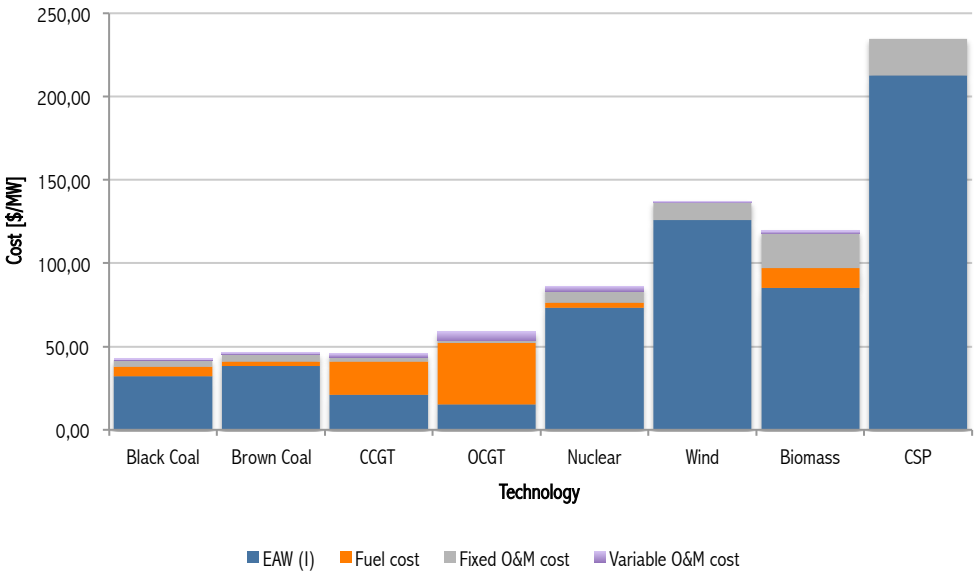

Figure 3.2 – Cost structure of the LCOE indexes obtained in paragraph 4.1

As can be seen on the graph, coal-fired power plants have a high initial expenditure and a small cost due to fuel and variable O&M. On the contrary gas-fired plants (OCGT and CCGT) have a smaller initial investment but a high operational cost, especially OCGT systems, due mostly to the high specific price of raw fuel. All other technologies (both nuclear and renewables) have a huge discrepancy between investment cost and all others with an unequivocal prevalence of the first ones.

All renewable sources, with the exception of biomass and HFR geothermal, have no costs for fuel for the nature of the source itself but just a very high initial capital investment, especially for solar technologies.

3.2.1 Detailed cost structure analysis for solar technologies with Solar Advisor Model

As seen above, the main cost for solar technologies is undoubtedly the initial expenditure for the solar field, with approximately 93% of the total costs for concentrating mirrors and other equipment in the CSP case. All other costs are referred only to fixed O&M since there are almost no expenses for variable O&M.
Analysing how this 93% is subdivided can make us understand a lot about how money are spent to build a solar power system, thus evaluating all the opportunities to cut part of these costs to make solar technology more appetizing and competitive.
This analysis has been made using *Solar Advisor Model (SAM)*, dedicated free software from the National Renewable Energy Laboratory of the United States (NREL) with an algorithm able to simulate the operation of different solar power generation option, such as CSP systems.

The simulation has been run considering a reference CSP solar trough system with a 100 MW nominal output range and with the following additional parameters

CSP solar trough system:

- *Collector*: Solargenix SGX-1
- *Receiver*: Schott PTR70 2008
- *Total land area occupied*: 865352 m^2
- *Power cycle*: 100MW with 0,3774 rated cycle conversion efficiency
- *Thermal storage*: full load 6 hours of TES, 1764,7 MWt thermal capacity, 26268,7 m^3 storage volume
- *Analysis period*: 30 years
- *Analysis type*: after-tax
- *Inflation rate*: 2,5%
- *Real discount rate*: 8%

The results of the simulation for this kind of system are resumed in the SAM screenshot shown in Figure 3.3:

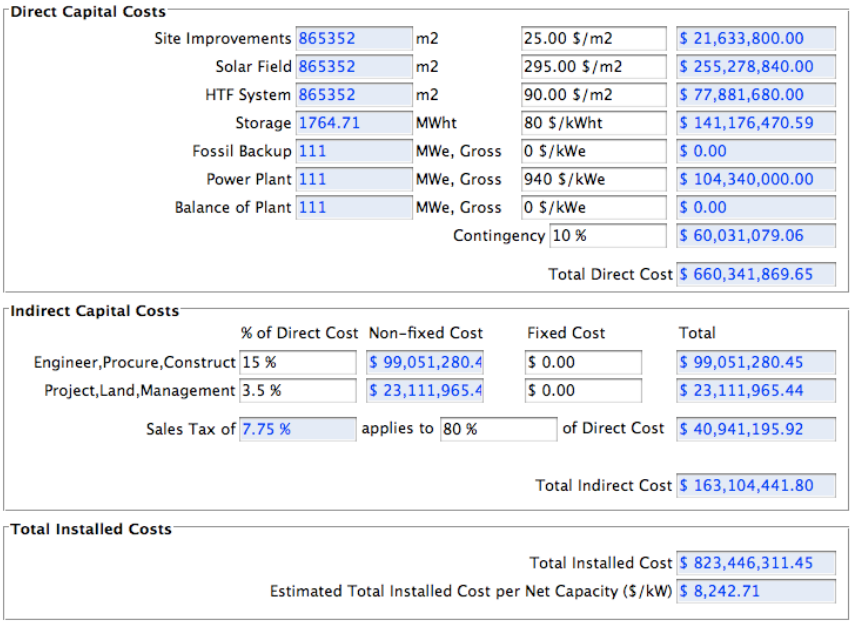

Direct Capital Costs

Site Improvements	865352	m2	25.00 $/m2	$ 21,633,800.00
Solar Field	865352	m2	295.00 $/m2	$ 255,278,840.00
HTF System	865352	m2	90.00 $/m2	$ 77,881,680.00
Storage	1764.71	MWht	80 $/kWht	$ 141,176,470.59
Fossil Backup	111	MWe, Gross	0 $/kWe	$ 0.00
Power Plant	111	MWe, Gross	940 $/kWe	$ 104,340,000.00
Balance of Plant	111	MWe, Gross	0 $/kWe	$ 0.00
			Contingency 10 %	$ 60,031,079.06
			Total Direct Cost	$ 660,341,869.65

Indirect Capital Costs

	% of Direct Cost	Non-fixed Cost	Fixed Cost	Total
Engineer,Procure,Construct	15 %	$ 99,051,280.4	$ 0.00	$ 99,051,280.45
Project,Land,Management	3.5 %	$ 23,111,965.4	$ 0.00	$ 23,111,965.44

Sales Tax of 7.75 % applies to 80 % of Direct Cost $ 40,941,195.92

Total Indirect Cost $ 163,104,441.80

Total Installed Costs

Total Installed Cost $ 823,446,311.45

Estimated Total Installed Cost per Net Capacity ($/kW) $ 8,242.71

Figure 3.3 – Structure of initial capital costs for a 100MW CSP solar trough system, computed with Solar Advisor Model

Those values can be put in an additional pie chart (Figure 3.4) to have an immediate visual feedback of how capital costs are structured and divided:

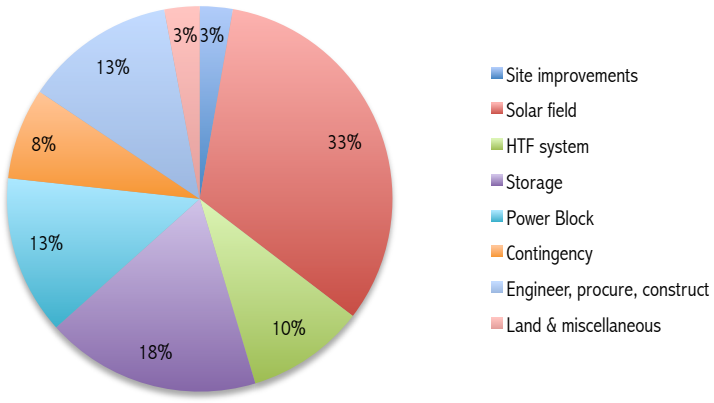

Figure 3.4 - Capital costs structure for a 100MW CSP solar trough system

From the chart clearly emerges the huge weight of the solar field in the overall capital expenditure balance. This is a cost that cannot be avoided and that can be reduced only with research and development, finding cheaper solutions and exploiting large-scale production advantages. But in a cost reduction point of view the cost listing of thermal storage (18% of the total capital expenditure) and HTF system (10%) are quite relevant, giving good possibilities for this aim. Power block slice is quite wide too (13%) and thus represents a further opportunity for a cost reduction, even if only partial because money has to be spent anyway in this sector. Finally there is a further possible contribution from land and miscellaneous costs, which is nevertheless very small (only about 3%).

In a realistic point of view, considering a very short-term period of time with no significant improvements from R&D, the cost reduction for an hybrid repowering system, compared to the layout simulated in SAM software, could be greater than 40% of the overall capital expenditure (see the case study analysis in chapter 4). This conclusion has been supposed by eliminating both the thermal storage and HTF systems slices, by reducing the power block intervention costs to 3% (instead of 13%), and by eliminating costs for land and miscellaneous. This means that the LCOE index for CSP technologies calculated in the first part of this chapter can decrease from 234,7 $/MWh to approximately 139 $/MWh, becoming much more attractive in the energy market context (see Figure 3.5).

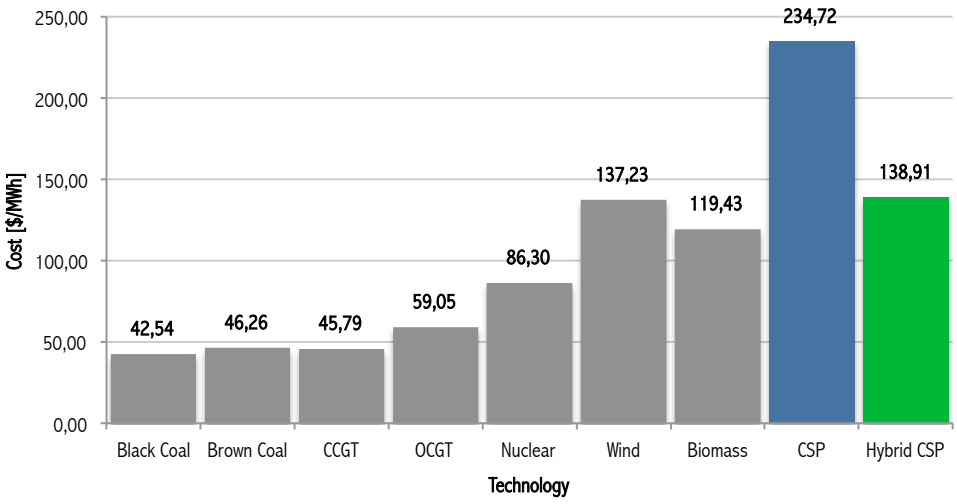

Figure 3.5 - Potential reduction on levelized cost of electricity index for hybrid CSP systems

3.3 Short-term utility planning

Short-term utility planning is used for setting up the day-ahead energy dispatching. It needs to be studied carefully on both sides of demand and supply with continuous daily forecast, for giving to consumers and distributors the best options in the energy stock market.

In the "demand side", planning is made basing on five main steps:

(1) Day-ahead electricity demand forecasting
(2) Day-ahead supply forecast
(3) Day-ahead ancillary services forecasting
(4) Setting the day-ahead dispatch schedule
(5) Day-ahead scheduling of utility-owned generation

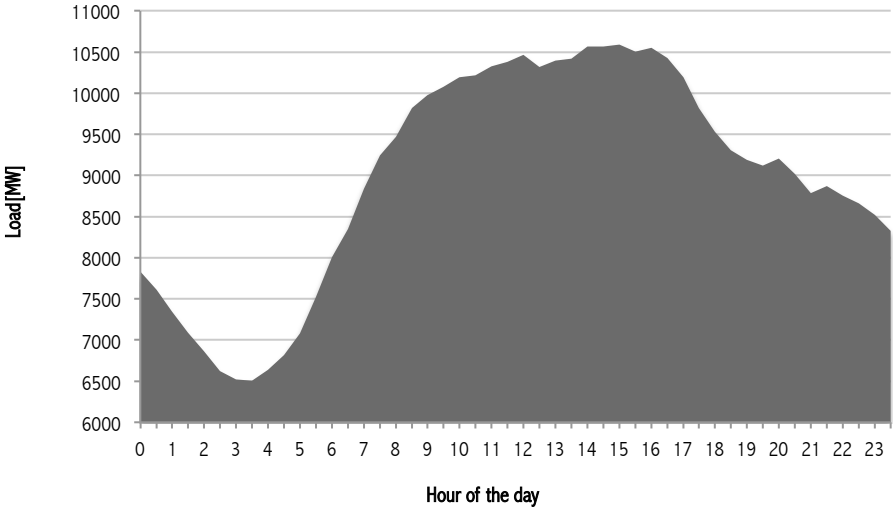

Figure 3.6 - Demand curve based on load data for NSW, for the 15th of January 2010

According to these parameters, a curve with the trend of demand is created. In Figure 3.6, the demand curve for NSW on the 15th of January 2010 is shown; the trend enlighten a very low consumption during nights with a constant growth, from about 4:30 a.m. in the morning till the peak at around 4:30 p.m. where the descent begins.

The other and last main block of short-term utility planning is the "supply side". Here, all sellers need to be analysed and classified according to a merit order, determined with a supply stack based on five parameters:

(1) *Capacity*: minimum and maximum operating capacity
(2) *Performance*: nominal efficiency rate and heat rate, heat rate curve, ramp-up and ramp-down heat rates and incremental heat rate
(3) *Grid-integration*: based on start-up time, minimum uptime, maximum downtime, ramp-up sequence and fuel start-up requirements
(4) *Costs*: variable operation & maintenance, start-up costs
(5) *Availability*: forced outage rate

Basing on these parameters, the supply merit order list is created and plotted in a scale graph (see Figure 3.7) as a function of total variable expenses (y-axis) and output of dispatched units [MW] (x-axis).

Unit	Fuel	Capacity MW	Efficiency	Heat rate GJ/MWh	Variable Expenses: Fuel $/GJ	Variable Expenses: O&M Var. $/MWh	Variable Expenses: Total $/MWh	Dispatch position
Aquarius	Hydro	320	n/a	n/a	n/a	2.25	2.25	base-load
Neptune	Nuclear	1200	35.6%	10.1	1.50	6.00	21.15	base-load
Venus I	Coal	900	36.0%	10.0	2.80	4.50	32.50	base-load
Venus II	Coal	800	35.0%	10.3	2.80	4.50	33.34	base-load
Orion	Gas	550	52.2%	6.9	7.45	4.00	55.41	int.-load
Pegasus	Gas	500	51.4%	7.0	7.60	4.00	57.20	int.-load
Mercury	Gas	250	34.3%	10.5	7.45	4.15	82.38	peak-load
Mars	Gas	250	33.6%	10.7	7.45	4.15	83.87	peak-load
Pluto	Gas	150	31.9%	11.3	7.45	4.15	88.34	peak-load
Haley	Gas	150	28.8%	12.5	7.45	5	98.13	peak-load

SOURCE: (Mazer 2007)

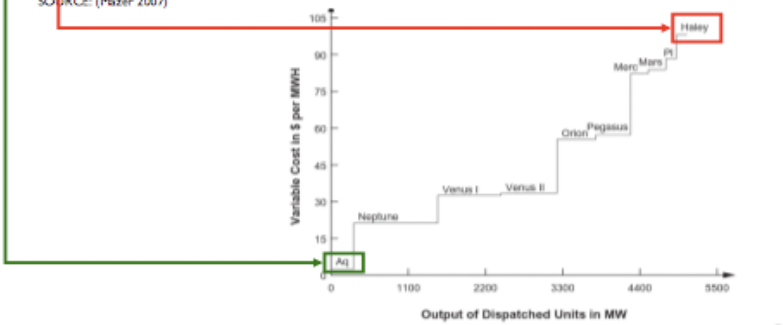

Source: *A. Pigneri, Economic Analysis for energy investment decision-making (2009)*

Figure 3.7 - supply merit order list and relative graph as a function of costs (y-axis) and power output (x-axis)

With the analysis on both demand side and supply side done, the obtained results need to be compared (see Figure 3.8) in order to determine which supplier has to sell electricity at that very instant of the day;

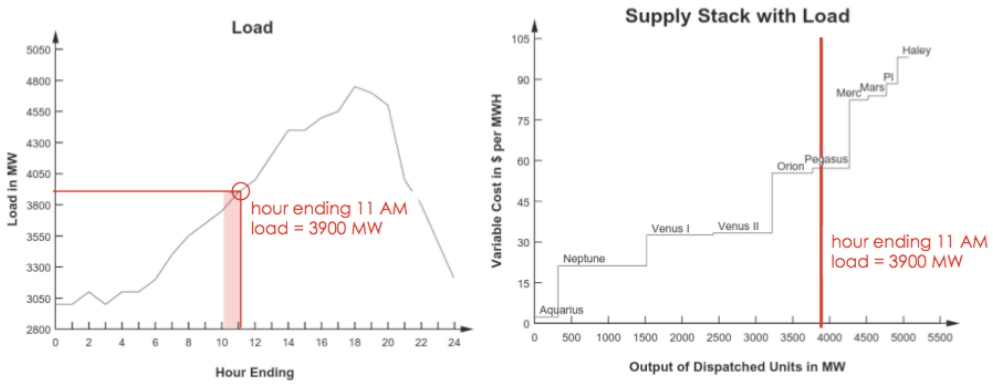

Source: *A. Pigneri (2009)*

Figure 3.8 - Crossing the data of a typical demand side curve (left) with supply side graph (right)

Once completed the crosscheck, the final 24 hour day-ahead dispatch schedule (Figure 3.9) is completed.

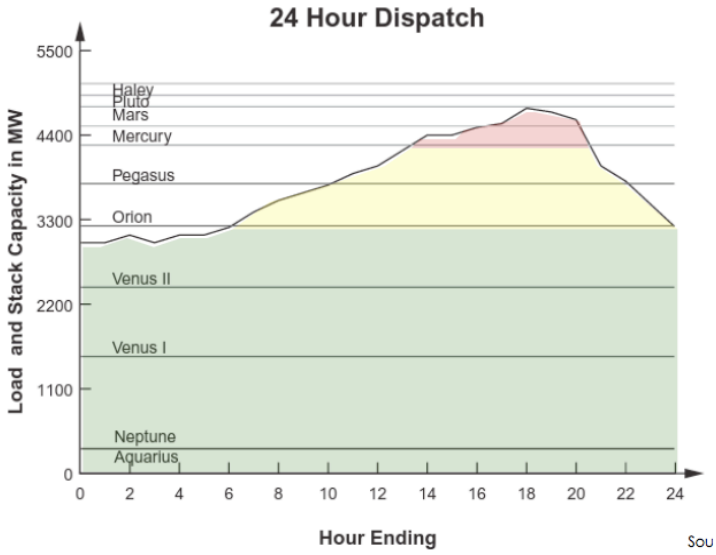

Source: *A. Pigneri (2009)*

Figure 3.9 - 24 hour day-ahead dispatch schedule

Since the demand of energy on the NEM (*National Electricity Market*) is not linear and fully predictable, the price for the energy trade is subject to variations according to the considered period of the day and the request of that particular interval of time. According to this, energy generation is divided into three main categories, based on the *capacity factor* of the power plants that indicates the continuity of energy generation and thus how the money is spent for producing energy.

The three categories are:

(1) *Base-load* power plants: characterized by continuous power output, they usually have low flexibility because of high start-up costs (e.g. coal-fired steam generators). Energy is sold at a low price.

(2) *Intermediate-load* power plants: this kind of systems have some flexibility to part-load operations. Their operation schedule is determined by trade-offs between costs of continuous operation and start-up costs (e.g. combined cycle gas turbine generators)

(3) *Peak-load* power plants: they have high operational costs, mostly due to expensive raw fuel, and are normally dispatched only during on-peak periods (e.g. open cycle gas turbine generators). Economic incoming is higher because energy is highly priced.

The reason why the economic incoming are in inverse proportion with the load (the lower the load, the greater the incoming) is due to the variation of the LCOE index as a function of the capacity factor (see Figure 3.10) It is very easy to deduce that, for small ACFs, the levelized cost of electricity is higher; this just means that the price paid to construct, operate and maintain the system is used to produce a smaller electricity output with the consequence of a smaller economic incoming and, thus, electricity needs to be priced highly.

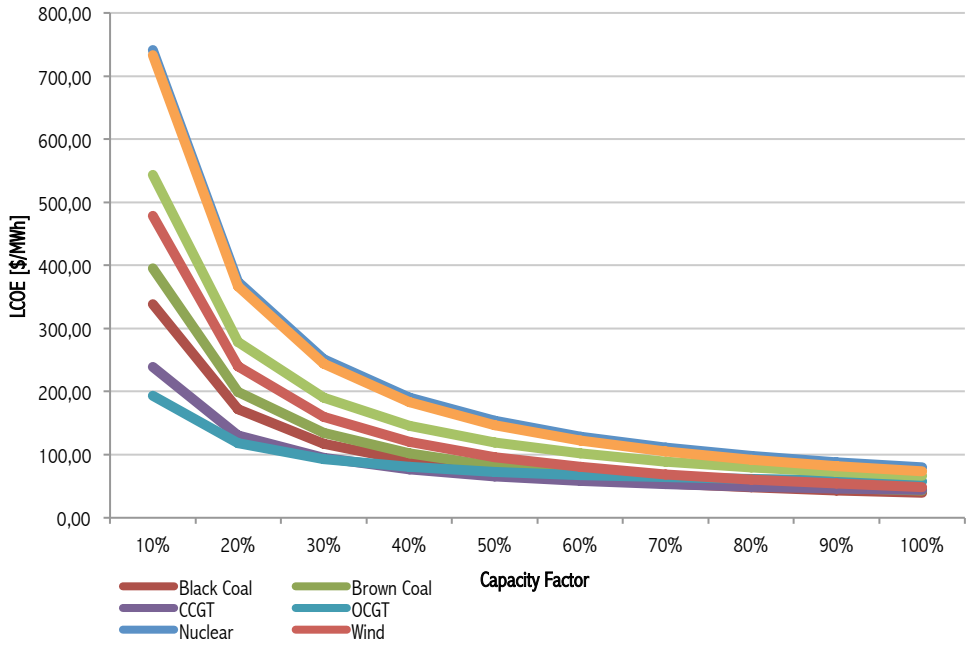

Figure 3.10 - LCOE variation as a function of the capacity factor

3.4 Long-term utility planning: the MCoE index

The *Marginal Cost per unit of Energy* (MCoE) is an index used for constructing a long-term utility planning of the energy sources, for investment and decision-making evaluation. This analysis is able to create, maintain and renew a generation, transmission and distribution resources portfolio, capable of providing least-cost electricity services. This index is also the base on which to construct useful graphs such as the *supply-resource screening* (see Figure 3.11) and the *load-duration curves* (see Figure 3.12).

3.4.1 How is the MCoE index calculated?

To explain the role of the MCoE index we first need to explain the main "bricks" that constitute it: the *Marginal Energy Cost (MEC),* the *Marginal Capacity Cost (MCC)* and the *LCOE* (or *Long Run Marginal Cost, LRMC*) indexes.

Respectively:

$$\boldsymbol{MEC} = \boldsymbol{f}\left(\boldsymbol{Ex_{FUEL,t}} + \boldsymbol{Ex_{O\&M\ var,t}}\right) \tag{2.11}$$

$$= \sum_{\boldsymbol{h=1}}^{\boldsymbol{8760}} \frac{\boldsymbol{C_{ENE,h}}}{\boldsymbol{\Delta ENE_h}} =$$

$$= \frac{\boldsymbol{1}}{\boldsymbol{8760}} \sum_{\boldsymbol{h=1}}^{\boldsymbol{8760}} \frac{\boldsymbol{Ex_{FUEL,h}} + \boldsymbol{Ex_{O\&M\ var,h}}}{\boldsymbol{\Delta ENE_h \cdot (1 - F_{loss,h})}}$$

where $Ex_{FUEL,h}$ [$/h] is the hourly expense for fuel, $Ex_{O\&Mvar,h}$ [$/h] is the hourly expense for variable operation and maintenance, $C_{ENE,h}$ [$×MW/h] is the cost of producing energy with marginal supply resource in hour h, ΔENE_h [MWh] is the increment of energy produced by marginal supply resource in hour h, $F_{loss,h}$ [%] is the value of the transportation and distribution losses, calculated with the ratio of the difference between the generated and sold amount of energy and the generated energy [$(ENE_{gen} – ENE_{sold}) / ENE_{gen}$].

$$\boldsymbol{MCC} = \sum_{\boldsymbol{t=0}}^{\boldsymbol{n}} \frac{\boldsymbol{I_t} + \boldsymbol{Ex_{LABOR,t}} + \boldsymbol{Ex_{O\&M\ fix,t}}}{\boldsymbol{\Delta CAP_j \cdot (1 + r)^t}} \tag{2.12}$$

where I_t [$] is the investment cost in year t for increments in supply capacity, $EX_{LABOR,t}$ [$/year] is the annual expenditure for labour in year t, $EX_{O\&Mvar,t}$ [$/year] is the fixed annual cost of operation and management, ΔCAP_j [MW] is the increment in generation capacity from marginal unit supply and r [%] is the applicable interest rate (in this case, again, the cost of capital). Furthermore, with the parameters calculated in previous equations is possible to obtain:

$$MC = MCC \cdot \Delta CAP + \frac{MEC \cdot \Delta ENE}{crf} \tag{2.13}$$

We can finally calculate the wanted *Marginal Cost per unit of Energy* (MCoE) index:

$$\begin{aligned} MCoE = \frac{MC \cdot crf}{\Delta ENE} &= MCC \cdot crf \cdot \frac{\Delta CAP}{\Delta ENE} + MEC \\ &= \frac{MCC \cdot crf}{8760 \cdot CF} + MEC \end{aligned} \tag{2.14}$$

This index is not significant itself, because it doesn't reflect the competitiveness of the technology on the market context. From the obtained value, for example, CCGT has a MCoE of 22202 $/MW and OCGT 42749 $MW but, from an economical and concrete point of view, even if much higher than CSP solar technology with its 1179 $/MW, they remain one of the most convenient ways to generate power. But the MCoE index is good for its extreme immediate visual feedback once outlined with the supply-screening curve (Figure 3.11).

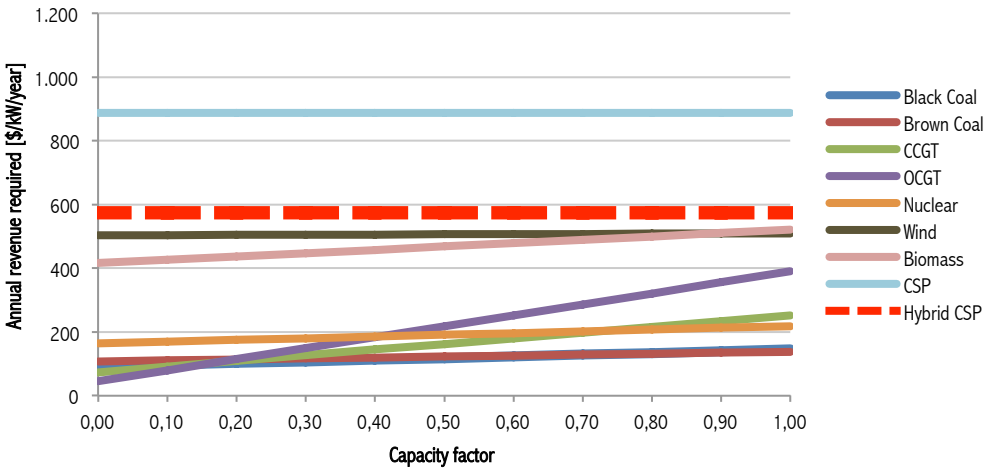

Figure 3.11 – Supply-resource screening curve

This graph represents a comparison between the annual revenue required on the y-axis ($/kW/year) and the annual capacity factor (ACF) on the x-axis. That's a very intuitive way to see which one, among the technologies, has the lowest running costs for each chosen ACF. Simply, the most convenient one is represented by the curve that stays under all the others.
The economic meaning of the chart is very simple; the interceptions of each line with the y-axis represent the fixed cost components (initial investment, fixed O&M, …) whereas the slope represents the amount of variable expenses during operation (labour, variable O&M, …). For example, coal technologies have higher initial investment than CCGT or OCGT plants but a flatter slope because, mainly, the used raw fuel (coal) is much cheaper than gas. This is the same reason why a completely horizontal line describes all renewables because in this case there are no expenses for fuel. This graph is a further confirmation that at the moment, basing on the most recent data, solar technologies are still quite far from economic competitiveness on the energy market panorama, but also that hybrid solar systems represent a concrete opportunity to reduce the gap with conventional power sources and start competing in the national energy market.

From supply-resource screening curve it is possible to construct another useful tool mad for long-term utility planning: the load-duration curve (see Figure 3.12).

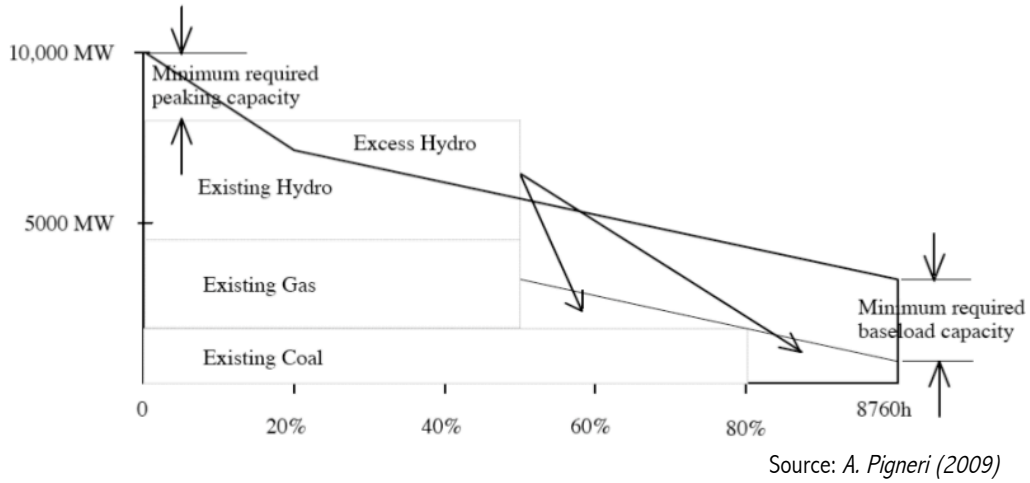

Source: *A. Pigneri (2009)*

Figure 3.12 - Explanation of the meaning of a typical load-duration curve

As final step, in order to develop the optimum energy mix for dispatch, crossover point from screening curve are plotted on load-duration (see Figure 3.13).

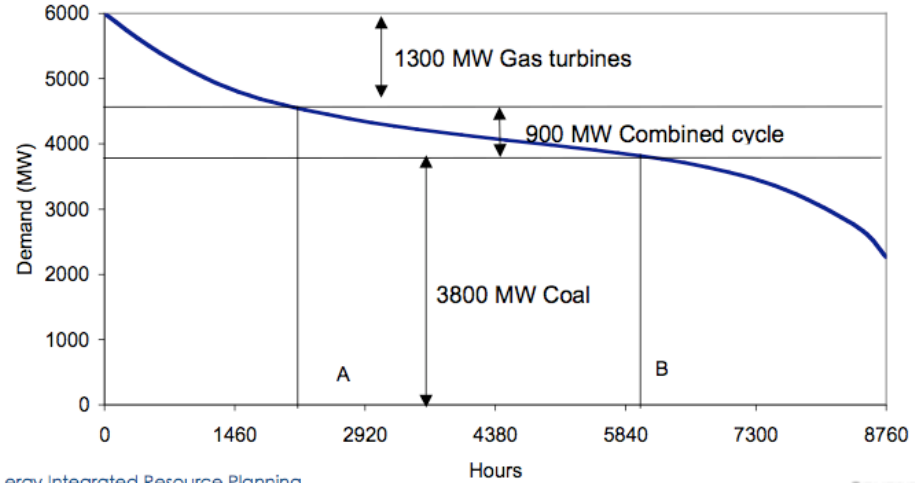

Source: *A. Pigneri (2009)*

Figure 3.13 - Screening curve crossed with load-duration curve

In reality, electric supply planning is more complex than the simple process illustrated using the load-duration curve because loads are variable and difficult to predict, and supply resources may not be available at all times.
These uncertainties are reasons for planning and maintaining a *reserve margin*, such that total supply capacity, at the generation, transmission and distribution levels, almost always exceeds the maximum expected demand.
One way to think about it is increase the levels of load by the requested margin along the whole load-duration curve; this extra generation, which is made available to meet unusual demands or deal with unforeseen outages or shutdowns in generations, is set to about 25% as generally accepted percentage of reserve, decreasing till 15% in large diversified and distributed systems
In practice supply resources are lumpy investments that come in discreet and often large sizes. A real utility investment plan must select individual types of plants in discreet sizes to begin service in specific years in order to meet present and anticipated (but uncertain) future demand.
The selection of these plants must maintain a balance between the different types of plants, according to the pattern of load growth and retirement of existing plants, in order to achieve the least-cost resource mix. The criterion to determine when and how much capacity to be added is the system peak

demand (*A.Pigneri, 2009*). Is just in this growing demand scenario that CSP must cut down its cost to start competing with traditional energy sources in the NEM. But totally R&D-based hopes are not enough; governments and big investors must act together to finance new project for stimulating large-scale production in order to make costs fall to a much lower level. In particular, dedicated energy programs based of funds, incentives and feed-in tariffs can give an important short-term boost to CSP market.

3.5 Australian National Energy Market (NEM): policy, targets and State funding

3.5.1 MRET (Mandatory Renewable Energy Target) and eRET (enhanced Renewable Energy Target)

In 2001 the Australian Government introduced the MRET, a Mandatory Renewable Energy Target of 9,500 GWh of new generation that was doubling the 1997 levels of renewable generation and increasing of about 3-4% the slice of renewables in Australia's total electricity generation panorama.
On 20 August 2009, to ensure that renewables in Australia achieve the target of 20% of electricity supply by 2020, the government has enhanced the Renewable Energy Target (eRET) with an increase from 9,500 gigawatt-hours to 45,000 gigawatt-hours (see Figure 3.14)

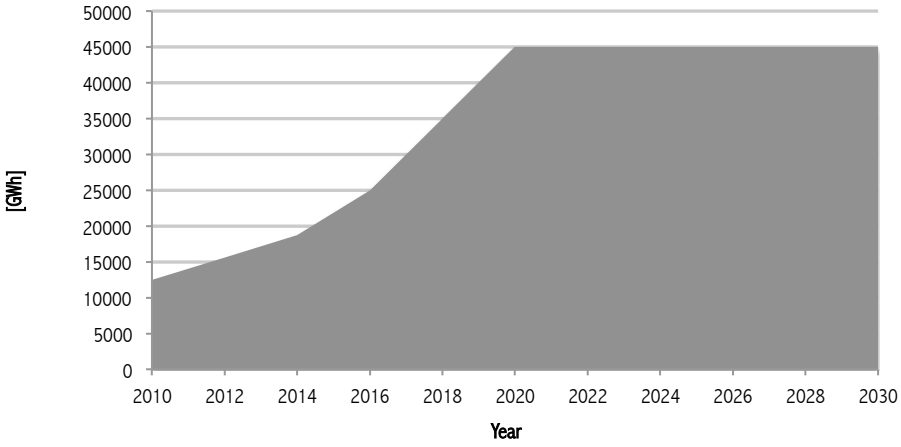

Figure 3.14 – Australian MRET 2010-2030 [15]

[15] Source: M. Watt, J. Wyder (2010). *National survey report of PV application in Australia 2009*. IT Power Australia with the support of ASI (Australian Solar Institute).

The scheme will last until 2030 because after 2020 the suggested ETS (Emissions Trading Scheme) and improved efficiencies in processes are expected to allow the MRET to be phased out by 2030.
A lot of people attacked the MRET because of a supposed inefficiency in reduction of the fossil fuel dependency of Australia as it is addressed only to generated electricity for domestic use an not to all energy sources. In fact, this is applied neither to the exported energy production (77% of the total amount of produced energy) nor to energy sources that are not used for electricity generation (such as oil in transportation). Taking those percentages into account and considering the total Australian electricity production, the flagged 20% of the MRET turns into the small 3-4% (less than 2% in the opinion of organizations that criticize the MRET).

3.5.2 Solar Flagship Program

In 2009 the Australian Government has announced a call for an allocation of a fund of 1,3 billion AUD to cover up to one third of the capital cost of 4 new solar thermal and PV power stations, to achieve the target of 1 GW of solar generation. In the first call eight project among PV companies, State and local governments, electricity retailers, financial institutions and research partners have been chosen. They divide into four solar PV and four solar thermal projects [16] but, in order to match the interest of this thesis, only the four CSP solar thermal projects of the Solar Flagship program have been listed:

(1) *Parsons Brinckerhoff:* is the leading part of the Solar Flair Alliance with Siemens (Technology partner), John Holland (Lead construction contractor), CS Energy (Market participant, generator, project host and long-term asset operator and manager), Infrastructure Capital Group (Lead commercial advisor and equity partner) and Queensland University of Technology (Lead research partner). The project aims to build a 150 MW solar thermal parabolic trough power plant near the existing Kogan Creek power station, close to Chinchilla, QLD (Queensland). The vision of the Solar Flair Alliance is to use Australia's abundant solar resource to start developing

[16] source: Australian Government, Department of Resources, energy and Tourism. Solar Flagship project descriptions – Round 1

infrastructures create a large scale solar thermal market able to provide affordable, secure and reliable electricity.
Criticisms: This is a US engineering firm and its proposal involves a joint venture with Queensland coal-fired generation company, CS Energy.

(2) *Transfield*: this is a project for the conversion of the Transfield coal fired Collinsville power station (QLD) into a 150 MW solar thermal plant. Transfield is a consortium consisting of Transfield Holdings, Novatec, Transfield Services and Transfield Services Infrastucture Fund.
Criticisms: Transfield could use taxpayer funds to convert an existing, small coal-fired power station in Queensland into a solar thermal plant in what could seem an opportunistic grab in order to extract value from a polluting asset. Transfield also part-owns coal-fired power plant Loy Yang A.

(3) *Wind Prospect CWP:* is a joint venture between Wind Prospect (a private company focused on renewable energy development) and Continental Wind Partners (CWP, a renewable energy development fund). They have formed a consortium with CS Energy Ltd (QLD largest energy generator), AREVA Solar and Mitsui & Co Australia Ltd (developer and owner of major power generation and infrastructure projects in Australia and overseas) to develop, build and operate a 250 MW solar thermal power plant at Kogan Creek (QLD) based on AREVA Solar's compact linear Fresnel reflectors (CLFR) technology.
Criticisms: As the name says, british Wind Prospect CWP could be seen as a consortiom with no experience in large scale solar generation.

(4) *ACCIONA Energy*: headquartered in Spain, is a leader in the development, production and management of renewable energy, water and infrastructures. Its strong capabilities in design, construction, project financing, operation and maintenance make ACCIONA lead a consortium, with Mitsubishi Corporation and Australia's BMD Constructions and GHD (an Australian engineering firm), that proposes the generation of 200 MW at a single site (QLD or South Australia, SA), using solar thermal parabolic trough technology. Nowadays ACCIONA has retired from the Solar Flagship project.

A second call for two more power stations will be made in 2013-2014 with a particular consideration for proposals that include local industry development to improve the status of local manufacture. All projects must include research programs with funding up to 400 MAUD available for research infrastructure.

3.5.3 Other ongoing national programmes

Solar Credits

Solar Credits system is a solution to increase incentives for the adoption of renewable power systems. The MRET (45000GWh by 2020) will continue to use the Renewable Energy Certificate (REC) mechanism, with each MWh produced by a renewable system eligible for one REC. PV systems, wind turbines and micro-hydro systems, for the first 1,5 kW of capacity, have Solar Credits available, a REC multiplier (x5 until 2012, x4 in 2013, x3 in 2014 and x2 in 2015). Everyone (privates, industries, schools, …) is eligible for Solar Credits.

National Solar Schools (NSS)

It started on 1 July 2008 and will finish on 30 June 2015. The program, with a total fund of 480 MAUD, offers a grant of up to 50000 AUD per school (without regards to local State Governments) to install PV, renewable power systems and take other measures to increase buildings energy efficiency and pull down their environmental impact. The average of power installed on schools is 2-4 kW each with an expectation of a total 20-40 MW in 2015 (In 2009 the budget allocation was oversubscribed). This program is focused on schools also to increase the awareness of students and understanding of PV with guided tours through the systems and increase the community acceptance level.

3.5.4 Ceased national programmes

Solar Homes and Communities Program (SHCP)

It operated from 2000 to 2009 and aimed to both accelerate the uptake of small-scale PV systems (residential and community buildings) and develop the local industry. It was based on a 8000 AUD refund for 1 kW PV systems installed on residential buildings and up to 50% refund on the systems price for community buildings willing to install up to 2 kW. From March 2000 to

December 2009 were installed a total amount of 84 MW of which 94% were grid-connected. The program has been replaced by the Solar Credit mechanism.

Renewable Remote Power Generation Program (RRPGP)

It operated from 2000 to 2009 too and, with a total fund of 300 MAUD and a refund of up to 50% of the capital cost, aimed to both accelerate the adoption of renewable technologies used for the displacement of diesel based installations in stand-alone power systems. In 2008 the Industry Support of the RRPGP provided additional 980000 AUD for the installation of 64,9 kW of PV in the Alice Spring Desert Knowledge Australia Solar Centre for tests on a wide range of PV systems and configurations. The total amount of capacity installed at the end of 2008 was 11,92 MW.

Chapter 4. Case study: Hybrid repowering of Munmorah power station (NSW, Australia)

This chapter wants to give an example of a real application of what said since now. An existing and operational coal-fired plant, Munmorah power station, in NSW (New South Wales) has been taken as reference for multiple studies on its repowering.
The whole analysis has been made with Thermoflex, a dedicated engineering software by Thermoflow, designed to simulate thermodynamic behaviour of ad hoc-designed power generation layouts.

The studio has been conducted in three main steps:

(1) Simulation of the performances with the existing coal layout

(2) Repowering with a NGCC (Natural Gas Combined Cycle), built keeping the same power output of the steam turbine

(3) Conversion of the NGCC into a hybrid ISCC

(4) Off-design simulation in two different locations: Munmorah lake and Perth

4.1 Munmorah power station: the location in the Australian context

Australia is one of the biggest producer and consumer of coal for power generation. In this context, with a worldwide rise of a "greener consciousness", the spread of renewable energy technologies becomes very significant.
Because of the low price of coal, Australia has a lot of coal-fired power located across the whole country (see Figure 4.1 for a graphical representation and Appendix 1 for a complete and detailed table of all coal-based facilities in the territory).

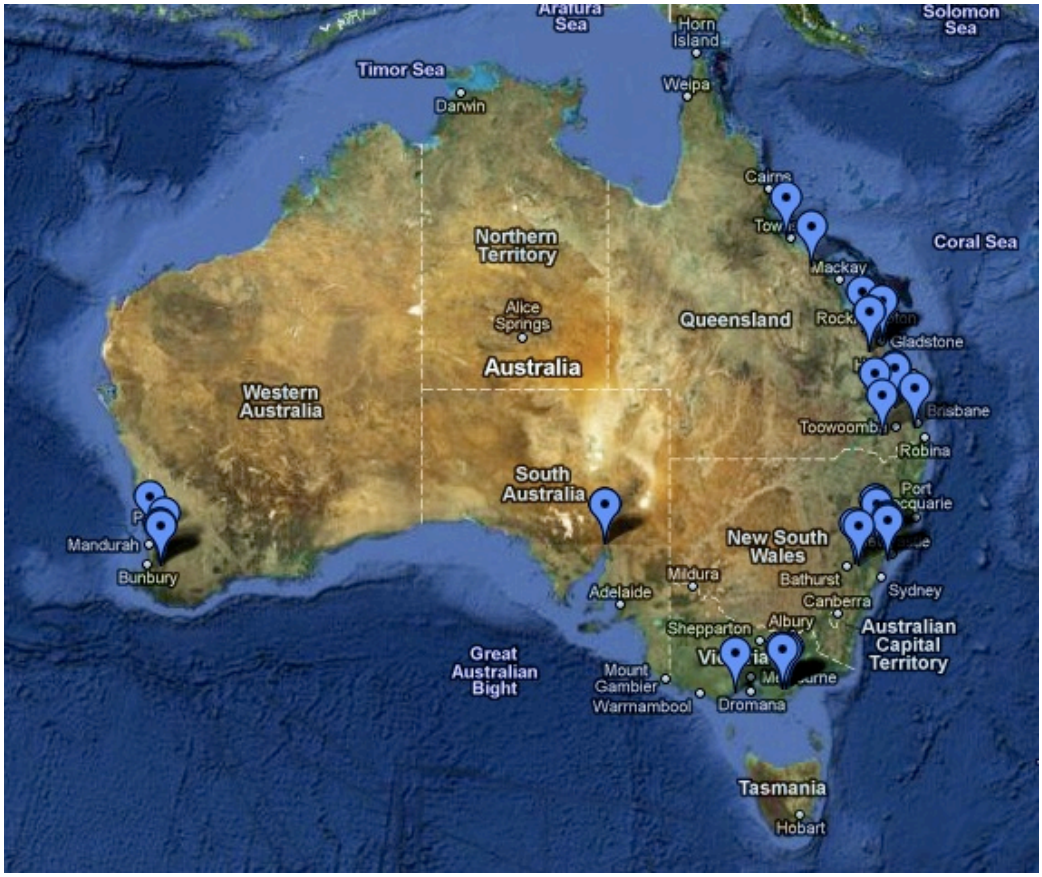

Figure 4.1 – Coal-fired power stations in the Australian territory

As can be noticed, all the power generation facilities are near big consumption centres such as Brisbane for Queensland, Melbourne for Victoria, Adelaide for South Australia, Perth for Western Australia and Sydney for both New South Wales and the small Australian Capital Territory, where Canberra is located. Tasmania has no coal-fired power station.

At the beginning of the studio, Munmorah has been chosen because of many reasons:

- From the results of a preliminary analysis (see figure 4.2) this facility has came out as one of the most interesting because of both the small power of its units (300 MW each) and the year of its construction (1969)

- Its proximity Sydney, the biggest Australian city and consumption centre and so one of the most interesting places in terms of growing energy demand.

- The higher availability of data (see Appendix 2), taken as basis for the simulations with Thermoflex software
- Being in Sydney makes it nearer to the UNSW (the University of New South Wales), the partner university where part of this thesis has been developed and, thus, there are more related interests

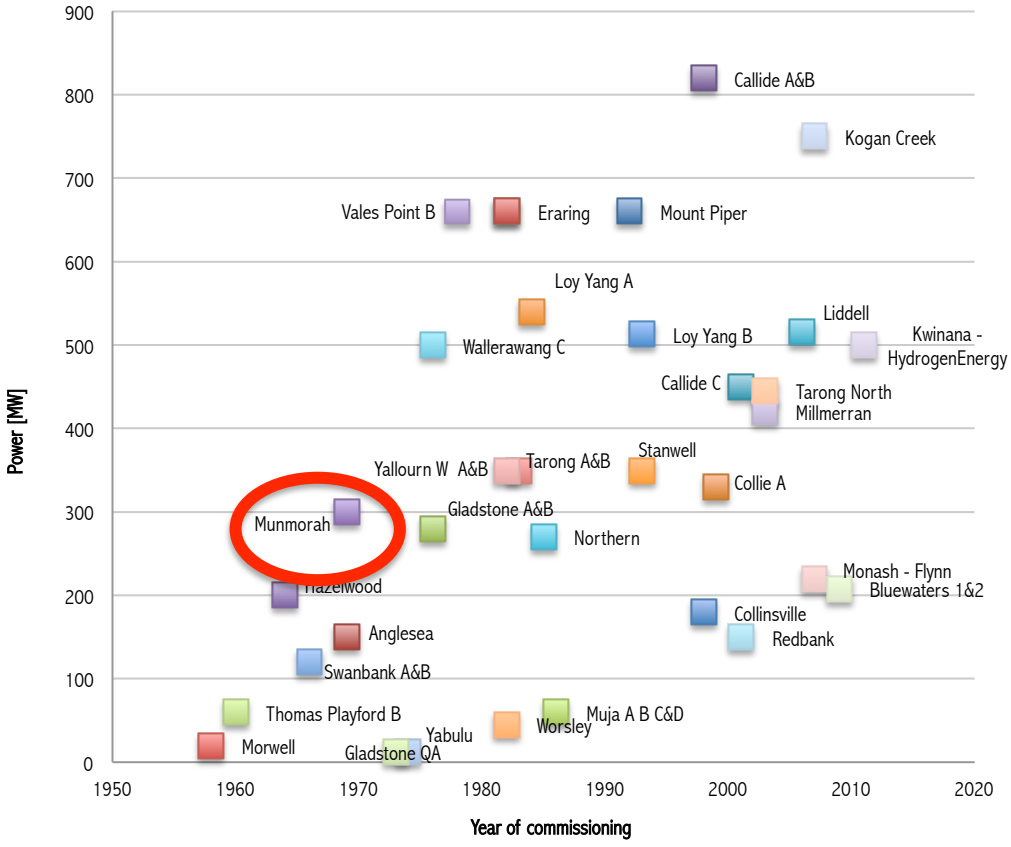

Figure 4.2 – Classification of Australian coal-fired power stations basing on their unit(s) power (y-axis) and year of commissioning (x-axis)

The most interesting options for a hybrid repowering are the facilities located in the bottom-left corner of the chart in figure 4.2, because of their small units and their high probability of revision in the short-term, being quite dated.

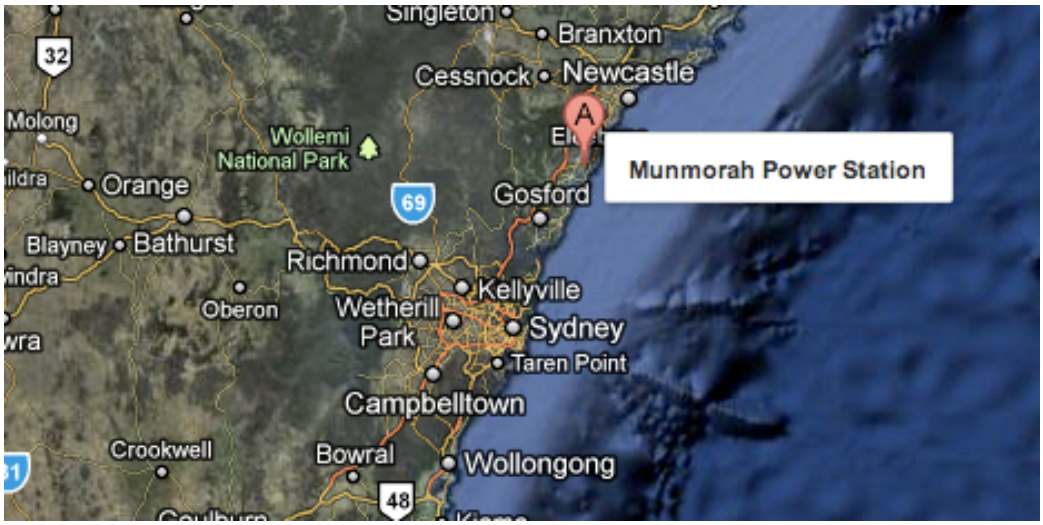

Source: Google Maps

Figure 4.3 – Location of Munmorah power station in respect of Sydney

Furthermore, in order to have a wider view on the possibilities for solar power integration in Australia, a comparison has been made taking the same 3-steps study, with the same plant layout, but in a different location, Perth (WA). Perth is a very good location for solar power installations because, if compared to Munmorah, it is characterized by a significantly higher DNI (989 W/m^2 vs. 668 W/m^2 as peak in January, see Appendix 3) and dryer and bright-sky weather conditions during the whole year and, in particular, in Summer where Perth has almost no rainfall, while Munmorah (Sydney) has more than 50% (see Figure 4.4).

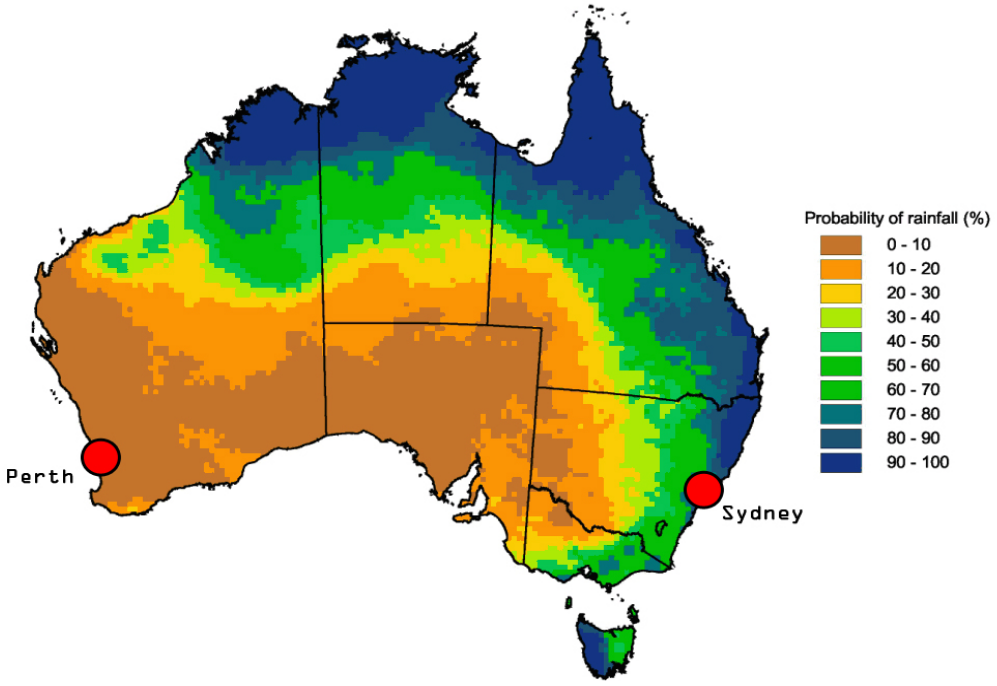

Source: *anra.gov.au, Australian Natural Resources Atlas*

Figure 4.4 – Probability of rainfall in the Australian territory, in summer

4.2 Munmorah power station: the facility

Munmorah power station has been built in 1969 near Colongra village, in a piece of land just on the shore of lake Munmorah (see Figure 4.5), a salted lake connected with another bigger salt-water basin: Tuggerah lake. Those two lakes are just about 200 m from the Pacific Ocean and, thus, represent an ideal location for a Rankine cycle-based steam cycle, because of a possible water-based cooling process.

The station was originally built with four English Electric 350 MW turbo-alternators, and had a total capacity of 1,400 MW. One unit was completed in 1967, another in 1968, and the remaining two in 1969. The alternators were de-rated in the 1980s to 300 MW each, and the oldest two units were shut down in 1990. By now, this power plant has only two 300MW steam turbines, fed with coal coming from two local underground mines and delivered by a conveyor belt. So, today Munmorah power station generates a total capacity of 600.01 MW of electricity[17].

[17] Source: Wikipedia, http://en.wikipedia.org/wiki/Munmorah_Power_Station

Source: *Google Maps*

Figure 4.5 – Current Munmorah power station occupation area

In September 2007, the New South Wales State Government announced the commencement of a trial of "clean coal" technology at Munmorah Power Station. The $5 million trial by the CSIRO and Delta Electricity will be the first part of a larger $150 million trial jointly funded by the coal companies.

Since the territory owned by Delta Electricity seems to be quite small for a big solar field, it has been supposed an extension of the occupied land (see Figure 4.6) to make a higher solar integration possible. In the first case (shown in Figure 4.5), in fact, the area that can be used to place solar collectors is approximately 500000 m^2 while in the second one, (represented in figure 4.6), it reaches approximately 1,5 million m^2.

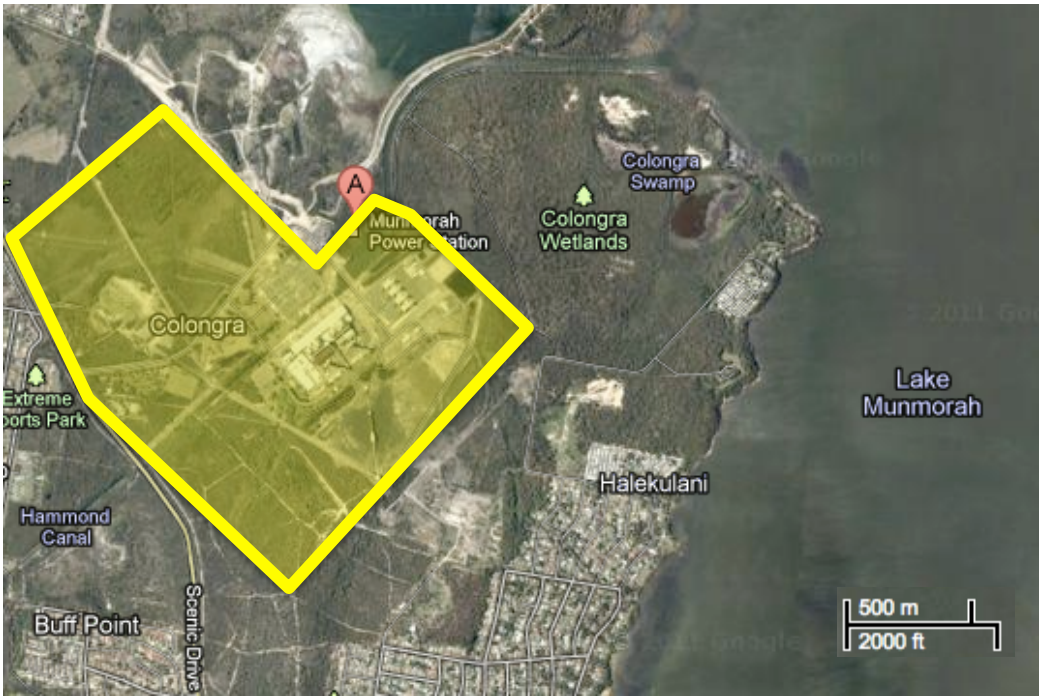

Source: *Google Maps*

Figure 4.6 – Extended Munmorah power station occupation area

4.2.1 Munmorah coal-based layout in Thermoflex: scheme of the system and results of the simulation

This layout has bees schematized in two different sections, the *boiler* side (Figure 4.7) and the *steam cycle* side (Figure 4.8). The cycle has been drawn with just one level of pressure, with the boiler made of the economiser that preheats water. Hot liquid water is than sent to the steam generator where it becomes steam that is sent in the superheater, which creates the required conditions for feeding the steam turbine inlet ($T_{IN,TV}$ = 565,5 °C).
The steam turbine is made of eleven stages, each with its dedicated bled-off fed regenerator. In particular, after the third stage, the steam returns to the boiler for being reheated up to a temperature of 540 °C.
As previously said the low-pressure fluid at the exit of the turbine goes to the water condenser, before being re-pumped in the economiser to be warmed up again.
There is also a deareator after the fifth regenerator (to separate liquid phase from gaseous one), while on the "boiler side" there is a rotating heat exchanger to preheat air sent to the boiler. Steam generator exhaust gases make the

superheating, reheating and preheating processes. After this, the residual heat is given to preheat boiler inlet air too so that, then, gases became cold reach the FGD section to be treated before being released in the atmosphere.

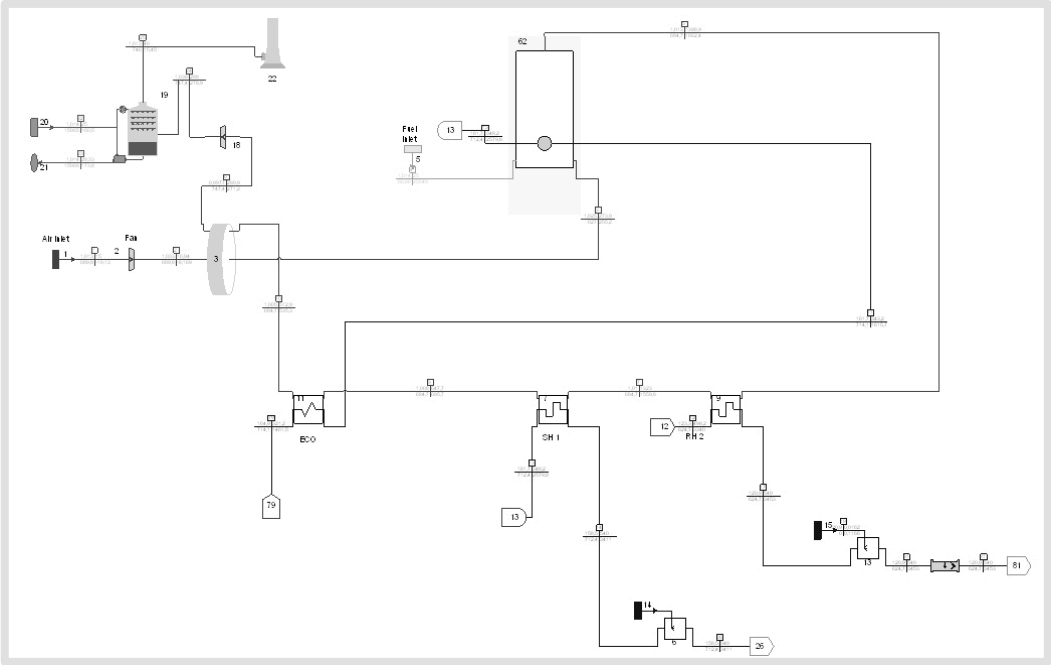

Figure 4.7 – "Boiler side" of the scheme for Munmorah coal layout

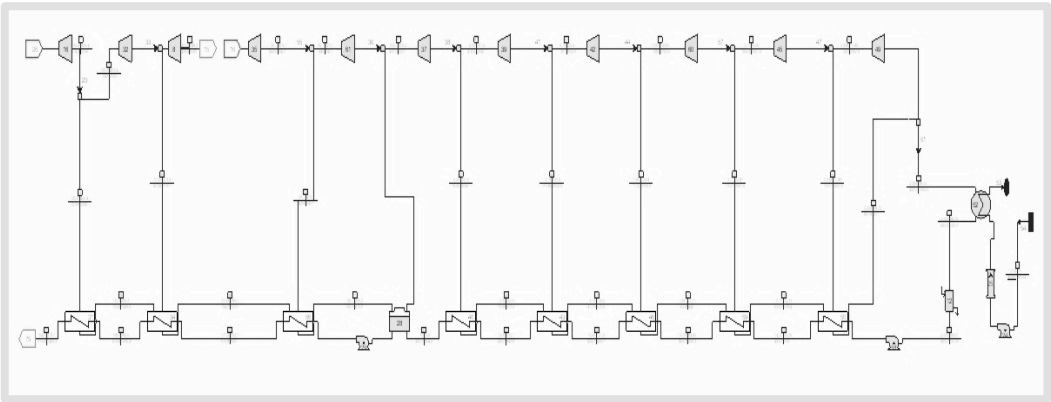

Figure 4.8 – "Steam side" of the scheme for Munmorah coal layout

After the simulations, in the thermodynamic mode (on-design), the results of the computation are shown in Table 4.1. As can be noticed the net power has been maintained almost the same of the one received by Delta Electricity, the owner of the power station (see Appendix 4). For the missing parameters, such as maximum pressure of the steam cycle, a typical layout of a coal-fired power plant has been taken as reference (the results can be seen in Appendix 5).
More, the obtained value for net electric efficiency is set to 40,58% and referred to LHV. This is a good value for a coal-fired power plant but remains average.
Finally, talking about emissions, after the FGD (Flue Gas Desulfurization) but with no CCS (CO_2 Capture and Sequestration), the CO_2 annual emission reach 778,9 kg/MWh for a total annual quantity of 4037348 kg, more than 4037 tons each year.

Table 4.1 – Results of the Thermoflex computation for the coal-fired layout

Parameter	*Unit*	*Coal*
Net electric efficiency	*[%]*	*40,58*
Net power	*[kW]*	*599997*
Net fuel input (LHV)	*[kW]*	*1478692*
CO2 annual emissions	*[kg/year]*	*4037348*
CO2 specific emissions	*[kg/MWh]*	*778,9*
P_max	*[bar]*	*161,67*
P_min	*[bar]*	*0,069*
T_SH	*[°C]*	*565,5*
T_RH	*[°C]*	*540*
Fuel mass flow	*[kg/s]*	*57,88*

4.2.2 Munmorah NGCC (*Natural Gas Combined Cycle*) layout in Thermoflex: scheme of the system and results of the simulation

This case represents the first evolution of the coal-fired layout for Munmorah. As said above, the system has been designed to maintain almost the same power output for the existing steam turbine. This means a significant power output growth for the whole combined cycle, from about 600 MW up to more than 1400 MW.
The previous "boiler side" has been thought as replaced by 3 Mitsubishi 701G gas turbines, with 334 MW rated power each, for a total of approximately 1

GW, only from gas machines. The simulation made with Thermoflex gives a real output power of 323337 kW for each turbine, for a total amount of 970011 kW from the whole gas section, with a 96,81% net efficiency in turbine thermal energy conversion.
Because of the presence of the turbogenerator itself, the steam cycle comes with no regenerator. In fact, in this configuration, the heat source, for producing steam to be sent at the steam turbine inlet, are the turbogenerator exhaust gases, that flow in the secondary stream from a inlet temperature of 603,9 °C to a outlet temperature of approximately 112 °C.

Among the detailed results of the simulation (see Appendix 6), the most significant ones are shown in Table 4.2. A particular observation must be done on environmental impact reduction of NGCC compared to coal-based cycles, mostly due to a significantly higher net efficiency of the combined cycle (55,17% vs 40,48) but also to the cleanest nature of the fuel (CH_4 vs. Coal). It is possible to notice that, although with a twice and a half grater power output, the annual CO_2 emissions remain approximately the same (4046268 kg/year for NCGG vs. 4037348 kg/year for coal layout), with a consequent more than halved specific CO_2 emissions (351 kg/MWh for NGCC vs. 778,9 kg/MWh for coal layout).

Table 4.2 – Results of the Thermoflex computation for the NGCC layout and comparison with the coal-based case

Parameter	*Unit*	*Coal*	*NGCC*
Net electric efficiency	*[%]*	*40,58*	*55,17*
Net power	*[kW]*	*599997*	*1396626*
Net fuel input (LHV)	*[kW]*	*1478692*	*2531380*
CO2 annual emissions	*[kg/year]*	*4037348*	*4046268*
CO2 specific emissions	*[kg/MWh]*	*778,9*	*351*
P_max	*[bar]*	*161,67*	*83,74*
P_min	*[bar]*	*0,069*	*0,0709*
T_SH	*[°C]*	*565,5*	*565,5*
T_RH	*[°C]*	*540*	*540*
Fuel mass flow	*[kg/s]*	*57,88*	*50,58*

Another evident difference is an almost halved maximum pressure of the steam cycle (83,74 bar vs. 161,67 bar), mostly due to a much lower mass flow at the first stage of the steam turbine inlet (274,8 kg/s vs. 604,6 kg/s). However, because of no bled-off circuit (due to a layout with no regenerators)

and with a multi-level thermal recovery, the mass flow at the outlet of the last stage of the steam turbine is almost equivalent to the one obtained in the coal-based system (339,9 kg/s for NGCC layout and 344,6 kg/s for coal layout).

4.3 Hybrid solar repowering in Thermoflex: ISCC layouts

Once terminated the simulations on the combined cycle system, the attention has been moved on the integration of the solar field in this system. Among all the possible systems configurations, the decision ended up being a DSG system with parabolic trough collectors. The justification of this choice has been widely treated in all previous chapters, but can be resumed as a matter of technical innovation and simplicity (DSG choice) matched with a proven technology, such as the one of the parabolic troughs, that, by now, remain undoubtedly the widely spread and secure way to produce thermal and electrical power from the Sun.
However, in this paragraph a step-by-step analysis is presented, showing also the results of possible alternative solutions, such as, for example, the one with LFR reflectors instead of PTCs (see paragraph 4.3.2).

4.3.1 Munmorah ISCC layout in Thermoflex: position of the solar field in the heating process

The first thing done has been an evaluation of the system performances as a result of two different layout configurations, one with the solar field put in parallel with the HRSG after the first high-pressure economiser (Figure 4.9) and one with the solar field put in parallel with the HRSG before the first, high-pressure economiser (Figure 4.10). The detailed results of both simulations can be found in Appendix 7 and Appendix 8.

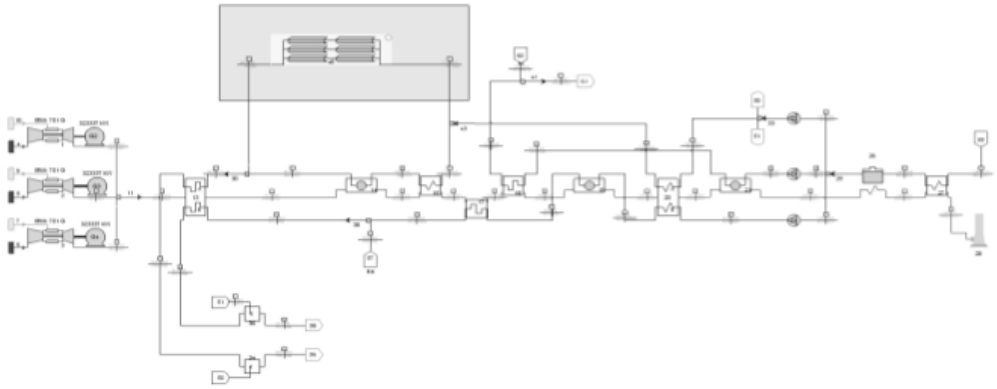

Figure 4.9 – ISCC layout in Thermoflex, with the solar field put in parallel with the evaporator only

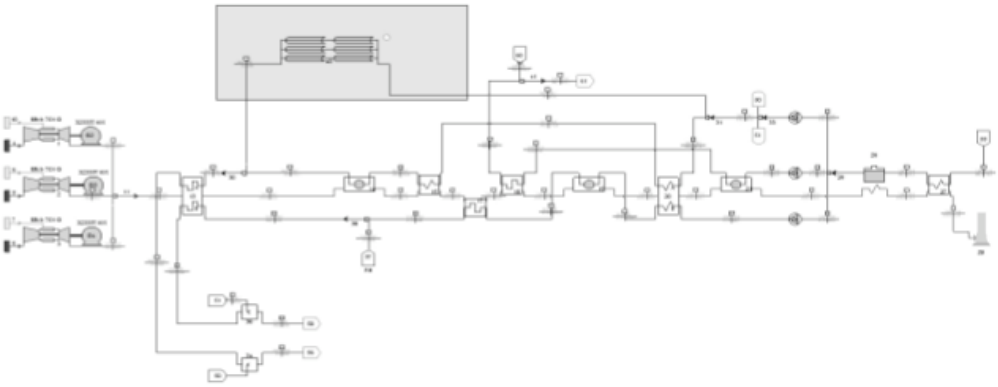

Figure 4.10 – ISCC layout in Thermoflex, with the solar field put in parallel with both the evaporator and the economisers

The most remarkable results, resumed in Table 4.3, are the ones that come out from the layout with the solar field put in parallel after the first, high-pressure economiser. This in enlightened by a relative 10+ % greater efficiency increase (2,71% vs. 2,43) in comparison of the system without solar field, a higher net power output (1446874 kW vs. 1439925 kW) and slightly lower specific CO_2 emissions (338,5 kg/MWh vs. 340,2 kg/MWh). It needs to be noticed that the parameters of the two configurations have been chosen accurately to have the same reflectors aperture area.

Thermodynamically, the configuration with the solar field covering also the pre-heating process is less convenient. This because the solar source is at very high temperature (approximately 5800K) and thus, in terms of exergy, the higher the temperature of the solar field system, the greater the efficiency. This is shown also in Carnot ideal efficiency that, with an unvaried minimum temperature of the system, rewards the system with higher maximum temperature. Basing on the results of the Thermoflex computation, this is once more confirmed (see Table 4.3); in fact, the solar field with doing evaporation only, with a water inlet temperature of 253,9 °C, behaves better than the one doing both preheating and evaporation, with a much lower inlet temperature of 108,1 °C. It must be noticed that a higher "efficiency decrease due to solar" parameter means a bigger contribution of the solar field. This because, with the solar energy considered at par with the one coming from gas, it is normal that efficiency is lower because the first one is converted in a steam cycle (more inefficient) while the second in a combined cycle.
There is to notice that, in this particular case, the argument is quite weak, because of a very low solar integration of the ISCC, set to approximately 4,78% (the solar field produces just 67480 kW of the 1446874 kW net power output). A further study with higher (11,1 %) solar integration is presented in paragraph 4.3.3.

Table 4.3 – Results of the Thermoflex computation for the two different configuration of the solar field positioning

Parameter	*Unit*	*Before*	*After*
Net electric efficiency w solar	*[%]*	*54,3*	*54,6*
Net electric efficiency w/o solar	*[%]*	*56,88*	*57,16*
Efficiency decrease due to solar	*[%]*	***2,55***	***2,56***
Net power	*[kW]*	***1439925***	***1446874***
Solar fuel input	*[kW]*	*120601*	*118683*
Net fuel input (LHV)	*[kW]*	*2531380*	*2531380*
CO2 annual emissions	*[kg/year]*	*4046268*	*4046268*
CO2 specific emissions	*[kg/MWh]*	*340,2*	*338,5*
P_max	*[bar]*	*92,32*	*94,1*
Fuel mass flow	*[kg/s]*	*50,58*	*50,58*
Reflector aperture area	*[m^2]*	*274042*	*274048*
Solar field mass flow	*[kg/s]*	*45,67*	*60*

As can be noticed, the maximum pressure at the steam turbine inlet is almost halved if compared to the coal-based layout. This has a negative impact on the

turbine efficiency (and thus on the overall efficiency of the ISCC, since farther from design conditions.

4.3.2 Munmorah ISCC layout: parabolic trough collectors vs. linear Fresnel reflectors

A further study has been conduced on the solar field main components: solar reflectors. This further analysis comes from the scarcity of available land in the considered location that, thus, needs to be optimized as more as possible. In order to do this, linear Fresnel reflectors represent a very interesting solution, also because of very big perspectives of growth in a short-term period.
As clearly shown in Figure 4.11, LFRs allow to have optimized land occupancy because there is no more need to have uncovered wide stipes of land to avoid reciprocal shadowing between solar collector rows. Thus the reflecting surface is much more "dense" that traditional parabolic through. However, by now, Fresnel reflectors have higher optical losses that make their efficiency lower than traditional parabolic trough collectors (approximately 67% vs. 75%).

Figure 4.11 – Differences in land coverage density between linear Fresnel reflectors (upper portion) and parabolic trough concentrators (lower portion)

Once more, all the result of the computation can be found in the Appendix section (Appendix 9), with the most significant ones resumed in the following table (Table 4.4).

Table 4.4 – Comparison between the main results of the two computations made with LFRs and PTCs, enlightening land occupation reduction.

Parameter	*Unit*	*PTC*	*LFR*
Net electric efficiency w/ solar	*[%]*	*54,60*	*54,60*
Net electric efficiency w/o solar	*[%]*	*57,16*	*57,16*
Efficiency decrease due to solar	*[%]*	*2,56*	*2,56*
Net power	*[kW]*	*1446874*	*1446870*
Solar fuel input	*[kW]*	*118683*	*118683*
Net fuel input (LHV)	*[kW]*	*2531380*	*2531380*
CO2 annual emissions	*[kg/year]*	*4046268*	*4046268*
CO2 specific emissions	*[kg/MWh]*	*338,5*	*338,5*
P_max	*[bar]*	*94,1*	*94,1*
Fuel mass flow	*[kg/s]*	*50,58*	*50,58*
Solar field mass flow	*[kg/s]*	*60*	*60*
Reflector aperture area	*[m^2]*	*274048*	*309674*
Collector field required land area	*[m^2]*	*624366*	*491376*
Land occupation reduction	[%]	*0*	***21,3***

The results clearly show that the reduction in occupied land is very significant, more than 21%. This result has been obtained with unchanged output parameters and indexes; in fact, it can be noticed that net electric efficiency, net power, solar fuel input, CO_2 specific emissions, solar field mass flow, steam cycle maximum pressure, etc. are unvaried.
The only parameter that changes is the "reflector aperture area", but this is due to the configuration of LFRs themselves that, being not parabolic, need a larger aperture area compared to PTCs. Furthermore, it must be said that Fresnel Reflectors have a marked performance (and thus efficiency) decline if operate at partial loads because of higher optical losses.

4.3.3 Munmorah ISCC layout with higher solar integration

The obtained result of the previous cases in Thermoflex where not satisfying, because of a small integration of the solar field (less than 5%). Because of this reason a change in the NGCC base layout has been made, to increase the solar field contribution in overall the power output balance.
As can be seen in figure 4.12, only one Mitsubishi 701 G turbogenerators has been considered in the turbo-gas section, while the steam turbine has been maintained with its eleven-stages, keeping the same performances but reducing the size.

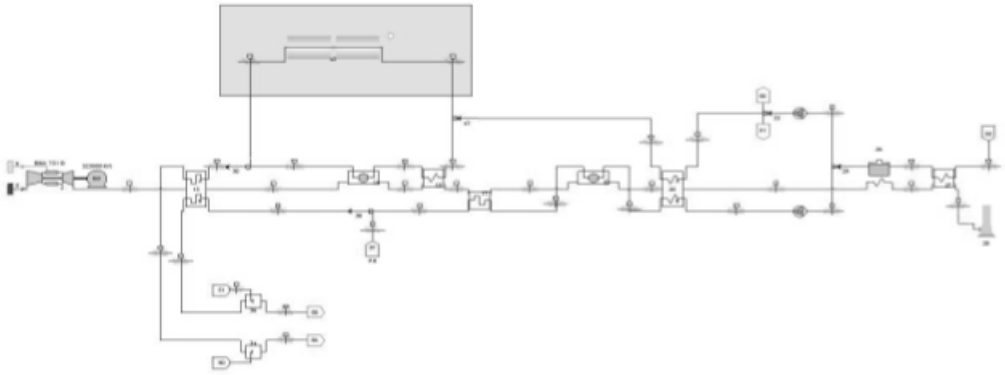

Figure 4.12 – ISCC layout in Thermoflex, with the solar field put in parallel with the evaporator only

According to the studio made in subparagraph 4.3.1, the chosen layout taken as reference sees the solar field put in parallel with the HRSG section after the first high-pressure economiser, with the aim of maximising the outputs in the computation (see Table 4.5).
The total power output of this new layout (with the contribution of the solar field) is quite similar to the one of the coal-based configuration, thus maintain the analysis valid for Munmorah power station, the facility chosen at the beginning of the studio. This further option can be considered as a plant conversion with a new, cleaner and partly renewable technology instead of a hybrid repowering.

Table 4.5 – Comparison between low solar integration layout and high solar integration one, both referred to PTC collectors.

Parameter	*Unit*	*ISCC low int.*	*ISCC high int.*
Net electric efficiency w/ solar	*[%]*	*54,60*	*49,13*
Net electric efficiency w/o solar	*[%]*	*57,16*	*54,58*
Efficiency decrease due to solar	*[%]*	*2,56*	*5,45*
Net power	*[kW]*	*1446874*	*517446*
Solar fuel input	*[kW]*	*118683*	*105192*
Net fuel input (LHV)	*[kW]*	*2531380*	*948118*
Level of solar integration	*[%]*	***4,69***	***11,09***
CO2 annual emissions	*[kg/year]*	*4046268*	*1347371*
CO2 specific emissions	*[kg/MWh]*	*338,5*	*313,5*
P_max	*[bar]*	*94,1*	*158,5*
Fuel mass flow	*[°C]*	*50,58*	*16,86*
Reflector aperture area	*[m^2]*	*274048*	*248310*
Solar field mass flow	*[kg/s]*	*60*	*60*

To all intents and purposes, it can be noticed that the level of solar integration of the new system configuration has been significantly raised (+236%) from 4,69% to 11,09%. The power output, as expected has fall down to about one third (-280%) of its initial value with related CO_2 annual emissions following the same trend, but with a greater decrease (-300%). Specific CO_2 emissions have been reduced too in comparison with all configurations (-248% compared to coal-based system, -12% compared to 3-GT and 2-GT NCGGs and -8% compared to low solar integration ISCC).
This high solar integration configuration gives a much higher efficiency decrease due to the solar field itself dropping from -2,56% to -5,45%, but a higher maximum pressure of the steam cycle increasing its efficiency, since closer to design mass flow.

4.4 Off-design simulations

Off-design simulations are run for understanding the system behaviour in real conditions and, so, how outputs vary as a function of input environmental and technical parameters.
In this studio, some different configurations have been analysed. These are combinations that come from two different Australian locations (lake

Munmorah, NSW and Perth, WA) and two different layouts of each system (ISCC with low solar integration and ISCC with high integration).
In particular, Perth has been chosen for its much higher DNI during the summer period (see Table 4.6) and for its geographical nearness to a medium-big consumption centre.

Table 4.6 - Maximum and minimum DNI values for Munmorah and Perth (*source: NREL database*)

Location	*Unit*	*Best month Max DNI*	*Worst month Min DNI*
Perth	*[W/m^2]*	*989 (Jan)*	*450 (Jul)*
Munmorah	*[W/m^2]*	*668 (Jan)*	*476 (May)*

A higher average annual temperature and a lower relative humidity characterize other environmental parameters. Instead of setting the same field size as in the low solar integration simulations, what has been done in high solar integration cases is set the same power output for the two solar fields, in order to see the reduction of needed collectors for the same target (see Table 4.7).

Table 4.7 – Comparison between the performances of a high solar integration plant in Munmorah and in Perth, and variations on the solar field size.

Parameter	*Unit*	*Munmorah H.I*	*Perth H.I*
Net power	*[kW]*	*517446*	*517447*
Net electric Efficiency w/ solar	*[%]*	*49,13*	*49,13*
Net electric Efficiency w/o solar	*[%]*	*54,58*	*54,58*
Efficiency decrease due to solar	*[%]*	*5,45*	*5,45*
Net Heat Rate (LHV)	*[kJ/kWh]*	*6596*	*6596*
CH4 fuel input (LHV)	*[kW]*	*948118*	*948119*
Solar fuel input	*[kW]*	*105192*	*105192*
Total net fuel input (LHV)	*[kW]*	*1053310*	*1053311*
Plant auxiliary total power	*[kW]*	*13108*	*13108*
CO2 annual emissions	*[kg/year]*	*1347371*	*1347371*

CO2 specific emissions	*[kg/MWh]*	*313,5*	*313,5*
Reflector aperture area	*[m^2]*	***248310***	***161531***
Collector field required land area	*[m^2]*	***683871***	***446724***
Land occupation reduction	*[%]*	***0,00%***	***34,68%***

The results enlighten that in Perth, although the two systems have the same outputs, there is a significant reduction of approximately 35% on the solar field size. This translates in a much lower initial capital expenditure, making Perth much more attractive for capital investments. But it need to be noticed a negative consequence, because of lower turbogenerator power output. In fact it must be taken into account that also the performances of the turbogenerators are highly dependant on environmental conditions (see Figure 4.13) with a strong relation with ambient temperature. The more that temperature grows, the lower the generated power by gas turbines.

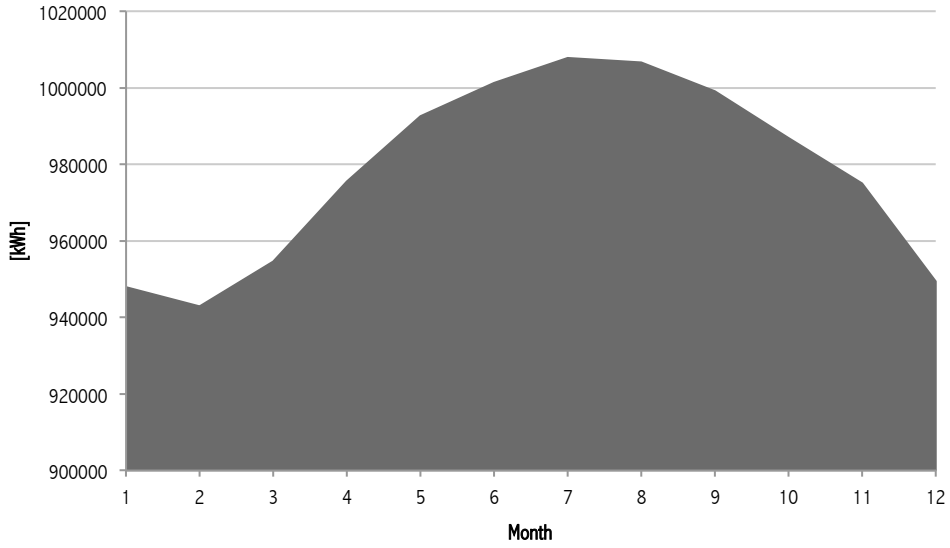

Figure 4.13 - Trend of the turbogenerators power output during the year, for the low solar integration ISCC in Perth

As a prove of that, with both cases of low solar integration systems as reference, is clearly shown that the net power output trend of the ISCC follows the exact path of the gas turbines power output one, with almost no

contribution from the solar field (see figure 4.14). This is more than evident, because the net power output increases just in summer, where the solar field slice of share in the overall power balance is at the lowest levels, while, on the contrary it decreases in winter (with the peak in January) when was expected to increase.

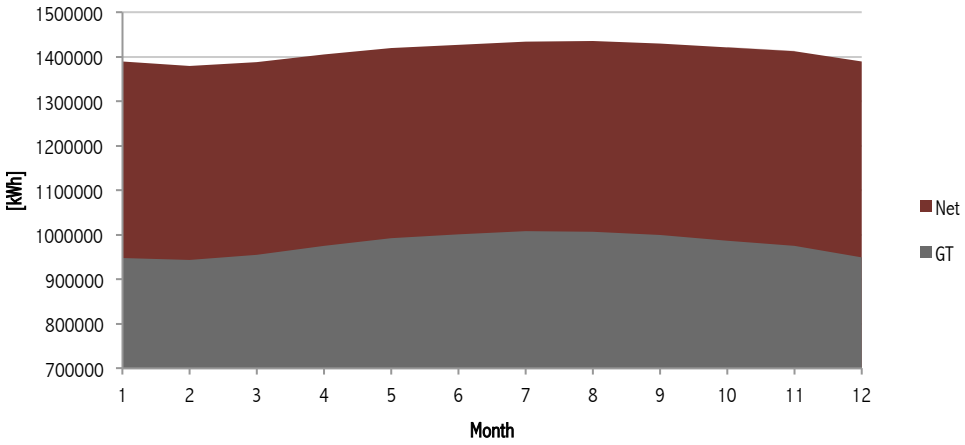

Figure 4.14 - Trends of net power output and Gas turbines power output, for the low solar integration configuration in Perth

In practice, this means that the turbogenerators performances reduction due to a higher ambient temperature is much more significant than the power given by the solar field, even in Perth where the solar radiation is high.
The situation is similar in the systems with higher solar integration, even if there is a little more balance, with an more constant net power output despite of a slightly variable annual power generation from the gas turbine, especially in summer months. This, again, is more evident in Perth (see Figure 4.15).

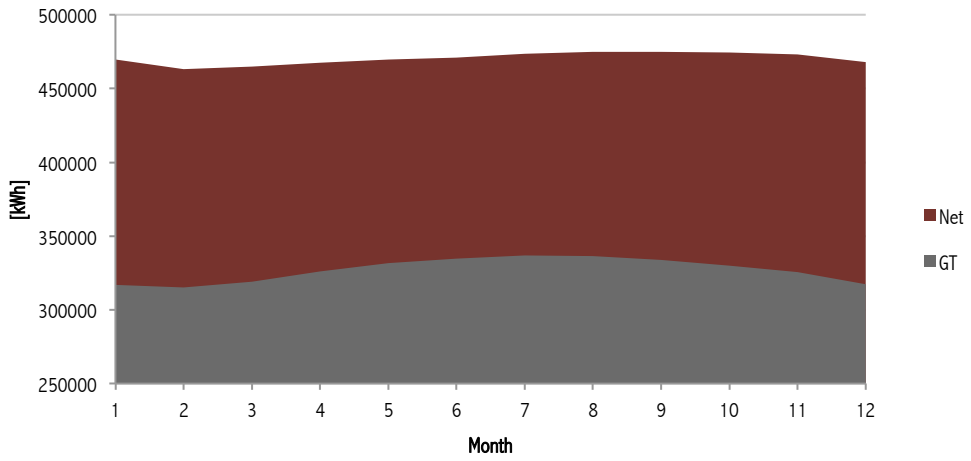

Figure 4.15 - Trends of net power output and Gas turbines power output, for the high solar integration configuration in Perth

An additional clarification must be done if the statistics and performances of the solar power system are analysed. In fact, comparing the charts of efficiency increase due to solar contribution (Figure 4.16) it may seem that Munmorah HI (high solar integration) ISCC behaves better than Perth one.

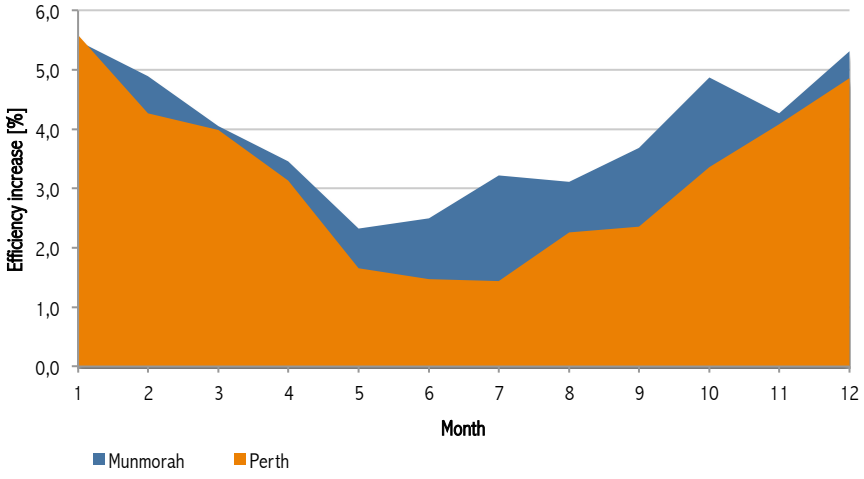

Figure 4.16 - Comparison between trend of efficiency increase in Munmorah HI ISCC and Perth HI ISCC.

Actually, this is not wholly exact because, even if the trends of the two cases are unequivocal and even if the differences in solar radiation are evident only in the hotter months of the year, it must be considered that, upstream, the dimensions of Perth solar installation are 34.68% smaller (see again table 4.7). This translates in a significant economical income due to saved capital expenditure that widely covers the abovementioned issue.
The same observations can be addressed to the trend of solar thermal power output and yearly produced energy, subordinated to the same issues and basis conditions. The comparison of annual trends of yearly-generated energy for both location of Munmorah and Perth can be found Figure 4.17.

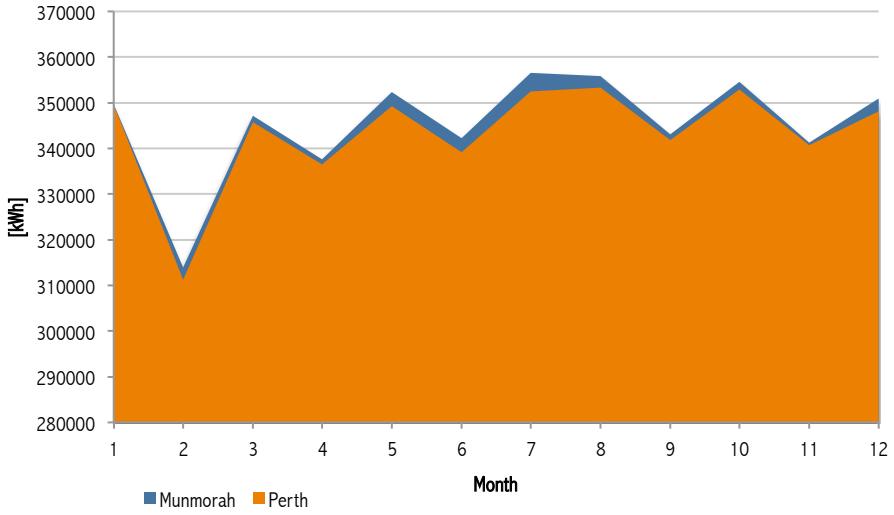

Figure 4.17 - comparison of annual trends of yearly-generated energy for Munmorah HI ISCC and Perth HI ISCC

Considering the energy balances of the four main cases[18], the total amount of energy delivered annually is resumed in the following table (Table 4.8):

[18] The order of the four cases has been set with Munmorah low-integration layout (Case 1) first, followed by Perth low-integration layout (Case 2), Munmorah high-integration layout (Case 3) and Perth high-integration layout (Case 4).

Table 4.8 - Annual energy produced the main power generation components of the system, in the four Cases

Parameter		*Case 1*	*Case 2*	*Case 3*	*Case 4*
SF energy	*[kWh]*	*161539624*	*221314800*	*190908393*	*168949486*
GT energy	*[kWh]*	*8614476300*	*8571826998*	*2875549032*	*2864006776*
ST energy	*[kWh]*	*3606806796*	*3569029255*	*1078832315*	*1087728374*
TOT energy	*[kWh]*	*12382822720*	*12362171053*	*4145289740*	*4120684636*

Once more, it need to be taken into consideration that in high solar integration cases (Case 3 and Case 4) the solar field has been sized basing on the same rated power output, in order to see financial benefits on capital costs. On the contrary, in low solar integration systems, the sizes of the solar field are the same, enlightening the benefits on yearly solar energy production (+37% in Perth, see Figure 4.18).

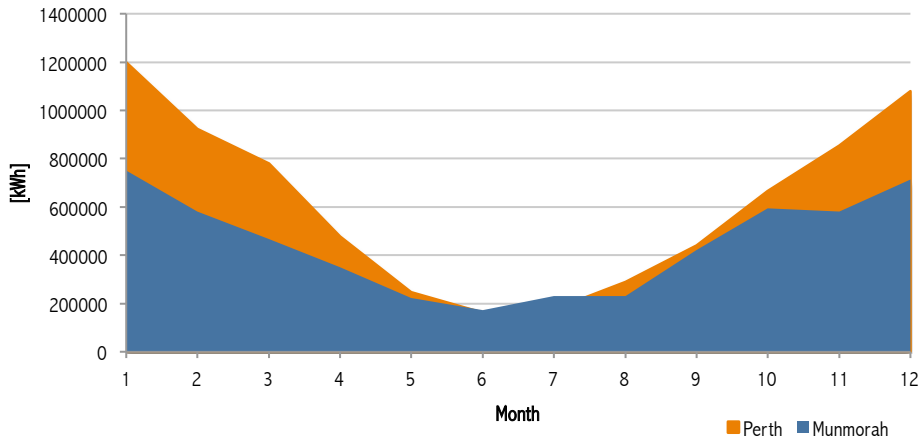

Figure 4.18 - Difference on daily energy production [kWh] between the two low solar integration cases, with the same solar field sizes.

Furthermore, with the aim of understanding the behaviour of the solar field during the day and the weight of the energy it produces in the overall energy balance, it is useful to compare the most productive hour of the sample day of each month with two other parameters: the total solar energy produced by the CSP system (see Figure 4.19 for low solar integration system and Figure 4.20 for high solar integration system) and the total energy produced by the ISCC

in the same time lapse (see Figure 4.21 for low solar integration system and Figure 4.22 for high solar integration system). In this case, the chosen location for the studio is Perth because of wider-range behaviour through seasons.

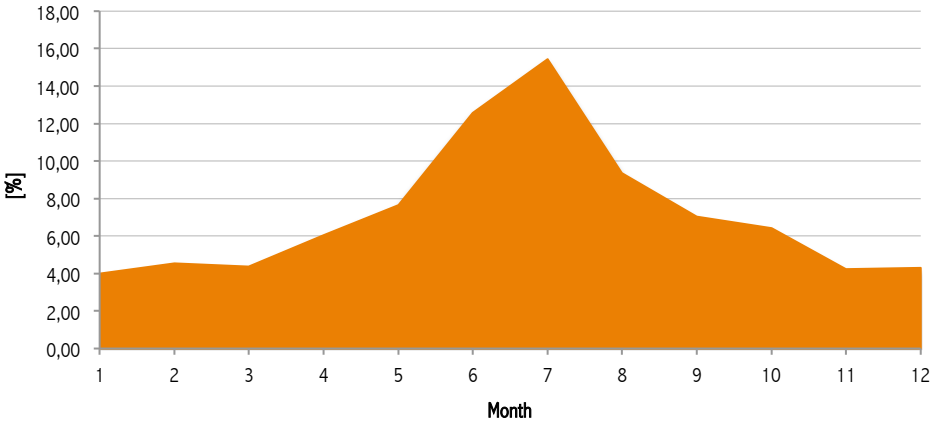

Figure 4.19 - Incidence of solar field "best hour" compared to the solar daily energy output, for the sample day of each month in the low solar integration Perth system

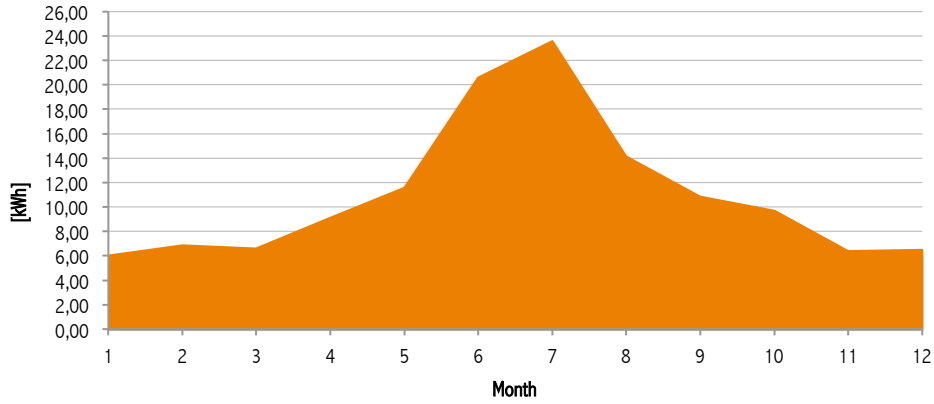

Figure 4.20 - Incidence of solar field "best hour" compared to the solar daily energy output, for the sample day of each month in the high solar integration Perth system

From above figures it can be noticed that, in both cases, in winter, the contribution of the central hour of the day is more than relevant, especially in

the high solar integration system with more than 23,5% coverage. On the contrary, in summer, the energy production of the solar field is more constant during the whole day and thus the incidence of the central hour is lower.
If we take the ISCC produced energy in the solar field best hour as term of comparison, the results "reverses" (see Figures 4.21 and 4.22);

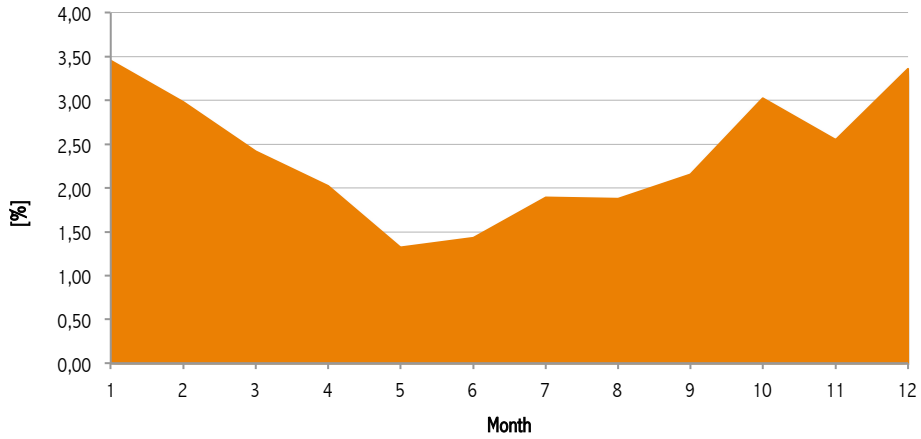

Figure 4.21 - Incidence of solar field "best hour" compared to the total ISCC energy output, for the sample day of each month in the low solar integration Perth system

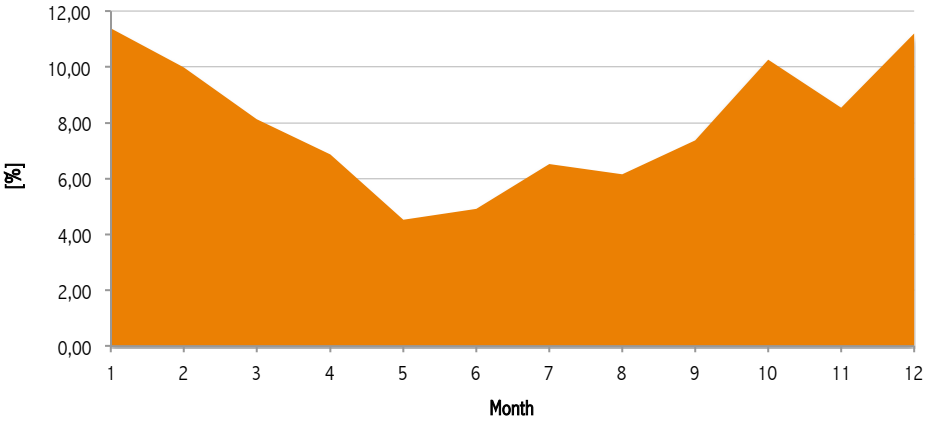

Figure 4.22 - Incidence of solar field "best hour" compared to the total ISCC energy output, for the sample day of each month in the high solar integration Perth system

In this second case, the solar contribution reflects the expected trend, being greater in winter and decreasing constantly with the lowest peak in May. The hourly contribution reaches a top 11,39% of share in January and for the high solar integration system, while for the other configuration the obtained maximum is much lower (3,45%), in January too.

In conclusion, for completing the studio on energy, the annual behaviour of the different components of the systems has been analysed. The annual energy produced by each sub-system has been quantified and put in a pie chart (see Figure 4.23) to obtain an immediate visual feedback.

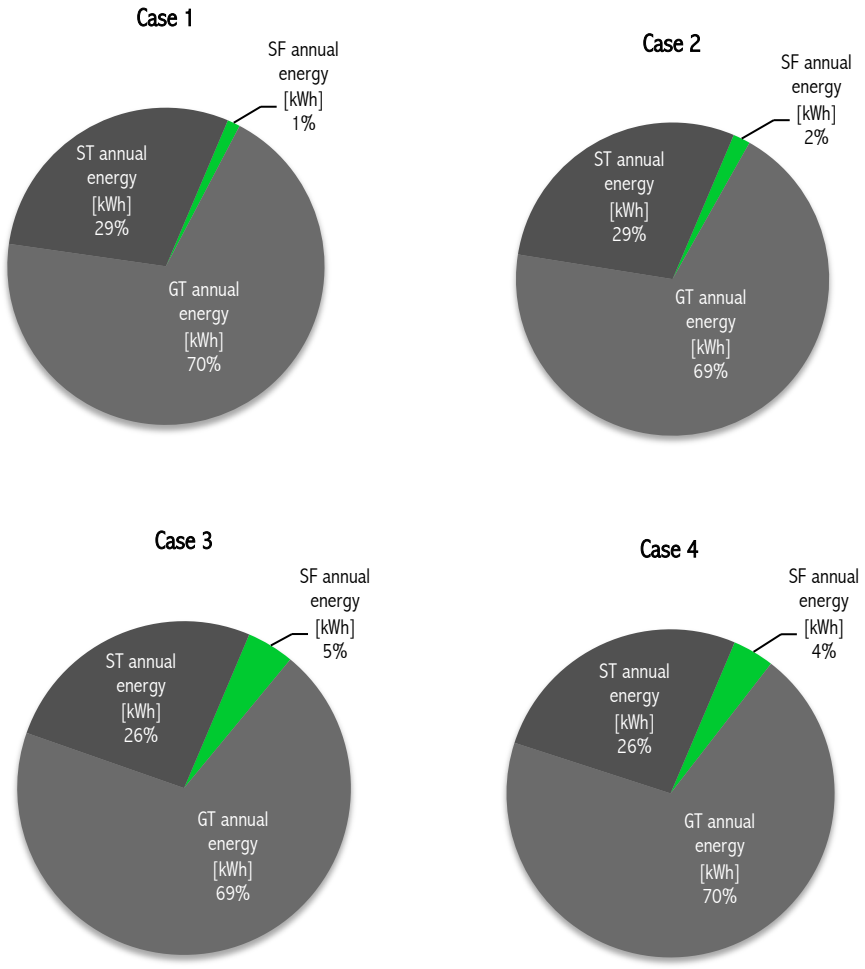

Figure 4.23 - Annual energy balances in Munmorah low solar integration (top left), Perth low solar integration (top right), Munmorah high solar integration (bottom left) and Perth high solar integration (bottom right)

As can bee seen from above figures, if we consider the two low solar integration systems, it is evident that the contribution of CSP generated energy is extremely low (2% in the best case, 1% in the worst) and thus almost negligible. In case of high solar integration, this percentage grows to a maximum of 5% for Munmorah and remains almost constant for Perth (4%) despite of 34,68% lower reflector aperture area. We could suppose that with a equally-sided solar field, the contribution of CSP energy would raise to 7÷8 %.

Conclusions

The study enlightens all the benefits and criticisms of ISCC hybrid systems. If compared to traditional coal-based facilities ISCCs have a much higher efficiency (approximately +15%) but with CO_2 emission cut to one third. The results also give an idea of different levels of solar integration, accenting high solar integration systems as a more sensible and preferable solution for who decide to have a net solar contribution. But also in the case of low solar integration, despite of an average 2% efficiency decrease due to solar field power cycle unable to exploit gas turbine benefits, the CO_2 reduction percentage is doubled, raising -4%.
Off design simulations confirm the big influence of environmental conditions on ISCC performances. In particular, of course DNI is a key parameter that need to be carefully evaluated during the design process, but also ambient temperature for its relation with turbogenerators power output, especially for low solar integration systems in the summer period.
More generally, the results of this thesis are the further confirmation that the needed change is possible. But huge efforts must be done to reduce the cost gap (measures according to the LCOE index) with conventional technologies that are still too far for competing in the global energy market.
To achieve this important target, a united action must be done, involving research and development on one side and States and governments on the other side, in order to rewrite the parameters of choice of big financial backers
On the "technology side" what can be done is huge; at first, synergies with industries can make the costs for solar field significantly lower, spreading a larger adoption and sustaining the development of related large-scale mechanisms. In this context, ISCC could have a key role to accelerate this process, being the missing link between fossil fuels and new renewable solutions. Hybrid systems, in comparison with coal-based facilities, have been proven as able to highly increase performances on one hand, significantly reducing polluting emissions on the other hand.
But all these efforts are not sufficient if considered isolated. On the "policy side", in fact, States and Governments must act together in order to sustain the development of the technology with concrete and rapid measure such as incentives and feed-in tariffs. This is absolutely mandatory.
But what should be done for boosting the renewable global scenario is to introduce a strong "carbon tax" with the aim of discouraging fossil-based energy by taxing it, reinvesting the related incomes for making renewable, and

thus solar, energy prices decrease. The effects on LCOE would be immediate, attracting private investors' capitals with the secondary effect of quickening the enhancement.

Appendices

Appendix 1.
Australian Coal Plants

NAME	STATE	OWNED	FUEL TYPE	TECHNOLOGY	N. ST	ST CAPACITY	N. ST	ST CAPACITY	N. ST	ST CAPACITY	TOTAL CAPACITY	UNITS	COMMISSION (lastest)	COMMISSION (to)	COMMISSION (first)
Mount Piper	NSW	Delta Electricty	Black Coal	Steam Turbine	2	660	0	0	0	0	1320	MW	1992	1993	-
Anglesea	VIC	Alcoa	Brown Coal	Steam Turbine	1	150	0	0	0	0	150	MW	1969	-	-
Bayswater	NSW	Macquarie Generation	Black Coal	Steam Turbine	4	660	0	0	0	0	2640	MW	1982	1984	-
Callide A&B	QLD	CS Energy	Black Coal	Steam Turbine	1	820	0	0	0	0	820	MW	1998	-	1965
Callide C	QLD	CS Energy (50%) and (50%) OzGen BV	Black Coal	Steam Turbine	2	450	0	0	0	0	900	MW	2001	-	-
Collie A	WA	Verve Energy	Black Coal	Steam Turbine	1	330	0	0	0	0	330	MW	1999	-	-
Collinsville	QLD	Transfield Services	Black Coal	Steam Turbine	1	180	0	0	0	0	180	MW	1998	-	1968
Eraring	NSW	Eraring Energy	Black Coal	Steam Turbine	4	660	0	0	0	0	2640	MW	1982	1984	-
Gladstone A&B	QLD	Comalco/NRG (37.5%)	Black Coal	Steam Turbine	6	280	0	0	0	0	1680	MW	1976	1982	-
Hazelwood	VIC	International Power Hazelwood	Brown Coal	Steam Turbine	8	200,4	0	0	0	0	1603,2	MW	1964	1971	-
Liddell	NSW	Macquarie Generation	Black Coal	Steam Turbine	4	515	0	0	0	0	2060	MW	2006	-	1971
Loy Yang A	VIC	Loy Yang Power Ltd	Brown Coal	Steam Turbine	4	540	0	0	0	0	2160	MW	1984	1987	-
Loy Yang B	VIC	International Power plc (70%)	Brown Coal	Steam Turbine	2	513	0	0	0	0	1026	MW	1993	1996	-
Morwell	VIC	Energy Brix	Brown Coal	Steam Turbine	1	20	3	30	1	60	170	MW	1958	1962	-
Muja A B C&D	WA	Verve Energy	Black Coal	Steam Turbine	4	60	2	200	2	227	1094	MW	1986	-	1965
Munmorah	NSW	Delta Electricty	Black Coal	Steam Turbine	2	300	0	0	0	0	600	MW	1969	-	-
Northern	SA	Alinta Energy	Black Coal	Steam Turbine	2	270	0	0	0	0	540	MW	1985	-	-
Stanwell	QLD	Stanwell Corp (33% NRG)	Black Coal	Steam Turbine	4	350	0	0	0	0	1400	MW	1993	1996	-
Swanbank A&B	QLD	CS Energy	Black Coal	Steam Turbine	4	120	0	0	0	0	480	MW	1966	1973	-
Tarong A&B	QLD	Tarong Energy	Black Coal	Steam Turbine	4	350	0	0	0	0	1400	MW	1983	1986	-
Thomas Playford B	SA	Alinta Energy	Black Coal	Steam Turbine	4	60	0	0	0	0	240	MW	1960	-	-
Vales Point B	NSW	Delta Electricty	Black Coal	Steam Turbine	2	660	0	0	0	0	1320	MW	1978	-	-
Wallerawang C	NSW	Delta Electricty	Black Coal	Steam Turbine	2	500	0	0	0	0	1000	MW	1976	1980	-
Worsley	WA	Worsley Alumina	Black Coal	Cogeneration	3	45	0	0	0	0	135	MW	1982	-	-
Yabulu	QLD	Queensland Nickel	Black Coal	Steam (cogeneration)	3	12,5	0	0	0	0	37,5	MW	1974	-	-
Yallourn W A&B	VIC	Auspower	Brown Coal	Steam Turbine	2	350	2	375	0	0	1450	MW	1982	-	1975
Gladstone QA	QLD	Queensland Alumina	Black Coal	Steam (cogeneration)	2	13	0	0	0	0	26	MW	1973	-	-
Millmerran	QLD	Millmerran Power Partners	Black Coal	Steam Turbine	2	420	0	0	0	0	840	MW	2003	-	-
Redbank	NSW	Alinta Energy/National Power Corporation (USA)	Black Coal	Fluidised Bed	1	150	0	0	0	0	150	MW	2001	-	-
Tarong North	QLD	Tarong Energy	Black Coal	Steam Turbine	1	445	0	0	0	0	445	MW	2003	-	-
Kogan Creek	QLD	CS Energy	Black Coal	Steam Turbine	1	750	0	0	0	0	750	MW	2007	-	-
Monash - Flynn	VIC	Monash Energy	Brown Coal	Gasification	1	220	0	0	0	0	220	MW	2007	2016	-
Bluewaters 1&2	WA	Griffin Energy Pty Ltd	Black Coal	Steam Turbine	2	208	0	0	0	0	416	MW	2009	-	-
Kwinana - HydrogenEnergy	WA	Hydrogen Energy (BP & Rio Tinto Joint Venture)	Black Coal	Gasification	1	500	0	0	0	0	500	MW	2011	-	-
Redbank 2	NSW	National Power Partners(USA) & Babcock&Brown	Black Coal	Fluidised Bed	1	132	0	0	0	0	132	MW	2005	-	-

Appendix 2.
Munmorah statistics

Temperature [°C]																							
Jan	*20,0*	*20,0*	*19,3*	*19,2*	*18,9*	*20,0*	*21,0*	*22,6*	*23,7*	*25,2*	*26,6*	*27,4*	*27,8*	*27,2*	*27,3*	*26,4*	*26,1*	*24,4*	*23,4*	*22,3*	*22,0*	*21,4*	*20,9*	*20,5*
Feb	*19,2*	*18,8*	*18,3*	*18,2*	*18,1*	*19,1*	*20,1*	*21,8*	*22,7*	*24,0*	*24,8*	*25,9*	*26,3*	*26,4*	*26,1*	*25,5*	*25,2*	*24,1*	*23,4*	*22,2*	*22,0*	*21,3*	*20,6*	*19,8*
Mar	*18,8*	*18,1*	*17,5*	*16,9*	*16,8*	*16,5*	*18,1*	*19,4*	*21,8*	*22,7*	*24,2*	*24,9*	*25,8*	*25,8*	*25,3*	*24,5*	*23,6*	*23,0*	*21,8*	*21,2*	*20,4*	*20,3*	*19,9*	*19,4*
Apr	*15,5*	*14,9*	*14,8*	*13,9*	*13,9*	*13,7*	*15,2*	*16,6*	*18,8*	*20,1*	*21,8*	*22,8*	*23,9*	*24,0*	*23,5*	*22,5*	*21,3*	*20,1*	*18,9*	*18,0*	*17,3*	*16,8*	*16,4*	*15,9*
May	*11,7*	*11,5*	*11,5*	*11,1*	*11,1*	*11,2*	*12,0*	*13,0*	*14,3*	*15,7*	*17,1*	*18,1*	*18,9*	*19,0*	*18,8*	*17,7*	*16,6*	*15,0*	*14,2*	*13,2*	*13,0*	*12,1*	*11,9*	*11,8*
Jun	*10,4*	*10,1*	*10,1*	*9,6*	*9,5*	*9,7*	*10,2*	*11,2*	*12,2*	*13,8*	*15,1*	*16,4*	*16,9*	*17,1*	*17,0*	*16,1*	*15,1*	*13,6*	*13,0*	*12,2*	*12,1*	*11,1*	*10,9*	*10,7*
Jul	*9,2*	*8,7*	*8,2*	*7,7*	*7,4*	*7,6*	*8,1*	*9,1*	*10,5*	*12,3*	*13,9*	*15,4*	*16,2*	*16,5*	*16,1*	*15,3*	*14,1*	*12,8*	*11,8*	*10,9*	*10,4*	*9,9*	*9,7*	*9,5*
Aug	*9,8*	*9,3*	*8,9*	*8,5*	*8,4*	*8,6*	*9,4*	*10,6*	*12,1*	*13,8*	*15,5*	*16,8*	*17,6*	*17,9*	*17,6*	*16,9*	*15,8*	*14,6*	*13,5*	*12,5*	*11,9*	*11,3*	*10,8*	*10,4*
Sep	*12,3*	*11,7*	*11,3*	*10,7*	*10,6*	*10,8*	*12,1*	*13,6*	*15,7*	*17,1*	*18,8*	*19,8*	*20,6*	*20,6*	*20,0*	*19,1*	*18,0*	*17,1*	*15,9*	*15,1*	*14,3*	*14,0*	*13,5*	*13,0*
Oct	*14,1*	*13,7*	*13,7*	*13,3*	*13,5*	*13,8*	*15,6*	*17,3*	*19,4*	*20,2*	*21,3*	*21,7*	*22,5*	*22,4*	*21,9*	*20,8*	*19,7*	*18,8*	*17,8*	*17,0*	*16,3*	*15,8*	*15,3*	*14,8*
Nov	*15,8*	*15,7*	*14,8*	*14,7*	*14,3*	*15,6*	*16,8*	*18,7*	*19,7*	*21,1*	*22,1*	*22,9*	*23,1*	*22,6*	*22,3*	*21,4*	*20,9*	*19,8*	*19,1*	*18,4*	*18,0*	*17,6*	*17,0*	*16,5*
Dec	*18,2*	*18,0*	*17,4*	*17,4*	*17,4*	*18,7*	*19,9*	*21,5*	*22,7*	*24,0*	*25,2*	*25,7*	*25,9*	*25,3*	*25,3*	*24,6*	*24,3*	*23,1*	*22,3*	*21,4*	*21,0*	*20,4*	*19,7*	*19,0*
Relative humidity [%]																								
Jan	*79*	*80*	*84*	*85*	*85*	*82*	*77*	*73*	*65*	*60*	*54*	*54*	*53*	*57*	*55*	*58*	*59*	*65*	*68*	*73*	*73*	*75*	*76*	*77*
Feb	*88*	*90*	*91*	*92*	*92*	*89*	*85*	*80*	*75*	*70*	*66*	*62*	*61*	*61*	*61*	*64*	*66*	*70*	*74*	*77*	*80*	*82*	*84*	*86*
Mar	*89*	*91*	*90*	*93*	*93*	*92*	*88*	*83*	*77*	*72*	*67*	*63*	*62*	*62*	*64*	*66*	*69*	*73*	*77*	*81*	*84*	*85*	*87*	*88*
Apr	*84*	*86*	*87*	*89*	*90*	*90*	*85*	*79*	*71*	*66*	*60*	*59*	*54*	*53*	*52*	*57*	*60*	*67*	*70*	*74*	*77*	*80*	*81*	*82*
May	*89*	*89*	*92*	*92*	*93*	*92*	*92*	*88*	*83*	*78*	*72*	*70*	*66*	*66*	*65*	*70*	*74*	*82*	*84*	*87*	*87*	*89*	*89*	*89*
Jun	*77*	*78*	*83*	*83*	*86*	*83*	*85*	*82*	*80*	*71*	*66*	*60*	*60*	*59*	*60*	*63*	*66*	*71*	*74*	*76*	*76*	*77*	*77*	*76*
Jul	*75*	*75*	*79*	*79*	*81*	*80*	*81*	*78*	*74*	*66*	*60*	*55*	*52*	*50*	*50*	*53*	*57*	*63*	*66*	*70*	*72*	*75*	*75*	*75*
Aug	*77*	*77*	*80*	*80*	*80*	*79*	*77*	*72*	*65*	*59*	*54*	*51*	*47*	*46*	*45*	*49*	*54*	*61*	*64*	*69*	*71*	*74*	*75*	*75*
Sep	*80*	*81*	*82*	*84*	*84*	*84*	*79*	*73*	*65*	*60*	*55*	*52*	*49*	*49*	*50*	*53*	*57*	*62*	*67*	*71*	*74*	*76*	*78*	*79*
Oct	*83*	*85*	*85*	*88*	*87*	*86*	*79*	*72*	*66*	*61*	*57*	*55*	*55*	*57*	*61*	*62*	*66*	*68*	*72*	*74*	*75*	*76*	*78*	*80*
Nov	*87*	*87*	*89*	*89*	*90*	*84*	*79*	*72*	*69*	*64*	*62*	*60*	*60*	*62*	*63*	*67*	*69*	*73*	*76*	*79*	*80*	*81*	*83*	*85*
Dec	*87*	*89*	*91*	*91*	*89*	*84*	*79*	*72*	*67*	*62*	*59*	*56*	*56*	*57*	*58*	*61*	*63*	*67*	*70*	*75*	*76*	*78*	*81*	*84*
DNI [W/m^2]																								
Jan	*0*	*0*	*0*	*0*	*0*	*48*	*341*	*476*	*499*	*605*	*609*	*612*	*668*	*579*	*577*	*521*	*409*	*163*	*4*	*0*	*0*	*0*	*0*	*0*
Feb	*0*	*0*	*0*	*0*	*0*	*14*	*196*	*339*	*369*	*421*	*480*	*547*	*622*	*605*	*532*	*490*	*330*	*126*	*1*	*0*	*0*	*0*	*0*	*0*
Mar	*0*	*0*	*0*	*0*	*0*	*3*	*166*	*435*	*495*	*469*	*389*	*413*	*479*	*512*	*535*	*425*	*208*	*15*	*0*	*0*	*0*	*0*	*0*	*0*
Apr	*0*	*0*	*0*	*0*	*0*	*0*	*46*	*403*	*482*	*485*	*484*	*478*	*435*	*497*	*432*	*336*	*45*	*0*	*0*	*0*	*0*	*0*	*0*	*0*
May	*0*	*0*	*0*	*0*	*0*	*0*	*8*	*182*	*405*	*414*	*418*	*469*	*450*	*476*	*414*	*201*	*6*	*0*	*0*	*0*	*0*	*0*	*0*	*0*
Jun	*0*	*0*	*0*	*0*	*0*	*0*	*1*	*137*	*393*	*482*	*507*	*500*	*409*	*394*	*377*	*149*	*1*	*0*	*0*	*0*	*0*	*0*	*0*	*0*
Jul	*0*	*0*	*0*	*0*	*0*	*0*	*2*	*190*	*471*	*583*	*558*	*559*	*507*	*470*	*390*	*172*	*7*	*0*	*0*	*0*	*0*	*0*	*0*	*0*
Aug	*0*	*0*	*0*	*0*	*0*	*0*	*30*	*379*	*502*	*495*	*445*	*416*	*437*	*482*	*482*	*352*	*30*	*0*	*0*	*0*	*0*	*0*	*0*	*0*
Sep	*0*	*0*	*0*	*0*	*0*	*3*	*139*	*343*	*472*	*494*	*540*	*509*	*489*	*519*	*463*	*355*	*93*	*1*	*0*	*0*	*0*	*0*	*0*	*0*
Oct	*0*	*0*	*0*	*0*	*0*	*57*	*311*	*495*	*556*	*618*	*562*	*566*	*570*	*542*	*446*	*383*	*150*	*4*	*0*	*0*	*0*	*0*	*0*	*0*
Nov	*0*	*0*	*0*	*0*	*5*	*135*	*368*	*472*	*487*	*455*	*418*	*413*	*449*	*496*	*511*	*451*	*275*	*35*	*0*	*0*	*0*	*0*	*0*	*0*
Dec	*0*	*0*	*0*	*0*	*5*	*110*	*321*	*477*	*483*	*500*	*556*	*572*	*618*	*641*	*605*	*517*	*321*	*115*	*2*	*0*	*0*	*0*	*0*	*0*

Appendix 3.
Perth statistics

Temperature [°C]																							
Jan	*18,6*	*17,7*	*17,7*	*16,8*	*17*	*17*	*19,1*	*20,9*	*23,7*	*25,4*	*27,5*	*29,2*	*30,4*	*30,9*	*30,2*	*29,8*	*28,6*	*27,8*	*25,6*	*24,2*	*22,4*	*21,7*	*20,6*	*19,5*
Feb	*21*	*20,3*	*20*	*19,1*	*18,9*	*18,6*	*20*	*21,3*	*23,5*	*25,1*	*27*	*28,7*	*29,9*	*30,5*	*30,2*	*29,9*	*28,9*	*28,2*	*26,4*	*25,2*	*23,8*	*23,2*	*22,4*	*21,7*
Mar	*18,8*	*18,2*	*18,3*	*17,3*	*17,2*	*16,8*	*18,3*	*19,6*	*21,7*	*23,3*	*25,3*	*27,1*	*28,2*	*28,8*	*28,2*	*27,9*	*26,6*	*25,6*	*23,7*	*22,4*	*21,2*	*20,5*	*19,9*	*19,1*
Apr	*16,1*	*15,8*	*15,8*	*15,2*	*15,1*	*15*	*15,8*	*16,7*	*18,2*	*19,5*	*21,1*	*22,5*	*23,3*	*23,7*	*23,3*	*22,9*	*21,9*	*20,9*	*19,4*	*18,3*	*17,3*	*16,8*	*16,4*	*16*
May	*13,2*	*13*	*12,8*	*12,4*	*12,2*	*12,2*	*12,8*	*13,7*	*15*	*16,5*	*18,1*	*19,5*	*20,4*	*20,8*	*20,5*	*19,7*	*18,5*	*17,1*	*15,8*	*14,7*	*14*	*13,5*	*13,3*	*13,2*
Jun	*11,9*	*11,6*	*11,3*	*11*	*10,8*	*11*	*11,3*	*12,2*	*13,2*	*14,9*	*16,3*	*17,7*	*18,4*	*18,7*	*18,4*	*17,7*	*16,6*	*15,3*	*14,2*	*13,3*	*12,7*	*12,3*	*12,1*	*11,9*
Jul	*10,8*	*10,6*	*10,3*	*10,1*	*9,9*	*10*	*10,2*	*10,9*	*11,9*	*13,4*	*14,8*	*16,2*	*17*	*17,4*	*17,2*	*16,5*	*15,5*	*14,2*	*13,1*	*12,1*	*11,5*	*11*	*10,8*	*10,8*
Aug	*10,7*	*10,3*	*10,1*	*9,7*	*9,6*	*9,8*	*10,3*	*11,2*	*12,3*	*13,8*	*15,2*	*16,6*	*17,2*	*17,5*	*17,1*	*16,7*	*15,8*	*14,9*	*13,8*	*12,9*	*12,2*	*11,7*	*11,3*	*10,8*
Sep	*11*	*10,6*	*10,5*	*10,1*	*10,2*	*10,4*	*11,6*	*12,8*	*14,6*	*15,8*	*17,3*	*18,3*	*19,2*	*19,5*	*19,3*	*18,6*	*17,7*	*16,7*	*15,5*	*14,4*	*13,5*	*12,8*	*12,2*	*11,6*
Oct	*13*	*12,5*	*12,5*	*11,9*	*12,1*	*12,1*	*13,8*	*15,2*	*17,4*	*18,6*	*20,1*	*21*	*21,9*	*22*	*21,5*	*20,8*	*19,7*	*18,8*	*17,4*	*16,4*	*15,4*	*14,9*	*14,2*	*13,5*
Nov	*14,8*	*14,2*	*14,2*	*13,6*	*13,9*	*14*	*15,8*	*17,3*	*19,6*	*20,8*	*22,3*	*23,3*	*24,2*	*24,3*	*23,9*	*23,2*	*22,1*	*21,2*	*19,8*	*18,8*	*17,6*	*17,1*	*16,3*	*15,7*
Dec	*18,7*	*18,2*	*18,5*	*17,7*	*18*	*17,9*	*19,9*	*21,5*	*24*	*25,3*	*27,1*	*28,3*	*29,4*	*29,7*	*29,1*	*28,6*	*27,4*	*26,4*	*24,6*	*23,3*	*21,9*	*21*	*20,1*	*19,1*
Relative humidity [%]																								
Jan	*71*	*74*	*72*	*75*	*73*	*72*	*63*	*56*	*48*	*42*	*37*	*33*	*32*	*32*	*35*	*35*	*39*	*41*	*48*	*53*	*59*	*61*	*65*	*70*
Feb	*61*	*63*	*63*	*66*	*67*	*69*	*63*	*58*	*51*	*47*	*42*	*38*	*37*	*36*	*38*	*38*	*41*	*42*	*47*	*50*	*55*	*55*	*57*	*58*
Mar	*60*	*61*	*60*	*63*	*63*	*65*	*60*	*55*	*48*	*44*	*39*	*35*	*33*	*33*	*35*	*36*	*39*	*42*	*48*	*51*	*55*	*57*	*58*	*60*
Apr	*76*	*77*	*77*	*78*	*79*	*78*	*76*	*73*	*68*	*61*	*56*	*50*	*49*	*47*	*49*	*50*	*53*	*58*	*63*	*69*	*73*	*76*	*77*	*78*
May	*80*	*80*	*82*	*82*	*84*	*83*	*83*	*79*	*75*	*67*	*61*	*56*	*53*	*51*	*51*	*53*	*58*	*64*	*69*	*75*	*78*	*81*	*81*	*80*
Jun	*80*	*80*	*81*	*81*	*82*	*82*	*82*	*79*	*76*	*68*	*63*	*58*	*56*	*56*	*56*	*60*	*64*	*70*	*74*	*79*	*81*	*83*	*83*	*82*
Jul	*84*	*83*	*86*	*85*	*87*	*86*	*88*	*85*	*81*	*74*	*68*	*63*	*59*	*57*	*57*	*60*	*64*	*71*	*76*	*82*	*85*	*88*	*87*	*85*
Aug	*87*	*88*	*91*	*90*	*91*	*89*	*89*	*85*	*82*	*73*	*66*	*59*	*58*	*56*	*57*	*59*	*63*	*67*	*73*	*78*	*82*	*85*	*86*	*87*
Sep	*84*	*84*	*85*	*86*	*86*	*85*	*81*	*77*	*71*	*65*	*59*	*55*	*52*	*51*	*52*	*54*	*58*	*62*	*68*	*73*	*78*	*80*	*82*	*84*
Oct	*81*	*83*	*82*	*83*	*82*	*80*	*74*	*68*	*60*	*56*	*51*	*48*	*46*	*46*	*48*	*50*	*54*	*58*	*64*	*68*	*73*	*75*	*78*	*80*
Nov	*73*	*75*	*75*	*77*	*77*	*77*	*69*	*62*	*54*	*50*	*45*	*42*	*40*	*40*	*42*	*45*	*48*	*51*	*56*	*60*	*65*	*65*	*67*	*69*
Dec	*65*	*66*	*64*	*66*	*64*	*65*	*57*	*51*	*44*	*41*	*37*	*35*	*33*	*33*	*34*	*36*	*39*	*43*	*47*	*51*	*55*	*58*	*61*	*65*
DNI [W/m^2]																								
Jan	*0*	*0*	*0*	*0*	*0*	*17*	*379*	*575*	*739*	*814*	*895*	*964*	*967*	*989*	*947*	*882*	*726*	*534*	*46*	*0*	*0*	*0*	*0*	*0*
Feb	*0*	*0*	*0*	*0*	*0*	*1*	*233*	*607*	*704*	*737*	*689*	*739*	*716*	*735*	*715*	*670*	*620*	*479*	*20*	*0*	*0*	*0*	*0*	*0*
Mar	*0*	*0*	*0*	*0*	*0*	*0*	*34*	*478*	*629*	*723*	*753*	*752*	*770*	*744*	*732*	*652*	*548*	*183*	*2*	*0*	*0*	*0*	*0*	*0*
Apr	*0*	*0*	*0*	*0*	*0*	*0*	*9*	*300*	*539*	*639*	*608*	*580*	*615*	*603*	*602*	*527*	*282*	*9*	*0*	*0*	*0*	*0*	*0*	*0*
May	*0*	*0*	*0*	*0*	*0*	*0*	*0*	*109*	*397*	*407*	*458*	*485*	*470*	*462*	*455*	*388*	*69*	*0*	*0*	*0*	*0*	*0*	*0*	*0*
Jun	*0*	*0*	*0*	*0*	*0*	*0*	*0*	*21*	*319*	*401*	*460*	*483*	*474*	*406*	*328*	*214*	*20*	*0*	*0*	*0*	*0*	*0*	*0*	*0*
Jul	*0*	*0*	*0*	*0*	*0*	*0*	*0*	*24*	*285*	*384*	*423*	*450*	*430*	*360*	*394*	*329*	*50*	*0*	*0*	*0*	*0*	*0*	*0*	*0*
Aug	*0*	*0*	*0*	*0*	*0*	*0*	*2*	*156*	*411*	*501*	*517*	*488*	*432*	*412*	*393*	*346*	*156*	*3*	*0*	*0*	*0*	*0*	*0*	*0*
Sep	*0*	*0*	*0*	*0*	*0*	*0*	*57*	*309*	*463*	*464*	*491*	*504*	*481*	*458*	*460*	*431*	*343*	*22*	*0*	*0*	*0*	*0*	*0*	*0*
Oct	*0*	*0*	*0*	*0*	*0*	*8*	*262*	*447*	*484*	*548*	*594*	*610*	*627*	*633*	*600*	*551*	*451*	*116*	*0*	*0*	*0*	*0*	*0*	*0*
Nov	*0*	*0*	*0*	*0*	*0*	*37*	*441*	*589*	*636*	*672*	*716*	*674*	*661*	*685*	*626*	*559*	*447*	*203*	*4*	*0*	*0*	*0*	*0*	*0*
Dec	*0*	*0*	*0*	*0*	*0*	*51*	*503*	*646*	*664*	*668*	*751*	*792*	*829*	*838*	*767*	*744*	*687*	*566*	*35*	*0*	*0*	*0*	*0*	*0*

Appendix 4.
Munmorah power station technical details

BOILERS

Number	4 x 350MW
Stop valve pressure	165,36 bar
Stop valve temperature	568,33 °C
RH pressure (inlet)	43,33 bar
RH pressure (outlet)	40,92 bar
RH temperature (inlet)	372,2 °C
RH temperature (outlet)	540,5 °C
Evaporation	308,69 kg/s

TURBINES

Number	4 x 350 MW (inactive)
Operating speed	3000 rpm
Number of steam turbines	2 x 300 MW

Turbine

Stop valve pressure	158,47 bar
Stop valve temperature	565,5 °C
RH pressure	37,89 bar
RH temperature	537,8 °C

Generator

Output	350 MW
Voltage	17,5 kV
Current	12840 A

Condenser

Number of tubes	34000 (per unit)
Number of units	4
Cooling water pumps	2 (per unit)
Cooling water pumps capacity	408362 l/h (each)
Total cooling water	3276000 l/h

FRESH WATER

Source	Hunter district water board
Storage	2 x 2957500 l
Demineralizing plant capacity	3185000 l/day

Appendix 5.
Munmorah coal layout in Thermoflex

Net power	599997 kW
Net electric efficiency	40,58 %
Net heat rate (LHV)	8872 kJ/kWh
Net fuel input (LHV)	1478692 kW
$P_{AUX,TOT}$	39902 kW
CO_2 yearly emissions	4037348 kg/year
CO_2 spec. emissions	778,9 kg/MWh

Figure 1 – Steam cycle layout

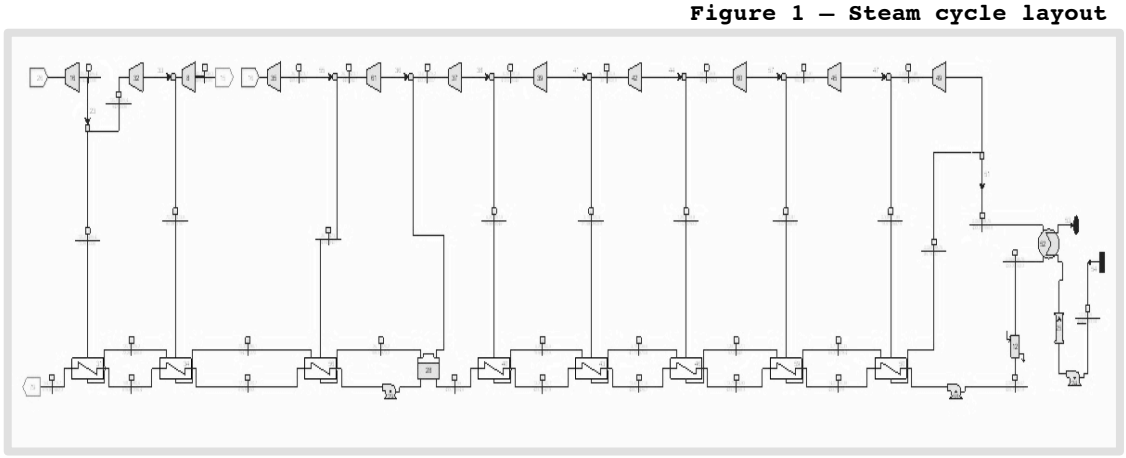

CONDENSER

Q	774553 kW
T_{SAT}	38,76 °C
P_{PUMP}	5677 kW
m flow (H_2O)	45420 kg/s
$T_{H2O,in}$	15°C
$T_{H20,out}$	19,07 °C
ΔT	4,07°C

Inlet

P	0,0690 bar
T	38,76 °C
x	0,748
h	1965,44 kJ/kg
m flow	429,5 kg/s

Outlet

P	0,0690 bar
T	38,76 °C
x	0
h	162,24 kJ/kg
m flow	429,5 kg/s

STEAM TURBINE(s)

N. of regenerator(s)	8
N. of deareator(s)	1
N. of turbine stages	11
TIT (first stage)	565,5 °C
P_{IN} (first stage)	158,5 bar
h_{IN} (first stage)	3480,45 kJ/kg
T_{OUT} (last stage)	38,76 °C
P_{OUT} (last stage)	0,0690 bar
h_{OUT} (last stage)	2373,91 kJ/kg
x_{OUT} (last stage)	0,918
m flow (last stage)	344,9 kg/s
stage 1 efficiency	0,82
stage 2 efficiency	0,84
stage 3 to 9 efficiency	0,87
stage 10 efficiency	0,89
stage 11 efficiency	0,90
stage 11 exhaust loss	15 kJ/kg

ECONOMISER

T_{IN}	319,7 °C
T_{OUT}	339,4 °C
P_{IN}	164,9 bar
P_{OUT}	161,67 bar
h_{IN}	1452,31 kJ/kg
h_{OUT}	1585,51 kJ/kg
DT_ln	27,54 °C
Q	80837 kW

SUPERHEATER

T_{IN}	348,2 °C
T_{OUT}	565,5 °C
P_{IN}	161,67 bar
P_{OUT}	158,5 bar
h_{IN}	2579,75 kJ/kg
h_{OUT}	3480,45 kJ/kg
DT_ln	273,9 °C
Q	545035 kW

REHEATER

T_{IN}	369,4 °C
T_{OUT}	539,2°C
P_{IN}	43,33 bar
P_{OUT}	40,88 bar
h_{IN}	3136,62 kJ/kg
h_{OUT}	3533,07 kJ/kg
DT_ln	830,7 °C
Q	181388 kW

BOILER

Air excess	10%
Waterwall surface	1382,7 °C
Heat transfer to waterwall	601699 kW
Heat losses	9024 kW
Bottom ah mass flow	1,47 kg/s
Fly ash mass flow	5,88 kg/s
Flue gas composition (Mole)	
O2	1,79 %
CO2	15,71 %
H2O	8,11 %
N2	73,48 %
Ar	0,883 %
SO2	0,028 %

Figure 2 – Boiler layout

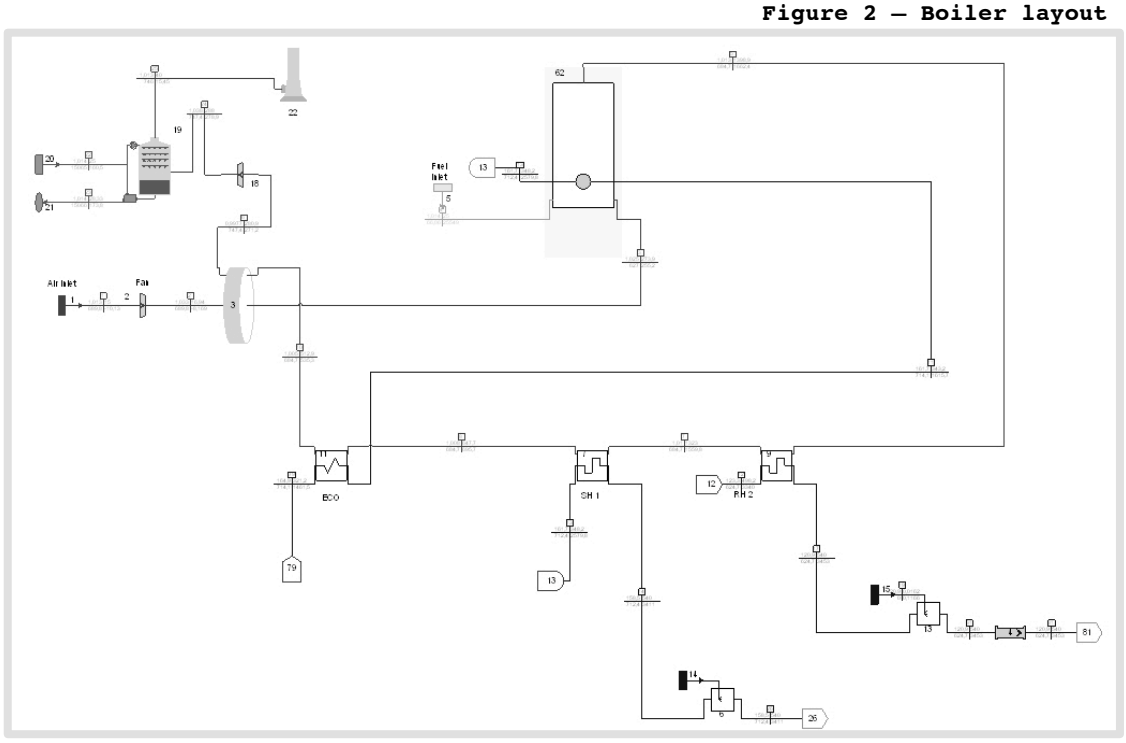

Boiler (water side)

T_{IN}	339,4 °C
T_{OUT}	348,2 °C
P_{IN}	161,67 bar
P_{OUT}	161,67 bar
h_{IN}	1585,51 kJ/kg
h_{OUT}	2579,75 kJ/kg
m flow	606,6 kg/s

Boiler (fuel side)

Type:	black coal
Source	Wallarah
P	1,01325 bar
T	25 °C
LHV	255493 MJ/nm^3
m flow	57,88 kg/s
m flow ash	7,350 kg/s

Boiler (air side)

T	273,9 °C
P	1,0251 bar
h	255,20 kJ/kg
m flow	549,4 kg/s
ρ	0,6503 kg/m^3

Boiler (outlet gases)

T	1398,9 °C
P	1,0126 bar
h	1662,37 kJ/kg
m $flow_{GAS}$	599,9 kg/s
m $flow_{ASH}$	5,880 kg/s

Appendix 6.
Munmorah NGCC layout in Thermoflow

Net power	1396626 kW
Net electric efficiency	55,17 %
Net heat rate (LHV)	6525 kJ/kWh
Net fuel input (LHV)	2531380 kW
$P_{AUX,TOT}$	26527 kW
CO_2 yearly emissions	4046268 kg/year
CO_2 spec. emissions	351 kg/MWh

CONDENSER

Q	767526 kW
T_{SAT}	39,25 °C
P_{PUMP}	5677 kW
m flow (H_2O)	45420 kg/s
$T_{H2O,in}$	15°C
$T_{H20,out}$	19,06 °C
ΔT	4,06°C

Inlet

P	0,0709 bar
T	39,25 °C
x	0,938
h	2422,65 kJ/kg
m flow	339,9 kg/s

Outlet

P	0,0709 bar
T	39,26 °C
x	0
h	164,39 kJ/kg
m flow	339,9 kg/s

TURBINE(s)

Steam

N. of regenerator(s)	0
N. of deareator(s)	0
N. of turbine stages	11
TIT (first stage)	565,5 °C
P_{IN} (first stage)	83,74 bar
h_{IN} (first stage)	3555,82 kJ/kg
T_{OUT} (last stage)	39,25 °C

P_{OUT} (last stage)	0,0709 bar
h_{OUT} (last stage)	2422,65 kJ/kg
x_{OUT} (last stage)	0,938
m flow (last stage)	339,9 kg/s
Stage 1 efficiency	0,82
Stage 2 efficiency	0,84
Stage 3 to 9 efficiency	0,87
Stage 10 efficiency	0,89
Stage 11 efficiency	0,90
Stage 11 exhaust loss	15 kJ/kg
total electrical power	453142 kW

Gas

Number of units	3
Turbine model	Mitsubishi 701G
Turbine rated power	334000 kW
TIT	1427,4 °C
$P_{IN,AIR}$	1,01325 bar
m $flow_{IN,AIR}$	729,7 kg/s
$P_{IN,FUEL}$	25 bar
m $flow_{IN,FUEL}$	16,86 kg/s
Fuel LHV	50046,7 kJ/kg
$T_{OUT,GASES}$	603,9 °C
$P_{OUT,GASES}$	1,074 bar
m $flow_{OUT,GASES}$	746,6 kg/s
unit shaft electrical power	323337 kW
total electrical power	970011 kW
Exhaust gas composition (Mole)	
O2	11,931 %
CO2	4,019 %
H2O	8,949 %
N2	74,208 %
Ar	0,894 %
SO2	0,000 %

ECONOMISER(s)

Low pressure

T_{IN}	39,4 °C
T_{OUT}	100,8 °C
P_{IN}	1,266 bar
P_{OUT}	1,241 bar
h_{IN}	163,55 kJ/kg
h_{OUT}	422,31 kJ/kg
DT_ln	60,58 °C
Q	88825 kW
m flow	343,3 kg/s

Intermediate pressure

T_{IN}	106,4 °C
T_{OUT}	226,4 °C
P_{IN}	29,25 bar
P_{OUT}	28,68 bar
h_{IN}	448,08 kJ/kg
h_{OUT}	973,3 kJ/kg
DT_ln	41,07 °C
Q	25525 kW
m flow	48,60 kg/s

High pressure 1

T_{IN}	107,7 °C
T_{OUT}	248,6 °C
P_{IN}	88,87 bar
P_{OUT}	87,13 bar
h_{IN}	458,00 kJ/kg
h_{OUT}	1078,94 kJ/kg
DT_ln	19 °C
Q	172360 kW
m flow	277,6 kg/s

High pressure 2

T_{IN}	248,6 °C
T_{OUT}	294,6 °C
P_{IN}	87,13 bar
P_{OUT}	85,42 bar
h_{IN}	1078,94 kJ/kg
h_{OUT}	1314,36 kJ/kg
DT_ln	33,81 °C
Q	65348 kW
m flow	277,6 kg/s

SUPERHEATER(s)

Low pressure

T_{IN}	133 °C
T_{OUT}	286,9 °C
P_{IN}	2,957 bar
P_{OUT}	2,899 bar
h_{IN}	2724,23 kJ/kg
h_{OUT}	3043,19 kJ/kg
DT_ln	37,75 °C
Q	5400 kW
m flow	16,93 kg/s

Intermediate pressure

T_{IN}	231,4 °C
T_{OUT}	290,3 °C
P_{IN}	28,68 bar

P_{OUT}	28,12 bar
h_{IN}	2803,13 kJ/kg
h_{OUT}	2975,66 kJ/kg
DT_ln	18,25 °C
Q	8301 kW
m flow	48,12 kg/s

High pressure

T_{IN}	299,6 °C
T_{OUT}	565,5 °C
P_{IN}	85,42 bar
P_{OUT}	83,74 bar
h_{IN}	2750,30 kJ/kg
h_{OUT}	3555,82 kJ/kg
DT_ln	90,63 °C
Q	221380 kW
m flow	274,8 kg/s

REHEATER

T_{IN}	388,5 °C
T_{OUT}	540 °C
P_{IN}	28,12 bar (IP)
P_{OUT}	27,57 bar (IP)
h_{IN}	3208,61 kJ/kg
h_{OUT}	3549,39 kJ/kg
DT_ln	75,29 °C
Q	110053 kW
m flow	322,9 kg/s

Appendix 7.
ISCC with solar field before the first parallel economiser

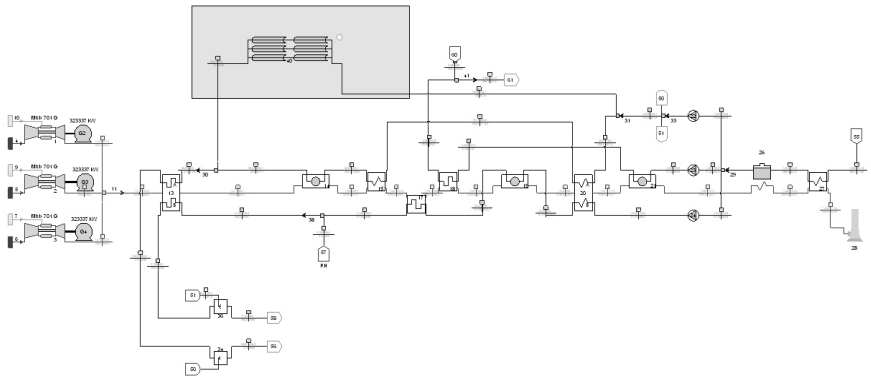

		Case 1	Case 2	Case 3	NGCC
Plant Summary					
Net power	[kW]	1429242	1439925	1450443	1396626
Net electric Efficiency w/o solar	[%]	54,5	54,3	54,1	55,17
Net electric Efficiency w/ solar	[%]	56,46	56,88	57,30	55,17
Overall efficiency increase due to solar	[%]	1,96	2,58	3,20	0
Solar equivalent efficiency	[%]	35,83	35,90	35,92	0,00
Net Heat Rate (LHV) w/ solar	[kJ/kWh]	6605	6630	6655	6525
CH4 fuel input (LHV)	[kW]	2531380	2531380	2531380	2531380
Solar Fuel input	[kW]	91042	120601	149811	0
Total net fuel input (LHV)	[kW]	2622422	2651981	2681191	2531380
Plant auxiliary total power	[kW]	28068	28446	28825	26527
CO2 annual emissions	[kg/year]	4046268	4046268	4046268	4046268
CO2 specific emissions	[kg/MWh]	342,8	340,2	337,7	351
T_SH	[°C]	565,5	565,5	565,5	565,5
T_RH	[°C]	540	540	540	540
Steam turbine					
T_in	[°C]	565,5	565,5	565,5	565,5
P_in	[bar]	90,25	92,32	94,41	83,74
P_out	[bar]	0,077	0,0791	0,0812	0,0709
x_out	[-]	0,937	0,937	0,936	0,938
m_flow HP	[kg/s]	296,9	304,1	311,1	274,8
m_flow IP	[kg/s]	346,8	354,5	362,2	322,9
m_flow LP	[kg/s]	366	374,4	382,8	339,9
Total electrical power	[kW]	487300	498361	509257	453142
Gas turbines					
N. of units	[-]	3	3	3	3
Turbine model	[-]	M 701G	M 701G	M 701G	M 701G
Turbine rated power	[kW]	334000	334000	334000	334000
Unit shaft electrical power	[kW]	323337	323337	323337	323337
Total electrical power	[kW]	970011	970011	970011	970011
Turbine rated efficiency	[kW]	39,3	39,3	39,3	39,3
Turbine net efficiency	[%]	38,32	38,32	38,32	38,32
Solar Field					
m_flow solar field	[kg/s]	34,5	45,67	56,99	-
T_in	[°C]	108	108,1	108,1	-
P_in	[bar]	104,52	106,87	109,19	-
h_in	[kJ/kg]	460,6	460,99	461,38	-
v_in	[m/s]	1,641	1,694	1,725	-
T_out	[°C]	395	395	395	-
P_out	[bar]	92,04	94,2	96,3	-

h_out	[kJ/kg]	3099,45	3094,75	3090,07	-
v_out	[m/s]	44,64	44,85	44,49	-
Heat transfer to network	[kW]	91042	120601	149811	-
Overall pressure drop	[bar]	12,46	12,68	12,89	-
Reflector aperture area	[m^2]	206761	274042	340599	-

Appendix 8.
ISCC with solar field before the first parallel economiser

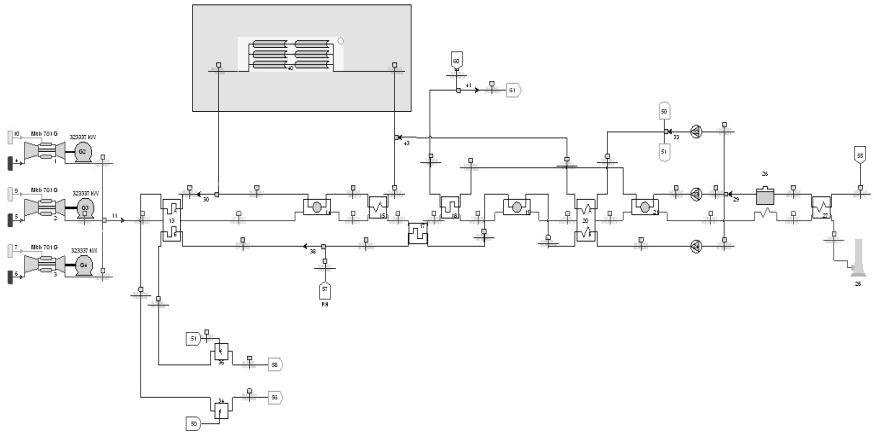

		Case 1	Case 2	Case 3	NGCC
Plant Summary					
Net power	[kW]	1434113	1446874	1459481	1396626
Net electric Efficiency w/o solar	[%]	54,72	54,6	54,49	55,17
Net electric Efficiency w/ solar	[%]	56,65	57,16	57,66	55,17
Overall efficiency increase due to solar	[%]	1,93	2,56	3,17	0
Solar equivalent efficiency	[%]	41,81	42,34	42,67	0,00
Net Heat Rate (LHV)	[kJ/kWh]	6579	6594	6607	6525
CH4 fuel input (LHV)	[kW]	2531380	2531380	2531380	2531380
Solar fuel input	[kW]	89652	118683	147302	0
Total net fuel input (LHV)	[kW]	2621032	2650063	2678682	2531380
Plant auxiliary total power	[kW]	28392	28889	29391	26527
CO2 annual emissions	[kg/year]	4046268	4046268	4046268	4046268
CO2 specific emissions	[kg/MWh]	341,6	338,5	335,5	351
T_SH	[°C]	565,5	565,5	565,5	565,5
T_RH	[°C]	540	540	540	540
Steam turbine					
T_in	[°C]	565,5	565,5	565,5	565,5
P_in	[bar]	91,35	94,1	96,81	83,74
P_out	[bar]	0,0764	0,0781	0,0799	0,0709
x_out	[-]	0,935	0,933	0,932	0,938
m_flow HP	[kg/s]	300,1	309,4	318,6	274,8
m_flow IP	[kg/s]	356,1	367	377,8	322,9
m_flow LP	[kg/s]	364,2	371,9	379,5	339,9
Total electrical power	[kW]	492495	505751	518861	453142
Gas turbines					
N. of units	[-]	3	3	3	3
Turbine model	[-]	M 701G	M 701G	M 701G	M 701G
Turbine rated power	[kW]	334000	334000	334000	334000
Unit shaft electrical power	[kW]	323337	323337	323337	323337
Total electrical power	[kW]	970011	970011	970011	970011
Turbine rated efficiency	[kW]	39,3	39,3	39,3	39,3
Turbine net efficiency	[%]	38,32	38,32	38,32	38,32

Solar Field

m_flow solar field	[kg/s]	45	60	75	-
T_in	[°C]	253,9	255,6	257,2	-
P_in	[bar]	105,76	108,83	111,88	-
h_in	[kJ/kg]	1104,75	1112,77	1120,59	-
v_in	[m/s]	2,24	2,178	2,256	-
T_out	[°C]	395	395	395	-
P_out	[bar]	93,18	95,98	98,75	-
h_out	[kJ/kg]	3096,98	3090,8	3084,6	-
v_out	[m/s]	50,22	47,03	46,97	-
Heat transfer to network	[kW]	89652	118683	147302	-
Overall pressure drop	[bar]	12,58	12,86	13,13	-
Reflector aperture area	[m^2]	206768	274048	340581	-

Bibliography

[1] F. Kreith, D. Goswami, *Handbook of energy efficiency and renewable energy* (2007). Taylor & Francis Group, LLC. Chapter 21.

[2] L. Pistocchini, *Concentrating Solar Power* (2010), Solar thermal engineering, course material.

[3] E. Hu, Y. Yang, A. Nishimura, F. Yilmaz, A. Kouzani, *Solar thermal aided power generation* (2005). Elsevier, www.elsevier.com/locate/apenergy

[4] Y. Cui, Y. Yang, J. Chen, *Utilization of solar energy in a coal-fired plant*. International conference on power engineering 2007, Hangzhou, China

[5] G. Odorica-Garcia, A. Vidal Delgado, A. Fernandez Garcia, *Novel integration options of concentrating solar thermal technology with fossil-fuelled and CO_2 capture processes* (2011). Elsevier, www.elsevier.com/locate/procedia

[6] M.J. Montes, A. Rovira, M. Muñoz, J.M. Martìnez-Val, *Performance analysis of an Integrated Solar Combined Cycle using Direct Steam Generation in parabolic trough collectors* (2011). Elsevier, www.elsevier.com/locate/apenergy

[7] H. Nezammahalleh, F. Farhadi, M. Tanhaemami, *Conceptual design and techno-economic assessment of integrated solar combined cycle system with DSG technology* (2010). Elsevier, www.elsevier.com/locate/solener

[8] P.Simshauser, *The hidden costs of wind generation in a thermal power system: what cost?* (2010). AGL applied economics and policy research.

[9] M. Watt, J. Wyder (2010). *National survey report of PV application in Australia 2009*. IT Power Australia with the support of ASI (Australian Solar Institute).

[10] Wikipedia: http://en.wikipedia.org/wiki/Munmorah_Power_Station

[11] U.S. Department Of Energy, http://apps1.eere.energy.gov/buildings/energyplus/cfm/weather_data.cfm